SEASON

Self-Managed Sustainable High-Capacity Optical Networks

This project is supported by the SNS Joint Undertaken through the European Union's Horizon RIA research and innovation programme under grant agreement No. 101096120

Deliverable D3.2

Optical systems enabling ultra-high-capacity access/metro networks

Editor L. Nadal (CTTC)

Contributors CNIT, CTTC, ADTRAN, UC3M, HHI, TIM, SSSA, INF-P, INF-G, WEST, ACC, ERI

Version 1

Date Dec 12, 2024

Distribution PUBLIC (PU)

Dissemination Level	Public

DISCLAIMER

This document contains information which is proprietary to the SEASON consortium members that is subject to the rights and obligations and to the terms and conditions applicable to the Grant Agreement number 101096120. The action of the SEASON consortium members is funded by the European Commission.

Neither this document nor the information contained herein shall be used, copied, duplicated, reproduced, modified, or communicated by any means to any third party, in whole or in parts, except with prior written consent of the SEASON consortium members. In such case, an acknowledgement of the authors of the document and all applicable portions of the copyright notice must be clearly referenced. In the event of infringement, the consortium members reserve the right to take any legal action it deems appropriate.

This document reflects only the authors' view and does not necessarily reflect the view of the European Commission. Neither the SEASON consortium members as a whole, nor a certain SEASON consortium member warrant that the information contained in this document is suitable for use, nor that the use of the information is accurate or free from risk, and accepts no liability for loss or damage suffered by any person using this information.

The information in this document is provided as is and no guarantee or warranty is given that the information is fit for any particular purpose. The user thereof uses the information at its sole risk and liability.

REVISION HISTORY

Revision	*Date*	*Responsible*	*Comment*
0.1	*July 31, 2024*	*L. Nadal*	*First draft*
0.2	*Sept 30, 2024*	*L. Nadal*	*Partner Contributions*
0.3	*Oct 16, 2024*	*L. Nadal*	*Integrated version*
0.4	*Dec 12, 2024*	*C. Pinho*	*Quality check*
0.5	*Dec 12, 2024*	*L. Nadal*	*Final version*

LIST OF AUTHORS

Partner	***Name Surname***
ADTRAN	*Lutz Rapp, Dominic Schneider*
CNIT	*Filippo Cugini, Margita Radovic*
CTTC	*Laia Nadal, Ramon Casellas, Josep Maria Fàbrega, Francisco Javier Vílchez, Ricardo Martínez, Luca Vettori, Carlos Hernández, Michela Svaluto Moreolo*
INF-G	*Antonio Napoli, Carlos Castro, Mohammad Hosseini*
INF-P	*Cátia Pinho, João Pedro, André Souza*
HHI	*Johannes K. Fischer, Behnam Shariati, Abdelrahmane Moawad, Juan Moreno Morrone, Laurenz Ebner*
WEST	*Carlo Centofanti, Andrea Marotta*
SSSA	*Nicola Sambo*
ACC	*Revaz Berozashvili*
TIM	*Marco Quagliotti, Mauro Agus*
UC3M	*José Alberto Hernández, David Larrabeiti, Fernando Díaz de María, Farhad Arpanaei, Alfonso Sánchez-Macián*
ERI	*Gianluca Gambari, Roberto Magri*

Dissemination Level	Public

EXECUTIVE SUMMARY

This deliverable reports the activities of WP3 during the second year of the SEASON project. The work is structured in two main parts. The first six chapters are dedicated to the data plane architecture, technology mapping, key performance indicators (KPIs) alignment and the development of optical subsystems, focusing on areas such as network design, transmission modelling, optimization, optical monitoring, and power-efficient solutions. The latter section describes the innovations/prototypes/components implemented within WP3, which are key elements in fulfilling the objectives and goals of the overall SEASON project.

The document first introduces a summary of the proposed novel network architecture designed to address the increasing demand for higher bandwidth and network capacity, as discussed in more detail in WP2 (see deliverable D2.1 [D2.1-24]). The proposed architecture is segmented into two main domains: Access-Metro and Backbone and it supports various levels of decentralization. Furthermore, we define a two-phase approach, with a Medium- (4 years) and Long-term (8 years) reference periods for implementing the proposed architecture and solutions are envisioned, introducing, and discussing key technologies such as new fiber types and multi-band transmission techniques. Data plane technologies are mapped within the envisioned SEASON architecture also discussing KPI alignment and development path.

To this end and based on WP2 outputs, SEASON project proposes innovative solutions for the optical data plane included in this document. In particular, the modelling of an end-to-end design of optical networks is investigated and presented, focusing on energy efficiency increase and power consumption reduction. In this regard, optical versus electrical aggregation and network optimization with digital subcarrier multiplexing (DSCM), enabling both point-to-point (P2P) and point-to-multipoint (P2MP) transceivers are analysed. Such solutions allow for more flexible and scalable network designs, reducing overall costs and energy consumption. In addition to DSCM, ROADM-free IP over wavelength division multiplexing (IPoWDM) networks are also explored. This approach eliminates the need for traditional reconfigurable optical add/drop multiplexers (ROADMs) and is driven by recent advances in coherent transceivers and packet-switching ASICs. These offer a more cost-effective and efficient solution for the Access-Metro segment. Initial performance studies suggest that ROADM-free networks can significantly reduce capital expenditures (CAPEX), particularly in scenarios where the traffic demand is lower than the available transceiver capacity.

In addition, in this document various scenarios for upgrading network capacity using both multiband (MB) and space division multiplexing (SDM) technologies are investigated and proposed. While MB transmission is currently the most cost-effective solution for increasing capacity over existing fiber infrastructure, SDM also offers significant long-term benefits. To support MB over SDM operation and manage the increasing demands of future networks, different node architectures and transmission solutions have been proposed and analysed. Furthermore, for supporting MBoSDM operation over C+S+L-bands, suitable optical subsystems including novel optical transceiver and switching solutions are implemented and preliminary assessed. These subsystems have been designed, in view of further enhancing performance, efficiency, flexibility and scalability of the network. Efficient network designs for power-optimized P2MP solutions in MBoSDM scenarios are also investigated for next generation optical networks. The investigation also included a cost benefit analysis.

Activities related to the front/mid-haul and access segment beyond 5G are also considered, analysing the radio access network (RAN) fronthaul network and promoting P2MP technology for next generation mobile transport, also proposing a spatial passive optical network (PON) architecture which ensures high performance and scalability by the exploitation of the spatial dimension.

Optical monitoring and power efficiency strategies are crucial topics that are also investigated in SEASON and reported in this document. Various approaches to reduce power consumption in optical networks are studied, emphasizing the role of pluggable transceivers and advanced monitoring techniques.

Finally, the document reports the main SEASON data plane prototypes/components/innovations (components C3.1 to C3.9) proposed as key solutions to meet the project objectives, goals and network requirements. These include:

- Advanced node and transceiver architectures (components C3.1-C3.4)
- Digital signal processing (DSP) receiver (Rx)-based monitoring (component C3.5)
- A predictive maintenance (PdM) system for MB amplifiers (C3.6)
- Optical monitoring and telemetry systems (component C3.7)
- Research activities on pluggable amplifiers and SmartNIC with coherent pluggable (C3.8-C3.9).

The proposed SEASON solutions will play a crucial role in ensuring an efficient operation and management of high-capacity MBoSDM optical networks, while addressing critical network challenges and requirements. All this WP3 technologies and achievements will be key towards fulfilling SEASON objectives and KPIs, in particular those related to providing: i) a sustainable network architecture able to scale up network capacity and cope with challenging user needs through improved power efficiency, reliability, and self-management capabilities; ii) a scalable, ultra-high capacity, and power efficient MBoSDM network infrastructure spanning from access to cloud; iii) novel optical systems and subsystems for MBoSDM transmission; iv) a pervasive monitoring infrastructure for secure and truly self-managed networking; and v) a control plane, monitoring and streaming telemetry solution.

WP3 components and results will be used in WP4 and WP5 activities facilitating the integration with the control plane and final demonstrations.

Table of Contents

1 INTRODUCTION

This deliverable D3.2 “Optical systems enabling ultra-high-capacity access/metro networks” describes the activities, during the second year, related to work package 3 (WP3) in the SEASON project. It defines the framework for the designing and operating of multiband (MB) and spatial division multiplexing (SDM) optical networks across multiple network segments, addressing the increasing demand for data and capacity/bandwidth. To meet these challenges the document summarizes various innovative SEASON data plane technologies and solutions (leveraging on MB, SDM and point-to-multipoint (P2MP) transmission), with a clear focus on minimizing power consumption and providing the required network capacity scaling. The main objectives of this work include:

- Designing a high-capacity, scalable, and flexible optical network architecture leveraging MB over SDM (MBoSDM) technology;
- Transmission end-to-end (E2E) modelling for MBoSDM and P2MP systems;
- Exploring power efficient solutions for P2MP and MBoSDM scenarios;
- Design, prototyping and experimental validation of novel optical network devices/systems for switching, amplification and transmission solutions capable to enable MBoSDM operation;
- Explore advanced network and switching options based on P2MP and SDM for front/mid-haul and access;
- Design and implementation of advanced monitoring solutions to enable efficient and flexible use of the network/fiber infrastructure.

This document reports on the progress of WP3 during the second year of activity of SEASON toward the above-mentioned objectives and is structured as follows:

Section 2 provides a comprehensive overview of the SEASON network architecture, also including the mapping of SEASON solutions into the overall proposed architecture and alignment and path towards fulfilling the project objectives and key performance indicators (KPIs).

Section 3 includes modelling, scenarios and design considerations of MBoSDM networks. It outlines the key challenges the project addresses, such as the increasing demand for bandwidth, network capacity, and energy-efficient solutions. It also includes activities on network optimization.

Section 4 covers the development and implementation of optical systems and subsystems, including advanced optical transceivers and switching solutions. Specifically, innovative transceiver and node architectures for high-capacity MBoSDM optical networks are investigated. This section provides a detailed analysis of the subsystems that support the MBoSDM networks, with a focus on energy efficiency, performance enhancement, and scalability. It also discusses power-optimized P2MP solutions, highlighting their role in enhancing network capacity and efficiency.

Section 5 examines the front/mid-haul and access segments beyond 5G, focusing on network design for mobile transport systems. This section presents innovative architectures, such as spatial passive optical networks (PONs), and promotes the use of P2MP technologies for future

mobile networks. It highlights how these technologies ensure scalability and high performance, critical for handling the increasing demands of 5G and beyond.

Section 6 focuses on optical monitoring and power efficiency strategies. It explores methods for reducing power consumption in optical networks, including the use of pluggable transceivers and advanced optical monitoring techniques. This section emphasizes the importance of energy-efficient solutions to meet the growing demands of future optical networks.

Section 7 details the data plane prototypes/components/innovations developed as part of the SEASON project. Here, we describe the components, their interfaces and initial experimental activities, including for example advanced node and transceiver solutions, a predictive maintenance (PdM) system for MB amplifiers, monitoring and telemetry systems and solutions, research activities on pluggable amplifiers and SmartNIC with coherent pluggable transceivers.

Section 8 provides the conclusions to the document.

1.1 Experimental validation of Optical Systems and Prototypes

The main SEASON data plane prototypes and components to be used in final project demonstration include:

- The advanced node and transceiver architectures (components C3.1-C3.4) that include:
    a. The MBoSDM node prototype (component C3.1)
    b. The Multi-Granular Optical node (component C3.2)
    c. The Spatial PON Node (component C3.3)
    d. The MBoSDM S-BVT prototype (component C3.4)
- The digital signal processing (DSP) receiver (Rx)-based monitoring (component C3.5).
- MB amplifiers with availability assurance via predictive maintenance (component C3.6)
- The optical monitoring and telemetry technique developed in the project (component C3.7)
- Pluggable Amplifiers (C3.8)
- SmartNIC with coherent pluggable (C3.9)

The components developed will be used in the final project demonstrations. Figure 1-1 displays the testbed and infrastructure to be used. The demo will deploy an open virtual museum in the City of L'Aquila. The transmission from the edge to the end-user of real-time profiled contents requires high throughput for multi-stream transmission of rendered content. Such a high throughput can be offered by densifying radio access points which in turn require dense and high-capacity optical transport. In the demo, the developed optical node prototypes will be employed as well as data plane components C3.7 to C3.9 to exploit coordinated SDN-control of high-density radio solutions (open RAN (O-RAN), cell-free) and high-capacity optical technologies (SDM-PON, MBoSDM, etc) for the radio fronthaul/midhaul and the metro connection with service instance at the edge.

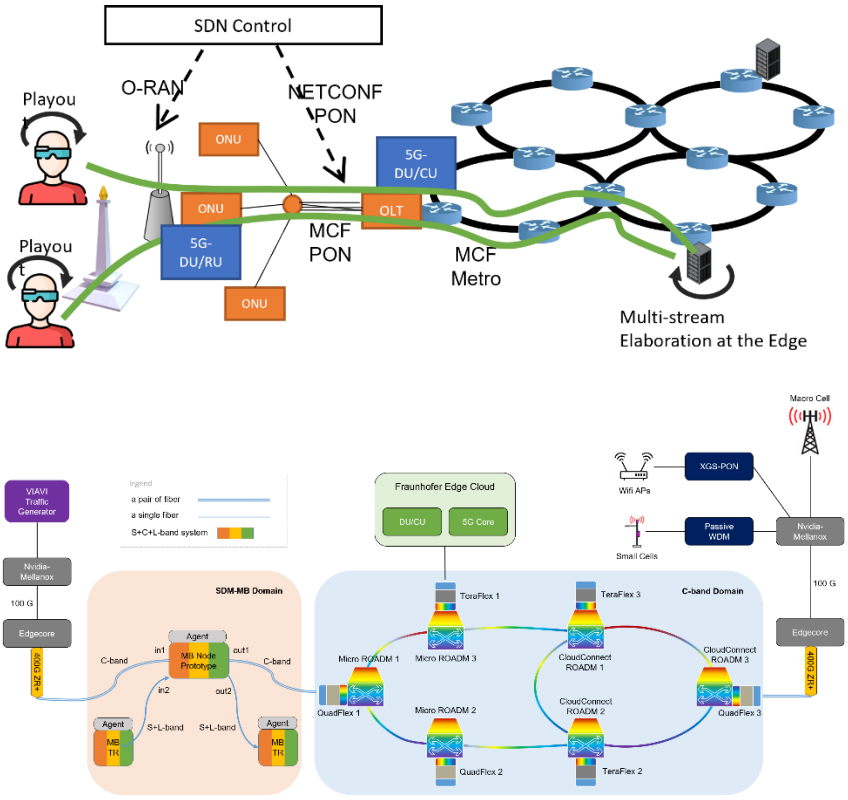

Figure 1-1: SEASON testbeds for final demonstrations.

The demo will go beyond the state of the art by deploying an AR solution which will exploit computation off-load from the user side to the edge.

2 PHYSICAL LAYER NETWORK ARCHITECTURE AND DATA PLANE SOLUTIONS MAPPING

2.1 NETWORK ARCHITECTURE OVERVIEW

The first design of the innovative architecture for the SEASON project was done in WP2 and reported in D2.1. This included the definition of a general framework that defines the network segmentation and the types of central office, the definition of the reference time periods for the studies and the definition of the network architectures for the medium term and the long term.

The proposed high-level framework provides a segmentation of the network into just two domains, Access-Metro (considered and optimized as a whole) and Backbone. Telco and service functions can be placed at three levels of decentralization (Cloud in the backbone, Edge, and Far Edge in the Access-Metro) which also correspond to three classes of Central Office (CO). The most peripheral type of CO is conceived to accommodate the Far Edge functions and is expected to be of low cost and low power consumption (mini containers or reinforced cabinets are possible practical implementations). They could replace all or part of the current aggregation or access legacy COs allowing considerable savings.

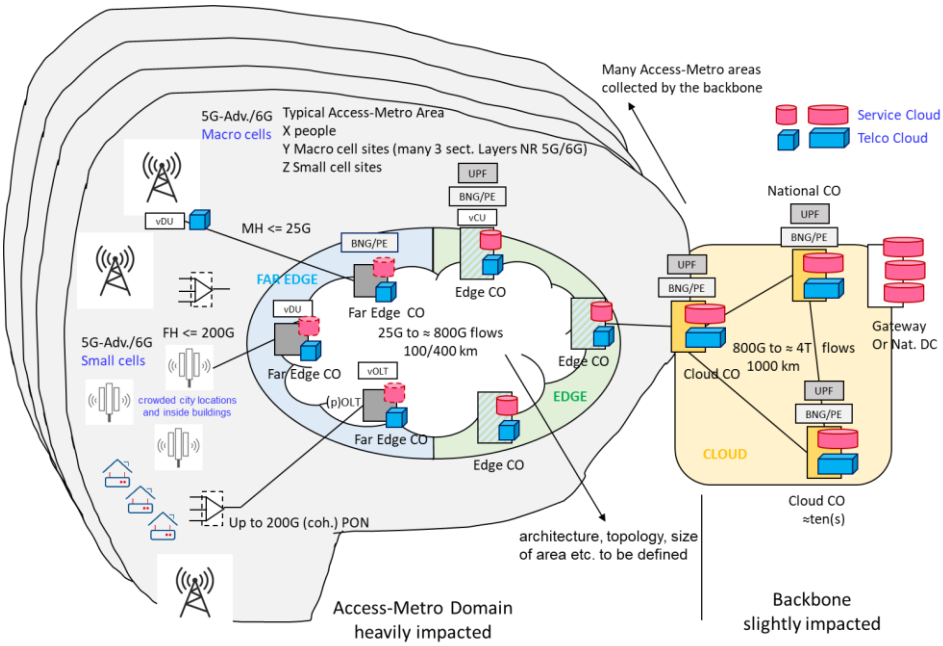

Figure 2.1-1: Overall high-level view of the SEASON architecture for the Medium-term.

Two reference periods are defined for architecture and solutions to be implemented in the project, the medium term, thought of 4 years from now (the late twenties) and the long term, 8 years from now, therefore beyond 2030. There are good reasons for this choice that are reported in D2.1 where the general characteristics and requirements are listed and argued for the reference architecture in the two periods. For example, the expected traffic growth in comparison to the current one is x5 for the medium term and of x10, and even up to x30, for the long term. Regarding mobile technology, however, it is assumed that in the medium term

Dissemination Level	Public

the system deployed will be 5G-Advanced (3GPP Rel. 18 or 19) while in the long term it will be 6G (Rel. 20 or later). Furthermore, with respect to the use of fiber and related multiplexing and transmission techniques, in the medium term a limited use of new fibers, few bands (C+L with at most one additional band) and multi-fiber as basic SDM technique is expected. In the long term, technologies will have to consider the use of new types of fiber (multi-core, hollow-core) with the exploitation of all bands and SDM extended to fiber or core switching. Taking into account everything all the above, the diagrams of the two medium term (Figure 2.1-1) and long term (Figure 2.1-1) architectures are provided with the main characteristic data, i.e., typical distances in the domains, data rates at the interfaces at the various network levels, probable positioning of the telco functions for the data plane (e.g., UPF, BNG) and more.

As indicated in Figure 2.1-1 and Figure 2.1-2, an Access-Metro area (grey multiple areas encompassing Access, Far edge and Edge) can extend from about 100 to 300-400 km and can be characterized by flows ranging between 25 Gb/s and 800Gb/s in medium term, and between 100 Gb/s and 1.6-3.2 Tb/s in the long term. Such a high variability of unitary flows could be effectively managed with a suitable mix of high capacity P2P, sub-carrier multiplexing P2MP and S-BVT. Higher data rate flows are expected between Far Edge CO and Edge CO or between pairs of Edge COs. The **Backbone Segment** is shown on the right side of Figure 2.1-1 and Figure 2.1-2 (yellow area including the Cloud). The capacity requirements for nodes interconnection in backbone segment is estimated to be of the order of Tb/s in medium term and up to ten Tb/s in long-term. From an architectural point of view, this backbone segment envisages a technological upgrade of nodes and transmission systems in the direction of the introduction of multi-band and SDM solutions.

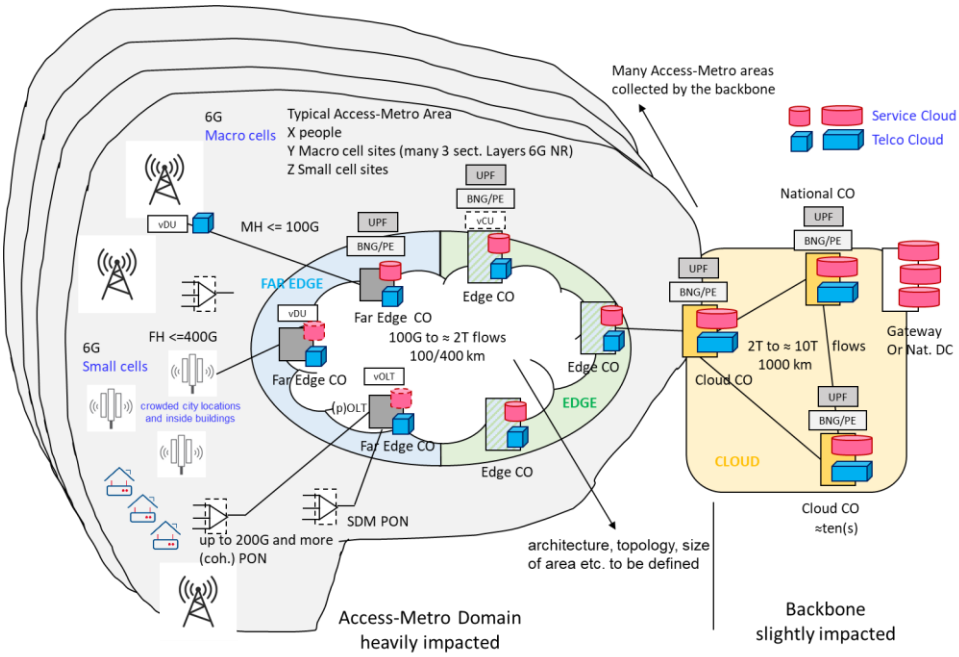

Figure 2.1-2: Overall high-level view of the SEASON architecture for the Long-term.

The architectures are to be considered as a reference both for the systems and subsystems developed in the project and to define the case studies of planning and dimensioning and technical-economic evaluations. The architectures in question refer to a reference framework for the data plane and must be completed with the physical topologies inspired by those

Dissemination Level	Public

provided by the operators (also included in D2.1 and made available as a shared dataset within the project). Important innovations are foreseen in the control plane too, with the introduction of pervasive telemetry and massive use of AI/ML solutions to support network operation and the coordination of the cloud resources of the Backbone with those of Access-Metro (Edge and Far Edge). This last feature can be obtained with an overreaching orchestrator that coordinates the control entities throughout the various network domains.

2.2 SEASON SOLUTIONS TOWARDS THE SEASON ARCHITECTURE

This section provides a detailed mapping of the data plane technologies and solutions proposed in SEASON and described in the following sections of this document into the high-level SEASON network architecture. In deliverable [D2.1] an initial mapping, considering different time periods (medium term and long term) was included. As denoted in the previous section, the SEASON architecture considered is segmented into two domains: Access-Metro and Backbone. The evolution of SEASON architecture considers both medium-term (4 years) and long-term (8+ years) with progressively advanced technologies addressing the expected traffic and requirements of future networks. So here, we also differentiate and map the proposed SEASON data plane technologies considering the identified two reference time periods.

2.2.1 Medium-term

In the medium-term, SEASON focuses on leveraging technology advancements to enhance the performance, efficiency and flexibility of the data plane. The following key technologies will be considered in different segments of SEASON architecture.

2.2.1.1 Access-Metro and Backbone segments

- ROADM-free IPoWDM networks (see related work in Section 3.3). SEASON focuses on the evolution of metro-aggregation networks based on cost-effective IPoWDM nodes eliminating the use of ROADMs, i.e., packet-optical switches/routers equipped with coherent pluggable transceivers enhancing cost efficiency and providing simplified network management.
    - **Mapping to SEASON architecture:** ROADM-free IPoWDM networks can be effectively implemented in the Access-Metro and Backbone segments where cost efficiency, simplified management, and low-latency communication are critical.
- Use of DPU/Smart NIC (component C3.9 detailed in section 7.9 and related work in Section 6.6): The integration of data processing units (DPUs) and smart network interface Cards (Smart NICs) featuring interfaces capable of supporting data rates up to 800G will play a key role in enhancing network performance while supporting monitoring capabilities. These technologies will enable both P2P and P2MP communication, particularly at the Edge and Far Edge of the network.
    - **Mapping to SEASON architecture:** the deployment of DPUs and Smart NICs will enable creating a highly efficient network infrastructure. By positioning these

units at the Edge and Far Edge (Access-Metro segment), SEASON enhances its capability to provide Telco functions (e.g., vDU) and Service functions (e.g., AI tasks) closer to end users, thereby minimizing latency and maximizing bandwidth utilization.

- Whiteboxes and Pluggable Transceivers: The use of L2/L3 switches and whiteboxes with pluggable transceivers (up to 800G) will be envisioned in the Access-Metro segment. These whiteboxes, compliant with standards such as OIF and OpenROADM, are critical in creating flexible, open line systems that accommodate modules from different manufacturers, and they can be easily upgraded with technological advances.
    - **Mapping to SEASON architecture**: In the SEASON architecture, these elements will be placed at Far Edge and Edge Central Offices (COs) of the Access-Metro segment, supporting both telco and service functions such as the vDU and vCU (virtualized distributed and centralized units).
- Coherent digital subcarrier multiplexing (DSCM) based P2MP and P2P transceiver up to 800G (related work in sections 3.1, 5.2 and 6.2): Implementation of DSCM based transceivers supporting data rates up to 800G also facilitating the transport of fronthaul (FH) flows (<=200 Gb/s) in the radio access network (RAN).
    - **Mapping to SEASON architecture**: the deployment of coherent DSCM-based P2MP and P2P transceivers will enable to optimize bandwidth utilization while enhancing power efficiency and performance in the Access-Metro domain. By leveraging the capabilities of these high-capacity transceivers, the growing demands of fronthaul traffic can be effectively managed, particularly in scenarios that require low latency, also resulting in power savings.
- 50G PONs and coexistence with coherent DSCM based P2MP and P2P pluggable transceivers (see deliverable D2.1 and Sections 3.2, 4.3, 5.3 and 6.5): SEASON also considers the use of 50G PON for aggregating endpoints within the access segment. In addition, it considers too, the introduction of coherent PON at 200G and wavelength division multiplexing (WDM) PON and DSCM based transceivers to enhance fiber capacity and effectively accommodate the increasing traffic.
    - **Mapping to SEASON architecture**: These technologies will be envisioned in the Access-Metro segment where high-density traffic aggregation is required. PON technologies will be used at Far Edge COs and aggregation points to efficiently connect access points and users, helping to handle the rapid growth in traffic while optimizing the use of existing fiber infrastructure.
- Pure filterless or hybrid filtered-filterless optical line systems (OLS) (see related work in Sections 3.2 and 4.3): The use of pure filterless or hybrid filtered-filterless optical line systems will be integrated with DSCM transceivers and multicarrier modulation (MCM) technologies to support both P2MP and P2P architectures. This will facilitate efficient transmission and optimize spectral efficiency and resource utilization.
    - **Mapping to SEASON architecture:** Advanced OLS based on filterless or hybrid filtered-filterless architecture in the Access-Metro domain with flexible and high-capacity transmission capabilities.
- Exploitation of MB transceivers (such as the MBoSDM S-BVT proposed within SEASON) operating in the C+L-bands, with potential extension to the S-band (component C3.4 in section 7.4): Adoption of MB transceivers (C+S+L) to enhance network capacity, scalability and spectral efficiency.

- **Mapping to SEASON architecture:** MB(oSDM) S-BVTs will enable the extension of the capacity of the existing fiber infrastructure and accommodate the growing data demands in both the Access-Metro and Backbone segments. The proposed SEASON MB(oSDM) receiver is designed using direct detection (DD) technology. However, coherent detection can also be implemented to significantly extend the transmission reach, making it more suitable for long-distance, high-capacity applications within the Backbone segment. This flexibility allows SEASON architecture to support a range of use cases, from shorter metro links to extended backbone connections, ensuring optimal performance across the network.

- Partially exploitation of the multigranular MBoSDM modular and flexible node (Components C3.1 in section 7.1 and C3.2 in section 7.2 and work included in Section 4.2).
  - **Mapping to SEASON Architecture**: The use of MB technology in both the Access-Metro and Backbone segments will require advanced switching node capabilities and granularities including band and wavelength switching. So, the proposed MBoSDM switching solution can be partially used in both segments.
- Advanced monitoring solutions (components C3.7 in section 7.7 and component C3.5 in section 7.5 and related work in Sections 6.3, 6.6 and 6.7): Advanced monitoring solutions based on fast fault and anomalies localization techniques, that use current digital signal processing (DSP) receiver (RX)-based transceivers or even simplified schemes/systems included in different network nodes.
  - **Mapping to SEASON Architecture**: Adoption of advanced monitoring solutions in different network nodes from both Access-Metro and Backbone segments to identify possible link faults or monitor different target figures of merit to efficiently allocate resources and establish optical paths accordingly.
- The implementation of radio access based on the O-RAN architecture providing double split 2 (MH) and 7.2 (FH) with open solutions (distributed or centralized) regarding the positioning of the vDU and vCU functions. The design aligns with the advanced functionalities expected in 5G Advanced (3GPP Releases 18 and 19), ensuring the network is prepared for future developments in mobile technology.
  - **Mapping to SEASON architecture:** the adoption of O-RAN's double split model for Split 2 (MH) and Split 7.2 (FH) is mapped to the Access-Metro segment, where efficient, flexible, and scalable deployment of radio access functions is essential.

2.2.2 Long-term

In the long term, SEASON envisions the deployment of even more advanced technologies in the data plane to handle extreme traffic demands and enable future network use cases such as 6G, metaverse, and AI-driven services.

2.2.2.1 Access-Metro and Backbone segment

- Next-Generation Whiteboxes and Pluggable Transceivers (see Section 3.3): Whiteboxes and pluggable transceivers will evolve to support data rates of up to 2 Tb/s per flow

preferably with the same form factor as today's 400G; evolution of other type of pluggable, EDFA and VOAs, with their higher level of integration and lower cost power consumption and footprint
    - **Mapping to SEASON Architecture**: These solutions will be deployed in the Far Edge and Edge COs to handle both telco and service functions, such as massive AI tasks at the Edge.
- Extensive deployment of DPU (or its evolution) featuring interfaces capable of handling data rates of 800G or higher, up to 2 Tb/s (see Component C3.9 detailed in section 7.9 and related work in section 6.6).
    - **Mapping to SEASON Architecture**: At the Far Edge, these DPUs will not only support essential Telco functions—such as the vDU in the RAN but also provide the computational power needed for running advanced service functions. This includes massive AI tasks to support services aligned with the Compute Power Networking (CPN) paradigm, where computation is distributed across the network and performed closer to the data source (or the user) to minimize latency and optimize resource use.
- Deployment and coexistence of coherent PON operating at 200G, WDM PON and SDM PON to address scalability and the increasing traffic demands of future networks (work related to Section 5.4 and component C3.3 in section 7.3).
    - **Mapping to SEASON Architecture**: Adoption of SDM PON node in the Access-Metro domain to cope with traffic demand growth from access points.
- Adoption of enhanced coherent DSCM-based P2MP and P2P transceivers, supporting data rates of 800 Gb/s and up to 2 Tb/s of total capacity (related work in Sections 3.1, 5.2 and 6.2).
    - **Mapping to SEASON Architecture**: Deployment of advanced coherent DSCM-based P2MP and P2P transceivers across both the Far Edge and Edge COs within the Access-Metro segment.
- Fully meshed connectivity in the fronthaul, leveraging coherent optical technologies and optical layer flexibility, to enable independent processes within the network to be dynamically and flexibly managed providing optimization in the cloud RAN (section 5.1). Use of coherent “lite” transceivers at >= 400 Gb/s for FH application (with 6G).
    - **Mapping to SEASON Architecture**: Fronthaul Optimization (real-time traffic management and resource optimization) in Access-Metro segment.
- Full exploitation of MB(oSDM) S-BVTs or future evolutions (component C3.4 in section 7.4): MB(oSDM) S-BVT with extended capabilities capable to operate beyond the C+L band and achieve aggregated bit rates of 1 Tb/s and higher, potentially scaling up to 10 Tb/s by means of using additional bands (beyond C+L+S-bands) or even different spatial channels (in the Backbone domain).
    - **Mapping to SEASON Architecture**: Advanced MB(oSDM) S-BVTs will be adopted and used within both the access-Metro and Backbone segments to dynamically allocate network resources, ensuring optimal performance. Thanks to its flexible, modular and scalable architecture, the transceiver can be adapted to maximize performance according to the target network domain.
- Full exploitation of the multigranular MBoSDM modular and flexible node or its evolution (Components C3.1 in section 7.1 and C3.2 in section 7.2 and work included in section 4.2)

  - **Mapping to SEASON Architecture**: Adoption in the Backbone segment of the advanced MBoSDM switching node with full capabilities enabling band, wavelength and spatial granularities to cope with the target network capacities.
- Exploitation of multiband amplifiers with availability assurance via predictive maintenance and pluggable amplifiers (component C3.6 in section 7.6): Multiband amplifiers will enable the amplification of signals across multiple bands beyond C+L. Implementing predictive maintenance (PdM) for optical fiber amplifiers will be investigated within SEASON to improve existing monitoring processes and minimize the risk of network downtime.
  - **Mapping to SEASON Architecture**: Multiband amplifiers will be strategically deployed within both the Access-Metro and Backbone segments. Depending on the network segment, they will be designed to cover extended operational bands.
- Implementation of radio access based on the O-RAN architecture. The implementation of radio access based on the O-RAN architecture supporting double split 2 (MH) and double split 7.2 (FH). This architecture allows for both distributed and centralized solutions regarding the placement of critical network functions, including the vDU and the vCU. Reference to functionality available with 5G Advanced (3GPP Rel. 18 and 19) ensuring compatibility with advanced services and improved operational efficiency.
  - **Mapping to SEASON Architecture**: integration of O-RAN architecture facilitating optimized deployment of vDU and vCU functions.

2.3 PROJECT OBJECTIVES AND KPIS

- ***Obj. 1****: Design a* ***sustainable network*** *architecture able to scale up network capacity and cope with challenging user needs* ***through improved power efficiency, reliability, and self-management capabilities****.*
  - **Results**: Design of a scalable horseshoe-and-spur filterless network architecture (see Sections 3.2 and 3.3), spectrum saving techniques (section 4.3), optimization of MB systems (Sections 3.2, 3.5 and 4.2.2), and application of RL for routing and spectrum assignment (section 3.4).
  - **Results**: Design and validation of MBoSDM sliceable bandwidth/bit rate variable transceiver (S-BVT) and switching node prototypes (Sections 4.1, 7.1, 7.2 and 7.4).
  - **Results**: Design of coherent mesh/ring with P2MP technology (section 3.2 and 4.2), SDM PON with spatial aggregation (Sections 5.4), and flexible activation/deactivation of subcarriers (section 6.2).
  - **Results**: Development of optical monitoring techniques (Sections 6.3 and 6.6), fault localization (section 6.7), signal quality monitoring (Sections 6.3), and AI/ML algorithms for failure management (Sections 6.7).
- ***Obj. 2****: Design and validate* ***a scalable, ultra-high capacity, and power efficient Multi-Band over Space Division Multiplexing (MBoSDM) network*** *infrastructure from access to cloud.*

- **Results**: Optical node design for MBoSDM (Sections 4.2, 7.1, 7.2), Investigations and comparison of different MB solutions (Sections 3.5), hybrid amplification (sections 3.3 and 7.6).
- **Results**: Analysis of power consumption of MBoSDM transceivers, integration with SDN control plane, and cost analysis of MBoSDM transceiver solution (Sections 3.4).
- **Results**: Initial assessment of energy-saving aspects of P2MP coherent use-cases in different scenario contexts within the C-band: 1) within WDM amplified ring architecture (Sections 5.1 and Sections 6.2), 2) through a comparison with other alternatives (i.e., P2MP and WDM) for FH traffic transportation (Sections 5.2) and 3) in metro aggregation structures in presence of daily variable traffic (Sections 6.2).

- ***Obj. 3**: Design and development of **novel optical systems** and subsystems for **multiband over SDM**.*
  - **Results**: MB S-BVT (Sections 7.4), filterless E2E design of metro-aggregation optical networks (sections 3.3 and 4.3), dynamic bandwidth allocation (section 6.2), and AI/ML-based failure management (Sections 6.7).
  - **Results**: Design and implementation of MBoSDM node prototype (Sections 7.1 and 7.2), insertion loss measurements (sections 7.1.4 and 7.2.4), and integration with SEASON MBoSDM transceiver (Sections 4.1).
- ***Obj. 4**: Develop an **innovative access and front/mid-haul transport solution** supporting power-efficient functional split implementations as well as cost-effective small/free cells solutions.*
  - **Results**: Access and front/mid-haul transport solutions (Sections 5.1, 5.2) covering different fronthaul configurations, including comparisons of P2P and P2MP options for scalable and power-efficient connectivity.
  - **Results:** Innovative, flexible, scalable and cost-effective node designs for PON spatial aggregation/ disaggregation leveraging on spatial switches (section 5.4).
- ***Obj. 5**: Develop a **pervasive monitoring infrastructure** for secure and truly self-managed networking*.
  - **Results**: Novel AI/ML algorithms for failure management (section 6.7), model-centric and data-centric approaches (section 6.6), and integration of monitoring solutions in control plane (section 6.3).
- ***Obj. 7**: Control plane, Monitoring and streaming telemetry.*
  - **Results**: Streaming telemetry solutions (section 6.7), intelligent data aggregation (section 6.6), and integration with SDN control plane (section 3.4).

2.3.1 KPIs

KPI 2.1

Increase the available bandwidth of the fiber from actual C-band (~35 nm) to O, E, S, L, U bands (~415 nm) that, together with the usage of SDM, e.g., with >10 fibers / cores, will make the available bandwidth to grow by a factor ×120.

Achieved, additional studies are in progress to finalize the validation. The actual increase of the available bandwidth depends on multiple factors, like distance, impairments, and number of active channels. First studies confirm that such increase can be effectively achieved by combining MB and SDM. For example, [Fer20] estimates for multiband transmission system exploiting wavelengths from 1260 to 1625 nm (bands O, E, S, C and L) a total single-fiber throughput of 450 Tb/s over a distance of 50 km and 220 Tb/s over regional distances of 600 km. This means a factor of ∼10× and 8× more than C-band transmission capacity respectively for 50 and 600 km, and ∼2.5× more than full C+L system. For long distance networks (1000 km and beyond), due to physical impairments, a reduction of the multiplication factor can be envisaged: for C-band we can expect a ∼ 5× factor, while for a full C+L system a factor of ∼2× can be esteemed. The evaluation done in [Fer20] considers 5 bands (O, E, S, C and L band, U is taken out of the analysis) and it is done with the widely deployed ITU-T G.652.D fiber without any optimization in transmission system design. Taking the above analysis into account, the factor x 120 required by KPI 2.2 is achievable thanks to the contribution of SDM, and in particular with system adopting multiple fibers in parallel (situation that is more likely the medium term) and with multicore fibers (more probable in the long term). The number of parallel multi-band systems that allow to reach the 120× factor or cores can be roughly estimated around 20-30.

Section 3 extensively analyses the technologies that allow the bandwidth used by a fiber to be increased from 35 nm (3.8 THz) to 400 nm (56.8 THz), Section 4 present some viable MSoSDM architectures while Section 7 include prototype implementations of MBoSDM nodes and transceivers developed with the contribution of SEASON.

Going in more details, section 3.5.2 presents a migration scenario from C-band only systems to multi-band and multi-fiber or multi-core systems. The migration is also discussed from an economic point of view and applies to bandwidth increases in single-fiber systems, that can achieve limited capacity increase factors (much lower than those required by KPI 2.2), and to multi-fiber and multi-core systems. The last ones are the only capable of obtaining multiplication factors of the overall capacity in the order of dozens or even one hundred times the capacity of a baseline C-band only system. In any case, the cost per bit is expected to increase both for multi-band (currently multi -band systems that share the same medium are more complex and expensive of the one of C-only band) and for SDM (new fiber, be it single or multi core, needs to be laid, and this is very costly). The conclusion is that the gain is achievable, but at the expense of an increased cost per bit, at least in an initial phase, in long term investments can be amortized.

Section 3.5.4 presents an analysis that goes in the direction of expanding the capacity available on the systems considering the potential of multi-core fibers. C+L+S-band with 268 channels of 75 GHz bandwidth is considered with MC fibers with 4, 7, 13 and 19 cores. The analysis is at network level in long or very long-distance networks (nationwide or continental wide), so the

bandwidth per channel ranges from 100 Gb/s to 600 Gb/s depending on the wavelength path distance and the evaluation gives results in terms of total throughput carried by the entire network, not in terms of line system capacity. It can be estimated that, given the fact that 3 bands and up to 19 cores are used, the capacity gain compared to systems made with C-band with single fiber could be in the order of 50x, less than 120x required by KPI2.2 but still an excellent value.

Section 4.2.2 addresses the MBoSDM node architecture issue by proposing several node architecture options that enable both MB and SDM. The architectures could be implemented with the technologies currently available at least for the case of C+L band plus a possible other additional band (S or E) and the parallelization (even with single fiber bundles) could ensure a significant capacity increase up to the order required by KPI 2.2. The economic aspect remains to be investigated, which could be particularly critical, but is difficult to address.

From the point of view of the prototype implementations that enable the MBoSDM technology that is essential for achieving, in perspective, the KPI 2.2 target on capacity increasing and to which SEASON project is contributing, we highlight the following components:

1. MBoSDM switching nodes presented in section 7.1 (component C3.1)
2. Multi-granular optical node prototype presented in section 7.2 (component C3.2)
3. MB(oSDM) sliceable bandwidth variable transceiver (S-BVT) the transceiver presented in section 7.4 (component C3.4).

KPI 2.2

50% CAPEX reduction by (1) designing an architecture that jointly leverages on parallel fibers (where fiber resources are abundant), multiple bands (where fiber resources are scares), and multi-core fibers (where fibers are not present, e.g., for cell densification); (2) limiting intermediate aggregation in routers thanks to the ultra-high capacity of MBoSDM and by exploiting smart coherent pluggable to remove aggregation layers and unnecessary O/E/O conversions.

Achieved, additional studies are in progress to finalize the validation. Several technologies developed to reduce the cost of future MBoSDM transmission systems are presented in this deliverable. However, more complete CAPEX and OPEX analysis of the proposed solutions will be presented in the techno-economic-specific deliverables (D2.2 and D2.3).

Section 3.2 presents novel, scalable network architectures based on a horseshoe-and-spur topology and digital subcarrier-based multiplexing (DCSM) P2MP transceivers. We propose filterless designs for transit nodes, reducing the number of O/E/O conversions. Section 3.4 presents a thorough cost and power consumption analysis assessing the performance and sustainability of the proposed transceiver prototype (described in detail in section 6.4) in a laboratory environment. This analysis is essential for future CAPEX and OPEX evaluations of the prototype. Section 3.5 describes the modeling and evaluates the throughput of different multi-core fibers.

In section 4.2, different node architectures are presented and evaluated for high-capacity, MBoSDM optical networks. The different node architectures, which provide advanced switching capabilities, trades-off flexibility/performance versus cost/complexity. The analysis presented in

this deliverable focus on the performance of the different solutions compared to a reference architecture, while cost/complexity evaluation will be performed in deliverables focused on techno-economic analysis (D2.2 and D2.3). Section 4.4 describes a novel architecture for interface nodes that reduces the number of O/E/O conversions using P2MP transceivers, especially when combined with the transit nodes filterless designs of Section 3.2.

KPI 3.1

Design and implement flexible and modular MBoSDM node prototypes able to switch/add/drop channels in at least 3 different bands (e.g., S, C, L) in an SDM/MCF fiber infrastructure featuring up to 10 fibers/cores, able to cope with switching capacities scalable up to between 2.4-3.6 Pb/s (considering a 4-degree node with 50% local add/drop and depending on the number of used bands and SDM cores/fibers) [SRIA, mid-term evo ~2028], by approaching (fractional) space-wavelength flexible architectures [Mar15].

Achieved. Additional studies are in progress to finalize the validation. In Section 4.2, different node architectures are presented and evaluated for high-capacity, MBoSDM optical networks. The different node architectures, which provide advanced switching capabilities, trades-off flexibility/performance versus cost/complexity. Key devices, such as spatial optical cross-connects (S-OXCs) or MB wavelength-selective switches (WSS), can be adopted to support the target switching capacity scaling efficiently. Although these architectures are not yet commercially available, they can be built with mature components such as band pass filters (BPF), fan-in/fan-out devices, OXCs, or WSS operating in a single or double band (C+L). Each degree of these switches can handle up to several hundred Tb/s, and a node with a degree greater than four can easily achieve an overall switching capacity in the Pb/s range.

To support the development of a scalable infrastructure that meets these high switching capacities, SEASON has developed and implemented two prototypes (C3.1 and C3.2), which enable both spatial (core) and spectral (wavelength/band) switching. These prototypes, outlined in sections 7.1 and 7.2, are designed to switch, add, and drop channels across at least three different bands (C+S+L) within an SDM infrastructure, aligning closely with the KPI requirements. Specifically, the node prototypes are able to switch/add/drop channels in at least 3 different bands (C+S+L) in an SDM infrastructure. The two prototypes, referred to as components C3.1 and C3.2, and detailed in Sections 7.1 and 7.2, have been preliminary evaluated. This includes measuring insertion losses for both prototypes, as well as assessing network performance for C3.1. In this case, initial capacity values have been measured. Section 4.1, demonstrates transmission of 3 slices of the MB(oSDM) S-BVT (prototype C3.4, section 7.4) at 41.3 Gb/s (C-band), 45.4 Gb/s (L-band) and 34 Gb/s (S-band). This MB flow is switched with the 3-degree prototype node C3.1 (section 7.1), which enables band (S+C+L) and core switching (with 19-cores multi-core fiber (MCF) available and 2 cores connected to the prototype). This scenario is critical for scalability analysis, as utilizing the full S+C+L band spectra over a 19-core MCF can greatly increase total capacity. With 350 channels at 25 GHz (S-band), 175 channels at 25 GHz (C-band), and 150 channels at 50 GHz (L-band), a transmission rate of 41 Tb/s is achievable. Including the spatial dimension with the 19-core MCF, this capacity could reach 0.5 Pb/s. Considering, a higher degree node, the target KPI switching capacities of 2.4-3.6 Pb/s could be envisioned.

The experimental assessment for node prototype C3.2 will be included in deliverable D3.3, along with alignment and analysis focused on meeting KPI 3.1. This additional evaluation will provide

further confirmation of the architecture's capability to meet the KPI, demonstrating that the SEASON project is on track to deliver a scalable, flexible, and high-capacity MBoSDM infrastructure capable of supporting next-generation optical networks.

KPI 3.2

MBoSDM transceivers able to increase the capacity of SoA transceivers [Nad22] up to 2× - 4× by exploiting enhanced wavelength/space dimensions while enabling appropriate slice/band/core/fiber selection according to the network path.

Achieved. Scalability analysis included in this deliverable. In Section 3.5, capacity upgrades scenarios with MB and SDM are presented and evaluated towards targeting this KPI. The required capacity scaling up to 2x – 4x could be envisioned by expanding transmission into S-, C, and L-bands and introducing SDM for additional spatial paths. In this regard, programable MB(oSDM) sliceable bandwidth/bit rate variable transceiver prototype (S-BVT), proposed in SEASON (component C3.4 described in section 7.4), supports flexible, sliceable bandwidth allocation across S-, C- and L-bands, providing scalability, improved network utilization and appropriate slice/band/core/fiber selection according to the network path. The prototype could be reconfigured by means of software defined networking (SDN) agents, which manage and adapt the transceiver programmable elements and reconfigurable devices based on the network requirements/demand. This transceiver design aligns with the project's KPI by allowing for adaptable use of spectral and spatial resources, thus achieving targeted capacity improvements. Specifically, preliminary experimental assessment has been performed (Section 4.1) showing that by utilizing the full S+C+L band spectra over 1 core of a 19-core multi-core fiber (MCF), aggregated capacity of 41 Tb/s could be envisioned if considering 350 channels in the S-band (SSB), 175 in the C-band (SSB), and 150 in the L-band (DSB). Compared to the SoA C-band S-BVT considering full population of the C-band (175 channels with SSB) about 8Tb/s could be envisioned. Hence, by the adoption of MB (S+C+L) an ideal maximum factor of 5x capacity increase could be envisioned, whereas this factor will also scale with the number of cores by including the MCF. However, transmitting across multiple cores and exploiting MB introduces additional challenges, such as stimulated Raman scattering (SRS) and crosstalk (XT), which will impact/limit the total achievable capacity and the corresponding scaling factor.

Additionally, SEASON also proposes the adoption of coherent pluggable transceivers that can be integrated into IPoWDM white-box network devices, eliminating the need for extra standalone components (Section 3.3). This reduces both space and power consumption, while enhancing the network's overall capacity. In particular, 400ZR and 400G OpenZR+ modules provide full tunability across C- and SuperC- bands (4 and 4.8 THz, respectively) with support for both 75 GHz and 100 GHz channel spacing. This flexibility maximizes spectral efficiency, enabling a single fiber pair to deliver up to 16-25 Tbps total capacity by multiplexing 40 to 64 individual 400 Gbps channels within the C and SuperC bands.

KPI 3.3

Optimized DSP for metro/core coherent applications, able to increase 4× data-rate, reaching up to 1.6Tb/s per port with power consumption suitable for future pluggable modules.

Partially achieved. Additional studied will be included in deliverable D3.3. The current work on optimized DSP for metro and core coherent applications is making strides toward supporting up to 1.6 Tb/s per port, aligning with the demands for future pluggable modules under the emerging 1600ZR standard. A key focus is the integration of novel low-power DSP architectures, specifically those employing frequency domain (FD) filtering for group velocity dispersion (GVD) compensation—a computationally intense task within DSP.

In Section 6.4, the FD filter architecture uses FFT and IFFT to facilitate GVD compensation by handling signal processing in the frequency domain. However, as symbol rates increase, the complexity and power demands of these DSP operations grow significantly, especially for symbol rates of 120 GBd and higher, due to the substantial increase in taps needed to manage accumulated GVD across longer fiber spans. Testing reveals that for high symbol rates, such as 240 GBd, complexity rises sharply beyond 100 km, underscoring the need for low-power designs capable of mitigating this power burden.

This effort, conducted as part of WP3 and still going on, demonstrates that achieving low-power DSPs while maintaining performance is critical to reducing computational demands through GVD compensation. Results will be part of the D3.3.

KPI 4.2

>50% contribution in energy saving via dynamic spatial channels aggregation and deactivation of unused transceivers at the OLT side basing on traffic conditions over total 70% energy saving targeted by [SRIA].

Partially achieved. The SEASON project has conducted a thorough evaluation of dynamic spatial aggregation as a method to achieve energy efficiency in Passive Optical Networks (PONs). The proposed architecture adopts spatial lane configurations based on traffic conditions, enabling the deactivation of unused transceivers at the OLT side to reduce energy consumption without impacting network performance.

Using simulation-based assessments, the analysis highlights the significant energy-saving potential of the proposed architectures. Results indicate peak energy saving up to 90% in low load conditions and average energy savings of 18–38% through dynamic aggregation of spatial lanes, depending on analyzed network scenario and PON configuration. The adaptive mechanism responds to traffic variations observed across different service patterns, including SOHO, Large Business, and Mobile. The scalability of the approach is evident, with energy savings increasing as the number of spatial lanes grows, saturating at around 8 lanes.

The evaluations emphasize that energy savings are influenced by the ratio of fixed power consumption (PF) to variable power consumption (PV). For PF/PV ratios near 1, maximum savings are achievable, while higher ratios reduce the relative gains. Even under less favorable conditions, the approach offers substantial contributions to operational energy efficiency.

Although the results are promising, further optimization opportunities remain. Future work will aim to refine the control mechanisms, ensuring seamless transitions between spatial lanes without service disruptions. Additionally, improvements in aggregation algorithms and integration with software-defined control systems will enhance adaptability to real-time traffic

dynamics. These efforts, coupled with advancements in hardware technologies, are expected to maximize the energy-saving potential of the proposed architectures.

KPI 4.3

400Gb/s RAN fronthaul ports capacity.

The KPI will be achieved. Studies indicate that achieving 6G capabilities within the next five years will require increasing the bandwidth to 400 Gbps in the Fronthaul segment. This substantial bandwidth expansion underscores the growing necessity to adopt coherent optical technology for efficient data transmission. As part of the SEASON project, we have chosen to explore and implement a WDM Mesh Network in the Fronthaul segment. By incorporating 400 Gbps transceivers, this architectural approach allows us to significantly enhance network capacity while introducing greater flexibility.

Coherent pluggable 400G transceivers, based on Open ZR+ specs, face challenges like low-power output and fixed amplifier gain, impacting OSNR and receiver sensitivity. Low-power versions require fixed attenuators, affecting power budgets. High-power versions (+3 dBm) reduce these issues, enabling longer distances and supporting up to 6 nodes with 15 wavelengths and 21 dB EDFA gain. At 200 Gb/s, up to 10 nodes are feasible.

KPI 4.4

High accuracy profile for IEEE 1588-2019 or better, evolving ±1.5 µs of LTE and Release-15 Standalone, aiming to ns with target IEEE P802.1CM A+ networks, demanding an accuracy better than 12.5 ns.

Partially achieved. Indoor 5G/6G networks, together with ongoing regional jamming and spoofing of GPS based GNSS networks, has increased the industry adoption of time & frequency synchronization distribution over the transport network. This is codified into the 'ITU-T Precision time protocol telecom profile for phase/time synchronization with full timing support from the network' [G.8275], based on Precision time Protocol, PTPv2 [IEEE 1588-2019]) for time synchronisation and SyncE [G.8261] to provide precise frequency reference. In the O-RAN disaggregation of the RU and DU, this has been adopted as the Sync- Plane (S-Plane) of the O-RAN open fronthaul [O-RAN.WG4.CUS.0].

For 5G precise network-based positioning (LCS) evolution towards 6G ISAC, combined with coherent/syntonized 6G cell-free, RIS, etc, the current time & frequency synchronization solutions are insufficient. Even the adoption of the new high accuracy profile [Rösel21], based on White Rabbit, will be required but may themselves be insufficient for the phase coherency needs for 6G cell-free.

For SEASON, the WP5 integrations and demonstrations will be based on 5G systems, integrating with the WP4 telemetry SDN controllers. It is required to maintain a precise synchronization accuracy between the RU's and DU's and a monitoring of the synchronisation over time to ensure a stable, consistent and reliable timing alignment between RU's and DU's in the fronthaul network.

Low relative time errors, in the nanoseconds range, in the S-plane between the different nodes and an improved frequency accuracy (low frequency variations) of the master clock will improve the overall performance of the fronthaul.

Depending on the fronthaul topology configuration that is used in the network (O-RAN defines 4 topologies: LLS-C1, LLS-C2, LLS-C3 and LLS-C4), timing requirements will be more strict per used component in the fronthaul in order to comply to the overall time error budget. For example, the allowed number of switches in the synchronization path of the fronthaul is limited by the frequency and time error contributions by all clocks in the chain.

KPI 5.1

Achieve sub-km (<500 m) and sub-dB (<0.5) resolution in the estimation of longitudinal fiber attenuation points and optical amplifier gain, respectively, using DSP-based monitoring scheme.

Partially achieved. Further validation will be included in D3.3. The SEASON project aims to enhance optical network monitoring by improving the resolution and accuracy of longitudinal power profile estimation using DSP-based techniques. Previous work in another project (B5G-OPEN) validated the use of the correlation method for anomaly detection and power profile monitoring, with applications in detecting amplifier characteristics and anomalies like gain tilt and narrowband compression.

The new focus in SEASON is to implement the Linear Least Squares (LLS) method, which promises higher accuracy in anomaly localization. This new method is currently in progress in [C3.5] and will replace the older correlation-based approach, which had lower resolution. The goal is to achieve sub-km (<500 m) and sub-dB (<0.5 dB) resolution in estimating fiber attenuation points and amplifier gain. The first version of the LLS approach is expected by the end of November 2024, with testing to follow in D3.3.

KPI 5.2

Performance improvement achievable with an optical spectrum analyzer (OSA) embedded in the amplifier setup and control identified for different link designs and applications.

Partially achieved. Dynamic gain equalization in erbium-doped fiber amplifiers (EDFA) using adaptive gain-flattening combined with spectral measurements in each optical amplifier embedded into a link has the potential to significantly improve link performance [Rap03]. However, additional cost introduced by the required components made this technique economically unattractive. Furthermore, an alternative technique based on a reconfiguration stage turned out to provide similar performance improvement at a lower cost.

However, cost has changed significantly since wavelength configurable devices have been must cheaper due to their large use in modern optical networks. Therefore, the concept of spectral reconfigurability has been revisited in view of the multi-band technology, in particular thulium-doped fiber amplifiers (TDFA) for the S-band. Some first results have been gained using a simplified model, but this will be redone with a more elaborate model based on coupled rate-equations is available.

KPI 5.3

OTDR Interrogator for latency / position measurement with 4 ns / < 1 meter accuracy respectively.

Partially achieved. The work on the KPI 5.3 started within the second half of the project, but without utilizing an OTDR. A summary of the ongoing work is reported in the subsections of Sec. 6.8. It is worth noticing that during the last year of SEASON, we might re-consider the option of employing an OTDR in the studies.

KPI 5.4

Applicability of modulation format insensitive optical signal-to-noise ratio (OSNR) measurement techniques in different scenarios determined, sources of inaccuracy identified, impact of signal distortions worked out.

Partially achieved. Spectral correlation has been shown to be a promising technique for monitoring signal quality in agile, disaggregated and open networks [Rap21]. In particular, it has been shown that the technique is able to capture the impact of all major propagation impairments in a standard single mode fiber. However, the measurement results also revealed that the measurement parameter reacts with different sensitivity to the different impairments. Therefore, it has been concluded that aligning the sensitivity of the measurement parameter should be further investigated for getting a universally usable GSNR value for characterizing link quality.

For this purpose, further investigations including additional postprocessing of the measurement results have been conducted in order to get a better alignment of the sensitivities. In fact, differences in the sensitivities to different effects could be reduced, but the achievements are not sufficient for qualifying as a universal tool for estimated link quality. Therefore, further investigation will be carried out.

KPI 7.3

Configuration of the MBoSDM node prototype agents for simple operations from the SDN control plane of O(100ms).

Not achieved yet. The activity is related to the integration of the MBoSDM node prototype with the SDN control plane and related agents has not yet started. Work on KPI fulfilment will continue, during the next months of the project. We have just started to identify node operation and programmable parameters and elements towards developing the corresponding SDN agent. The work will be part of D3.3 and D4.3.

3 MODELLING AND END-TO-END DESIGN OF OPTICAL NETWORKS

3.1 OPTICAL VERSUS ELECTRICAL AGGREGATION

Internet traffic is aggregated in Access and Metro-Aggregation networks and is delivered to metro-core and core networks. Traditionally, to convert individual small optical flows to a larger one, first the individual streams are converted to electrical and then aggregated electrically and re-converted to optical domain. This allows a single high-capacity transceiver to transmit a large amount of data over optical transport networks (OTNs).

However, with the advent of coherent P2MP transceivers, a single optical channel can be divided into several small digital subcarriers using Nyquist multiplexing technique. Therefore, each end leaf node with low-capacity demand can have its own dedicated end-to-end optical paths to the high-capacity transceiver located in hub nodes. The optical aggregator can be simple passive optical couplers or some kind of modified ROADMs. By removing electrical aggregation, we can reduce the cost, simplify the networks and reduce power consumption. This is a highly relevant result as the ICT sector accounts for 3% of global emissions and 5-9% of electricity use.

Figure 3.1-1 shows an illustration of optical aggregation using digital subcarrier-based multiplexing (DSCM)-based P2MP transceivers (b) and the traditional electrical aggregation with dedicated transceivers for each end-user.

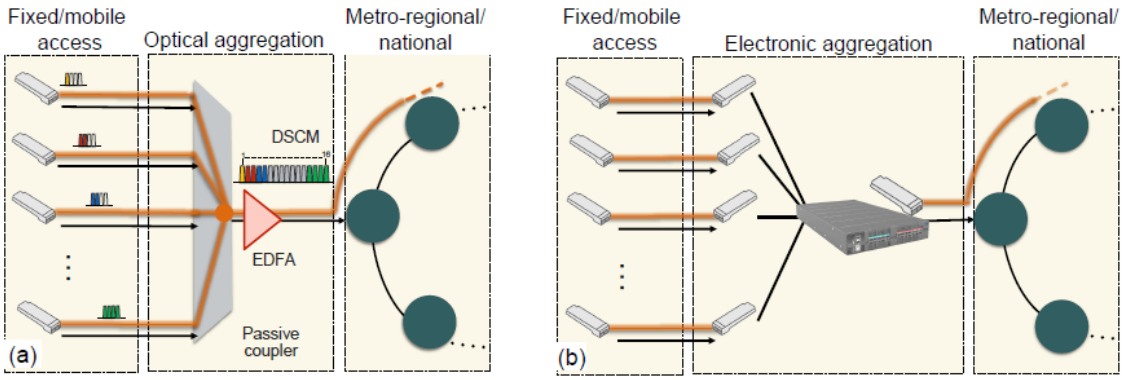

Figure 3.1-1 : (a) Optical and (b) Electronic aggregation approaches.

In a submission to OFC 2025, we explored the coherent P2MP approach to reduce energy consumption in telecommunications networks thanks to the DSCM and the enabled optical traffic aggregation. In this work, we considered the network illustrated in Figure 3.1-2, and we concluded that coherent P2MP offers similar transmission quality – with respect to traditional coherent P2P – but with a lower power consumption. In fact, for each removed router, we save ≥ 200 W, with potential OPEX saving of ≥ 1 million euros only for the Telecom Italia network in Italy presented within WP2.

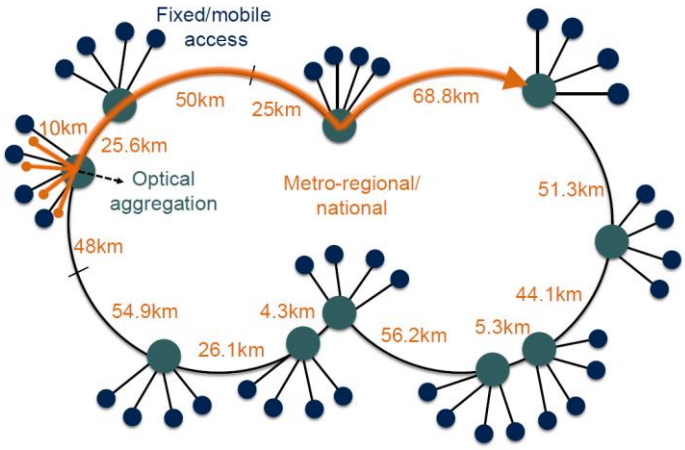

Figure 3.1-2: Considered network scenario.

3.2 NETWORK OPTIMIZATION WITH P2P AND P2MP TRANSCEIVER

We propose a novel, scalable network architecture based on horseshoe-and-spur topology and DCSM P2MP transceivers. This design enables gradual expansion through optical spurs without affecting the core horseshoe structure. By minimizing optical line reconfigurations using splitters/combiners with different ratios, we address the amplifier minimization while considering critical operational expense (OPEX) and service disruption concerns of network operators during network expansion.

Hub and leaf nodes function as endpoints and transit nodes add or drop optical signals to or from the main horseshoe. Leaf nodes uniquely serve both as direct connections to hubs and as intermediate points for neighboring leaf node traffic (see Figure 3.2-1). Our architecture is optimized for long-term traffic growth by offering two primary scaling methods:

- Geographic expansion: Adding leaf nodes and transceivers in different locations.
- Capacity increase: Deploying denser P2MP transceivers within existing leaf nodes.

While providing flexibility and scalability, the horseshoe-and-spur topology exhibits a trade-off in fault tolerance compared to simpler horseshoe designs. A spur link failure isolates only the affected spur, whereas a main horseshoe link failure still allows all leaf nodes to communicate through at least one hub.

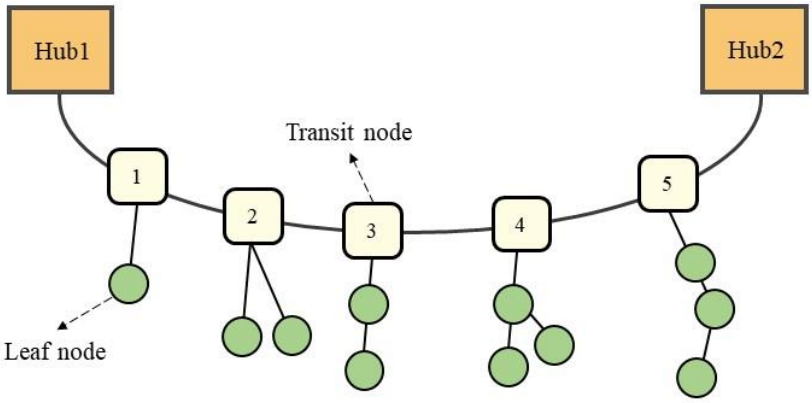

Figure 3.2-1: Illustration of a typical horseshoe-and-spur topology.

Filterless designs maximize simplicity but may require additional amplifiers. This study focuses on two basic filterless node architectures for transit nodes as shown in Figure 3.2-2: one using couplers and the other splitters/combiners. While couplers are simpler, splitters offer more optimization flexibility.

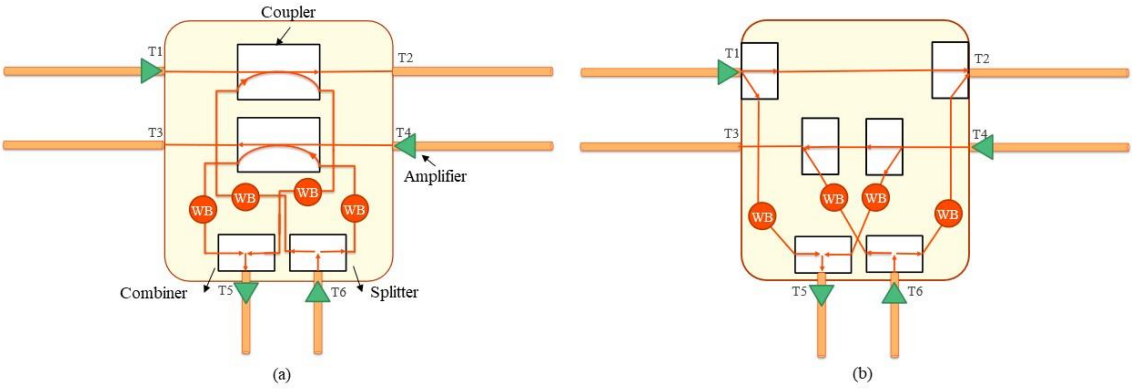

Figure 3.2-2: Horseshoe filterless node architecture using (a) Node Architecture 1: 1-by-2 splitters/combiners and 2-by-2 couplers and (b) Node Architecture 2: only 1-by-2 splitters/combiners.

We analyzed data from 495 links across 13 metro-aggregation networks (each consisting of one or multiple horseshoes, horseshoe-and-spur topologies) operated by Telecom Italia Mobile networks to create a statistical distribution to generate new links and networks. Numerous potential distributions such as log-normal, Weibull, and Gamma can be used to fit the available data. However, the quality of fitness must be assessed based on goodness-of-fit criteria such as Kolmogorov Smirnov and chi-squared tests. In Figure 3.2-3 the normalized histogram of empirical link lengths is compared with the probability density functions (PDFs) of the mentioned distributions obtained through Maximum Likelihood Estimation (MLE). The fundamental idea behind MLE is to find the values of the model parameters that maximize the likelihood function. Based on the results of Kolmogorov-Smirnov test, the log-normal distribution demonstrated a better fit compared to the other considered distributions, with a mean of 12 km and a standard deviation of 11.3 km. This distribution is referred to as the baseline distribution for the rest of this paper. Additionally, we introduce a second log-normal distribution, called extended distribution, with a mean of 24 km and a standard deviation of 15.8 km, representing a set of longer horseshoes.

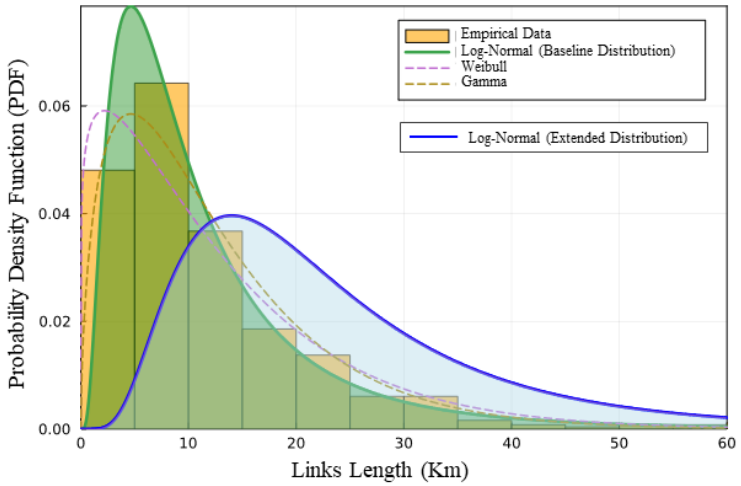

Figure 3.2-3: Probability Density Functions (PDFs) of fitting distributions to empirical link data utilizing Log-normal, Weibull, and Gamma distributions through Maximum Likelihood Estimation (MLE) and an extended horseshoe distribution.

An integer linear programming (ILP) optimization framework is developed to simulate and optimize different network instances. Since we have assumed dual-polarization 16-QAM, a minimum receiver input power of Ps=-24 dBm per SC for both low data rate and high data rate transceivers is set, which is aligned with OpenZR+ MSA. These parameters are scaled for 4 Gbaud SCs instead of the original 60.1 Gbaud single carrier signal. The launch power, variable within a range, is considered Pl =-12 dBm per SC for leaf and hub nodes transceivers, corresponding to an output power of 0 dBm for a 400 Gb/s signal using 16 SCs. To operate with negligible penalties from nonlinear interference due to transmission over optical fibers, the nonlinearity power threshold is set to Pn = -8 dBm per SC and is enforced at the ingress of every fiber span. The maximum allowable SCs power difference is Px = 8 dB. We also assume that all links are made of single-mode fibers with a loss of 0.22 dB/km. We assume a fixed power budget ranging from 0 to 13 dB per tree/spur.

We examine four distinct passive device configurations. The first employs balanced 50/50 splitters and combiners. The second utilizes exclusively 20/80 devices, while the third is limited to 30/70 and 10/90 ratios. Scenario four encompasses all ratios between 10% and 90% in 10% increments. Couplers follow the same scenarios but offer fewer configuration options due to their combined drop and add functionality. For example, an 80/20 coupler transmits 80% of express power to the other express port and drops 20%. Conversely, only 20% of added power enters the express path, with the remainder directed to the drop port. To account for inefficiencies, a consistent 0.5 dB excess loss is added to the coupling insertion loss.

All results are reported with both the average values and their corresponding 90% confidence intervals, obtained through Monte Carlo simulations of 10 different networks.

Figure 3.2-4 shows the average number of amplifiers for 10 horseshoes made of 5 transit nodes and links obtained from the first distribution. Overall, when setting a higher target power budget in the branches, more amplifiers are needed. This trend holds irrespective of the scenario and node architecture. For instance, consider the 2-by-2 coupler-based node architecture results shown in Figure 3.2-4 (a). Scenario 1 leads to the highest number of amplifiers ranging from

more than 5.5 to about 12 when the power budget increases from 0 dB to 13 dB. The reason is that there is no degree of freedom for coupler selection and all nodes are the same in terms of the architecture. Conversely, Scenario 4 delivers the lowest number of amplifiers compared to the other scenarios. The higher number of coupler types available for selection allows us to meet the problem constraints with a smaller number of amplifiers. Nevertheless, it is important to highlight that: (i) Scenario 3 leads to an average number of amplifiers that is only marginally higher than that of Scenario 4 while relying on only two types of couplers; (ii) at medium to high power budgets, Scenario 2 is also very competitive (almost the same number of amplifiers as Scenario 3) and uses only one type of couplers. Figure 3.2-4(b) illustrates the results for the 1-by-2 coupler-based node architecture. The number of amplifiers is slightly higher compared to the 2-by-2 coupler-based node architecture. This is mostly since the use of two discrete elements (one for drop and one for add) instead of a single one is impacted by additional division and excess losses.

Suburban deployments, for instance, tend to have longer networks. Considering a link length distribution roughly double that of our baseline scenario, the average total horseshoe length for a topology with 5 transit nodes and 6 links approximates 145 kilometres. Figure 3.2-4 (c) and (d) plot the number of amplifiers for different scenarios when considering the two node architectures and the longer horseshoes. Albeit the fiber losses are higher in the horseshoes generated with the extended distribution, the loss of passive devices is still dominant.

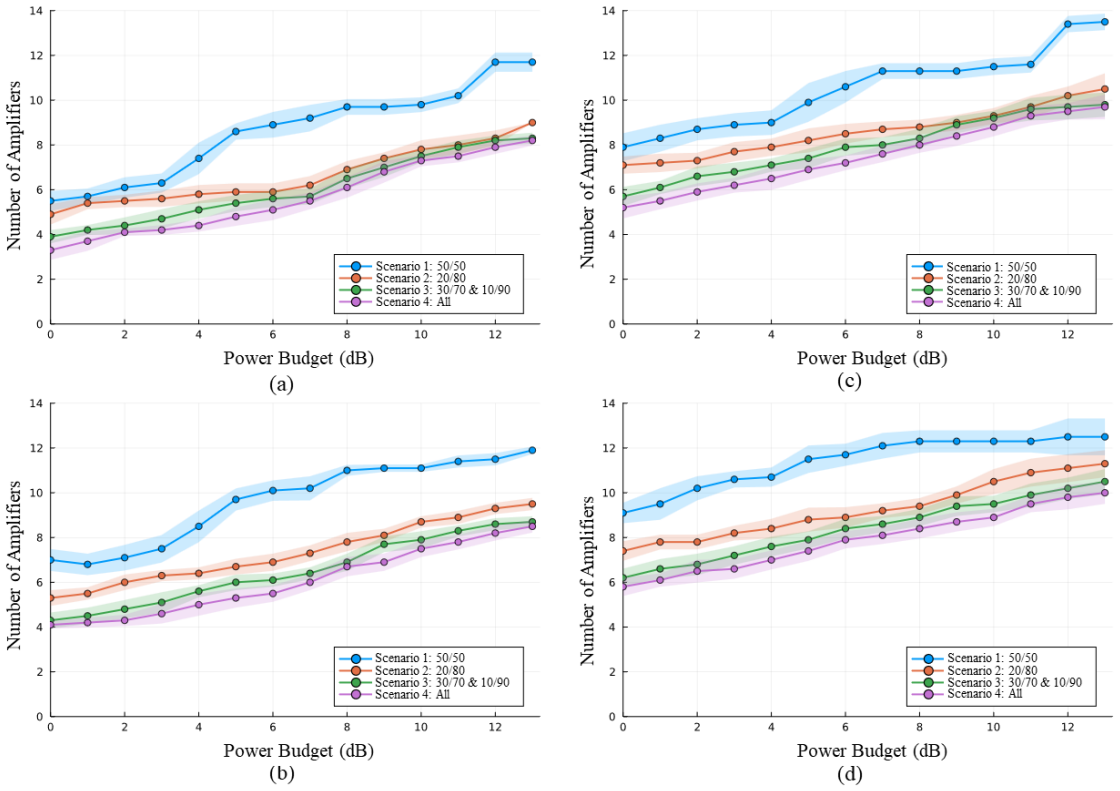

Figure 3.2-4: Optimized average total number of amplifiers (90% confidence intervals are highlighted for each curve) versus considered branches power budget for the defined scenarios based on (a) Node Architecture 1 and (b) Node Architecture 2 while considering the Baseline Distribution (shorter horseshoes), and (c) Node Architecture 1 and (d) Node Architecture 2 while considering the Extended Distribution (longer horseshoes).

The number of amplifiers is on average 10% to 45% higher than the shorter counterparts. At low power budgets, the increase in number of amplifiers is more significant compared to higher power budgets.

We also explored how to minimize disruption in case of multi-stage power budget upgrade while the network can be partially reconfigured/reoptimized. We investigate three upgrade scenarios when increasing the power budget from 6 dB to 12 dB:1) passive devices are fixed. Amplifiers can be re-optimized, 2) existing amplifiers remain in place but passive devices can be reconfigured, and 3) both existing amplifiers location and the network layout (node architecture) are fixed. New amplifiers can be added.

We simulate these scenarios by running the ILP twice, using the first run's output to fix the necessary parameters for the second. As shown in Figure 3.2-5, for the "70:30 & 90:10" coupler scenario, more amplifiers are needed compared to a scenario where the entire network can be reconfigured (one-shot planning shown by the dashed line). Specifically, when passive devices are fixed, the number of amplifiers increases to an average of 17.7, compared to 15.9 amplifiers when deployed amplifiers cannot be relocated. The composition of amplifiers is different. For instance, the "Fixed amplifiers" scenario requires more express amplifiers. The final scenario offers the least flexibility and requires over 50% more amplifiers than a design that allows full reconfiguration (but likely with higher OPEX and disruption). As a result, filterless horseshoe-and-spur architecture with P2MP transceivers can provide more flexibility if spending more upfront and considering a high-power budget. However, it is important to consider other factors like network dynamics, and availability constraints.

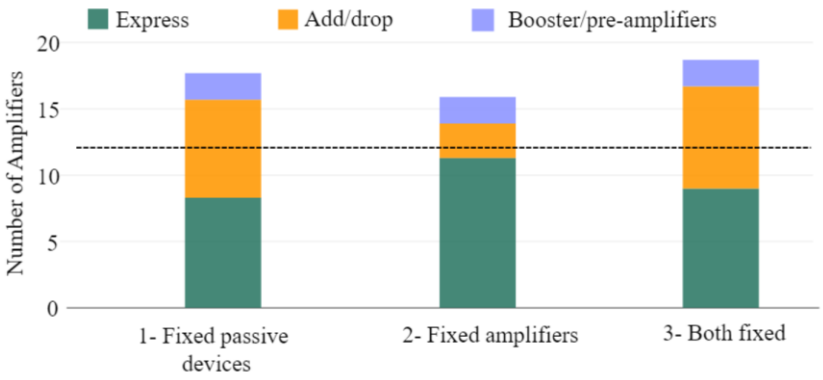

Figure 3.2-5: Optimized average number of amplifiers when upgrading power budget from 6 dB to 12 dB.

3.3 ROADM-FREE IPOWDM NETWORKS

SEASON focuses on the evolution of metro-aggregation networks based on cost-effective IPoWDM nodes, i.e., packet-optical switches/routers equipped with coherent pluggable transceivers.

Traditionally, IPoWDM nodes have been interconnected using Reconfigurable Optical Add/Drop Multiplexers (ROADMs). A ROADM is mainly built with several elements, mainly ROADMs on Blade (RoB) and Multi-Cast Switches (MCS). Each node degree needs of a RoB, which integrates

a pair of Wavelength Selective Switches (WSS) and optical amplifiers, for handling both TX and RX side. For example, Figure 3.3-1 (a) shows an IPoWDM switch equipped with coherent transceivers that relies on a two-degree ROADM to interconnect to remote IPoWDM nodes. The ROADM is composed of two RoB (one for east and one for west sides). A third RoB is also included to serve as add/drop module. The add/drop module is typically implemented using lower cost technologies, like multicast switches (MCS). This overall multi-layer node architecture enables effective optical bypass in intermediate nodes. Indeed, electronic processing in such ROADM-based optical networks only occurs at the source and destination IPoWDM nodes.

In SEASON we performed a first investigation of a novel *ROADM-free* network infrastructure. The motivation behind this study is related to the extraordinary technological improvements that coherent transceivers and packet switch ASIC have experienced in the last few years, driven by the hyperscalers (e.g., Google, Microsoft, etc) due to the significant growth of traffic among their data centers. In fact, transceiver line rate is nearly doubling every two years, at a pace much higher than Telco traffic growth. Coherent transceivers operating at 800Gb/s are nowadays commercially available and the first prototypes at 1.6Tb/s have been already announced by multiple companies.

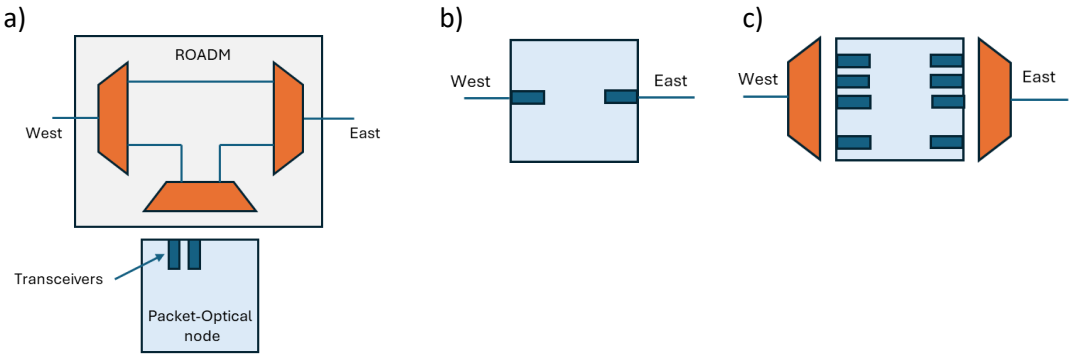

Figure 3.3-1: (a) Traditional multi-layer node in a ROADM-based packet-optical network. (b) node architecture in a ROADM-free metro-aggregation network where packet-optical nodes are directly connected without using ROADMs and using a single transceiver. (c) as in (b) but using multiple transceivers aggregated using RoB. For simplicity only two degrees are here represented

A ROADM-free network does not exploit optical bypass, always terminating the optical connection at the adjacent IPoWDM node. Such network infrastructure can be implemented in three different ways, depending on the amount of data to be exchanged and the distance between the nodes.

In the first implementation, the node architecture of Figure 3.3-1 (b) is adopted where only one coherent transceiver per direction (two in the figure, there can be more) is used for the interconnection to the adjacent IPoWDM node. That is, the transceiver is directly attached to the optical fiber. No optical amplification is adopted. This implementation is suitable for short distances among nodes (e.g., few tens of km, given the limited sensitivity of the transceivers, in the order of -10dBm) and relatively limited capacity (the one provided by a single transceiver). In case additional capacity is needed some management problems need to be addressed since the line needs to go offline to enable the insertion of coupler/splitters or RoB to serve additional transceivers.

In the second implementation, suitable for larger distances (up to few hundreds of km), optical amplification is introduced. Two cases can be considered: (i) traditional EDFA or (ii) innovative pluggable amplifiers. This implementation, still considering a single transceiver per direction (i.e., relatively limited capacity), may also require the same complex upgrade procedures.

In the third implementation, suitable for larger capacity, multiple transceivers per direction are considered. To aggregate multiple signals in a single fiber, different options are available:

- Fixed AWG. Pros: low cost; low insertion loss; no upgrade issues, scales well to accommodate a large number of transceivers. Cons: rigidity in spectrum allocation due to fixed filtering; it may not be future proof with the increase of baud rate.
- Splitters/Coupler. Pros: Low cost; no filtering constraints. Cons: possible slight transmission issues due to non-filtered signals; insertion loss increases with the splitting ratio, making it suitable to practically accommodate only very few transceivers. Upgrade issues.
- RoB. Pros: relatively low insertion loss; no upgrade issues, no rigidity in spectrum allocation; suitable to accommodate large number of transceivers; future proof with the increase of baud rate. Cons: higher cost.

The latter RoB-based option, given the better scalability performance even if more expensive, is the one considered in the following, and shown in the node architecture of Figure 3.3-1(c). Optical amplification needs to be encompassed to compensate at least for insertion loss. Both traditional and pluggable EDFAs can be considered.

A preliminary comparison of the ROADM-based versus ROADM-free solution is provided considering a 7-node ring network and the node architectures shown in Figure 3.3-1.

The relative CAPEX cost of the utilized components is reported in [Arp24b]. In particular, a 100G coherent transceiver is assumed with a cost of 1 unit. The 800G transceiver has a cost of 3 units. Each RoB has a cost of 1,6 units. For simplicity, the add/drop module is considered of the same cost of the RoB used for express traffic (but it can be easily updated considering lower cost multicast switches). The cost of the seven IPoWDM nodes is not considered since the same for both network solutions.

Two traffic scenarios are considered.

In the first scenario, any to any communication is assumed, considering traffic demands at 100G**.** Routing is performed along the shortest side of the ring and no protection is considered.

In the case of ROADM-free networks, each direction needs to accommodate six traffic demands at 100Gb/s, i.e., 600Gb/s of aggregated traffic considering both locally originated/terminated traffic and transit traffic. Thus, a single 800G transponder per direction is sufficient, i.e., two per IPoWDM node (one west and one east as in Figure 3.3-1(b)) and 14 in total. This leads to a network cost of 42 units.

In the case of ROADM-based networks, using 800G Transceiver is not effective since all connections are transparently forwarded at 100G towards the destination IPoWDM node. Thus, each IPoWDM node has 6 transceivers at 100G. In addition, a ROADM with 3 RoD needs to be considered, as in Figure 3.3-1(a). The overall network cost is 75.6, significantly *higher* than the ROADM-free infrastructure.

In the second scenario, each traffic demand is at 800G.

In the case of ROADM-free networks, each direction needs to accommodate six traffic demands at 800Gb/s, requiring six 800G transceivers per direction, i.e., 12 per IPoWDM node. Furthermore, one RoD per direction is required to aggregate the six transmitted signals, as shown in Figure 3.3-1(c). This leads to 14 RoDs in the network. The overall network cost is 274.4 units.

In the case of traditional ROADM-based networks, all connections are transparently forwarded at 800G, exploiting optical bypass in intermediate nodes. Thus, each IPoWDM needs only six transceivers at 800G besides the 3-RoD ROADM. The network cost is 159.6, which in this scenario is significantly *lower* than ROADM-free infrastructures. These results are summarized in Figure 3.3-2.

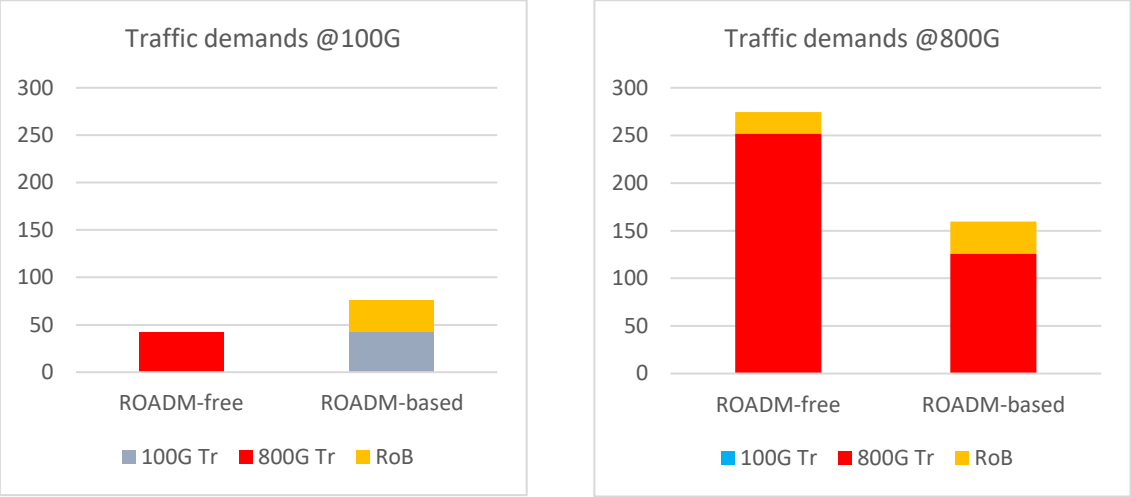

Figure 3.3-2: Cost comparison of ROADM-based and ROADM-free physical architecture on an exemplary 7-node optical network, considering either 100Gb/s (left) or 800Gb/s (right) traffic demands.

Although the considered network and traffic scenarios are only exemplary, these first results show that the choice between traditional ROADM-based solutions or innovative ROADM-free solutions, from a CAPEX perspective, depends on the considered scenario. The ROADM-free solution generally appears effective when the amount of *transit* traffic is limited and when traffic demands are significantly smaller than transceiver rates. Given the continuous and remarkable increase of transmission rates, ROADM-free solutions might become particularly relevant in multiple METRO scenarios.

Beside CAPEX considerations, ROADM-free solutions bring further benefits including:

- Drastic simplification of control procedures since each optical link is terminated at each IPoWDM node. That is, no need to execute complex routing and spectrum assignment algorithms, complex impairment validation assessment, complex equalization procedures handling transparent interconnections across multiple ROADMs.
- Significant improvement of failure management, simplifying failure localization and recovery performance while typically reducing the recovery time since no multi-layer procedures are involved.

- Overall management procedures simplified by the management of a single-layer IP/MPLS network, which has the potential to be handled by a single team of experts without requiring highly skilled optical experts.

Potential drawbacks include:

- Additional power consumption due to processing of transit traffic, only partially compensated by the reduced number of RoDs to be powered on.
- Additional latency due to electronic conversion and processing in transit nodes. However, IPoWDM nodes equipped with 800G transceiver introduce an overall latency lower than 1us, with negligible jitter.

Given the above preliminary analysis, additional and more accurate techno-economic assessment will be performed in WP2 considering SEASON reference networks. Moreover, specific simplified control plane solutions will be designed and validated by WP4, aiming at avoiding current control solutions based on complex Optical SDN Controller when ROADM-free networks are employed.

3.4 MB(oSDM) S-BVT COST AND POWER CONSUMPTION EVALUATION

A thorough cost and power consumption analysis was conducted to assess the performance and sustainability of the proposed transceiver prototype in a laboratory environment. The multi band over spatial division multiplexing (MBoSDM) sliceable bandwidth/bitrate variable transceiver (S-BVT) prototype (component C3.4) is described in detail in section 7.4. This analysis provides valuable insights into its cost, energy usage and efficiency, excluding the power consumption of all electrical components that comprise the optical devices/modules and related digital signal processing (DSP).

On the one hand, a comparison of the cost associated with 2x50 Gb/s S-BVTs based on direct detection (DD) and 4x 25 Gb/s channels with coherent detection is presented in [Nad20]. This comparison indicates that adopting a DD implementation offers intrinsic cost savings. However, the proposed MB(oSDM) S-BVT, illustrated in Figure 7.4-1, introduces additional cost factors due to the use of MB technology. Therefore, a cost analysis of the proposed transceiver solution that utilizes external modulation and basic DD photodetection is presented in [Nad23]. For this cost analysis, we consider that the optical aggregator/distributor component of the MB(oSDM) S-BVT includes wavelength selective switches (WSSes) operating within a specific frequency band, as well as bandpass filters (BPFs) necessary for implementing MB technology. Table 3.4-1, shows the number of components required for a DD-based S-BVT with 3 slices enabled at different bands (S+C+L) at a rate/slice of 50 Gb/s. Ideally, a WSS operating in C+S+L-band should be included avoiding the use of BPFs and enhancing overall transceiver flexibility. However, such device is still not commercially available.

Table 3.4-1: Number of elements for a MB(oSDM) S-BVT with DD.

Component	MB(oSDM) S-BVT DD
MZM	3
Driver	3
DAC	3 ports
ADC	3 ports
(Laser source) LSS	1
LSC	1
LSL	1
WSSTxS	1 port
WSSTxC	1 port
WSSTxL	1 port
WSSRxS	1 port
WSSRxC	1 port
WSSRxL	1 port
BPFTx	3 outputs
BPFRx	3 outputs
Photodetector (PD)	3

Thus, the unitary cost of a building block in the C-band of the proposed MB(oSDM) S-BVT based on DD is calculated by applying Eq. 1 and Eq. 2:

$$C_{BVT_{xC}} = C_{LS_C} + C_{MZM} + C_{driver} + \frac{C_{DAC}}{M} + \frac{C_{WSS_{TxC}}}{N} + \frac{C_{BPF}}{B} \quad \text{Eq. 1}$$

$$C_{BVR_{xC}} = C_{PD} + \frac{C_{ADC}}{M} + \frac{C_{WSS_{RxC}}}{N} + \frac{C_{BPF}}{B} \quad \text{Eq. 2}$$

M and N represent the number of DAC/ADC and WSS ports, respectively, while B denotes the number of BPF outputs, corresponding to the number of bands. It is assumed that the WSS units operating in a specific band at both the transmitter and receiver are identical. The unit cost for building blocks in the L-band and S-band relies on the same individual components, which include the LS, MZM, driver, DAC, WSS, PD, ADC, and BPF.

However, the costs of specific components, such as the LS and WSS used in the S- and L-bands, are higher than those in the C-band due to differences in availability and technology maturity for the specified bands. For instance, the cost of the S-band LS used in the SEASON transceiver prototype is nearly five times greater than that of the C-band LS from the same manufacturer. Similarly, when comparing WSS modules from the same provider, the cost of the WSS in the L-band can be 1.3 times higher than that of the C-band. To account for these variations, we introduce scaling factors α, β, γ and ϵ (all greater than 1) to define the cost relationships of the LS and WSS in the S- and L-bands compared to their C-band. Considering all these factors, the total cost for the 150 Gb/s MB(oSDM) S-BVT (3 x 50 Gb/s) can be defined as follows in Eq. 3:

$$C_{S-BVT} = (1 + \alpha + \beta) \times C_{LS_C} + 3 \times C_{MZM} + 3 \times C_{driver} + 3 \times \frac{C_{DAC}}{M} + \\ +3 \times C_{PD} + 3 \times \frac{C_{ADC}}{M} + 2 \times (1 + \gamma + \epsilon) \times \frac{C_{WSS_C}}{N} + 6 \times \frac{C_{BPF}}{B} \quad \text{Eq. 3}$$

According to equations and reference [Nad20], the cost of the MB(oSDM) S-BVT, when only enabling the C-band, will slightly increase compared to a S-BVT that can not enable MB

technology. Specifically, this increase is mapped with the cost term of using BPFs ($2 \times \frac{C_{BPF}}{B}$), which are static filters using very cheap technology of the order of few hundred euros. Also, specific devices such as the LS and WSS will have increased costs when operating beyond the C-band. The extra cost of deploying the MB(oSDM) S-BVT is justified by the substantial improvements it brings to the optical network's capabilities. In particular, the increased available spectral resources and the dynamic capacity scalability by enabling multiple slices in different bands beyond C-band. It is also worth to point out that due to the higher-cost of technology beyond C-band it will exist a trade-off between performance/capacity and cost. This trade-off introduces a strategic decision point that network planners and operators will carefully evaluate from a general network perspective before taking specific actions.

On the other hand, the estimated power consumption of the main components of the MB(oSDM) sliceable bandwidth/bit rate variable transmitter (S-BVTx) and receiver (S-BVRx), as considered in the experimental setup shown in Figure 4.1-1, have been derived and measured in the lab, with results presented in Table 3.4-2 andTable 3.4-3. In most cases, power consumption values were derived from intensity measurements. A total transceiver power consumption of 30.73W was estimated for the transmission and reception of 120 Gb/s S+C+L data flow in B2B, assuming uniform loading and a capacity of 40 Gb/s per band.

Table 3.4-2: Estimated power consumption assessment for the MB(oSDM) S-BVTx.

Band	Element	Power consumption [mW]
S-band	Laser	1638.05
	MZM	145.8
	Driver	2239.2
	DAC	750
C-band	Laser	714.01
	MZM	336.2
	Driver	2745
	DAC	750
L-band	Laser	1377.8
	MZM	627.2
	Driver	2754
	DAC	750
Aggregator	TF	2500
	WSS	5200

For the MB(oSDM) S-BVTx, estimated power consumption values are 4.77W for the S-band, 4.54W for the C-band, and 5.51W for the L-band, considering key transmitter elements such as lasers, MZMs, drivers, and DAC. The optical aggregator, including a WSS/TF for SSB modulation within the C- and S-band, respectively, consumes a total of 7.7W. The C-band transmitter is the most power-efficient, as illustrated in Figure 3.4-1 (a) and (b). Notably, the same laser module with a fixed output power of 6 dBm consumes less power in the C-band compared to the S-band and L-band, with power consumption increasing by a factor of 1.9 and 2.3, respectively.

Table 3.4-3: Estimated Power consumption analysis for the MB(oSDM) S-BVRx.

Band	Element	Power consumption [mW]
S-band	TDFA	1300
	PIN	108.57
	OSC	302.5
C-band	EDFA	43.84
	WSS	5200
	PIN	108.57
	OSC	302.5
L-band	EDFA	429
	PIN	108.57
	OSC	302.5

An offline DSP implementation is used in this work. For reference, in [Kim20], a DSP power of 68 mW is reported for a 32-point FFT with frequency-domain equalization, and in [Vat20], a 512-point FFT with increased complexity and more clock cycles per FFT calculation results in 472 mW (2.37 pJ/b). Since our offline DSP also includes a 512-point FFT for OFDM modulation, this can serve as a suitable approximation for its implementation in an application-specific integrated circuit (ASIC).

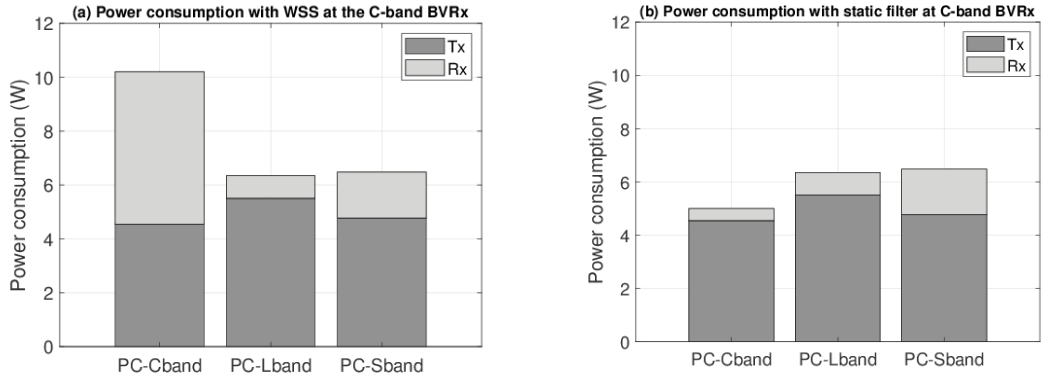

Figure 3.4-1: Power consumption of each S-BVT building block/BVT considering (a) a WSS or (b) a static filter at the C-band BVRx.

The estimated MB(oSDM) S-BVRx power consumption is 8.2W, corresponding to 1.71W for the S-band, 5.65W for the C-band, and 0.84W for the L-band receivers (see Figure 3.4-1 (a)). Using a C-band WSS at the receiver side instead of static filters significantly increases overall power consumption, but the programmable filter enhances receiver flexibility to adapt to the desired laser optical carrier. Replacing the WSS with a static non-programmable filter reduces C-band receiver power consumption to 0.45W, making the C-band receiver the most power-efficient option (see Figure 3.4-1 (b)). Additionally, L-band EDFA and S-band TDFA solutions consume 9.8 and 29.6 times more power than C-band EDFA, respectively.

This analysis, as previously mentioned, does not include the electrical components of the optical modules, focusing only on the power consumption of the device when the optical output is enabled. Higher power consumption values are expected when considering the essential electronic components required for module/device control. The overall L-band amplifier module

consumes 15W, while only 0.429W is needed to enable the optical output for signal amplification. The S-band amplifier module consumes less than 20W, with only 1.3W required to activate the optical output. The bench-top C-band amplifier in the experimental setup consumes a maximum of 50W, as it is a multi-stage EDFA with three pump lasers. Despite this, C-band amplification shows the lowest power consumption when only the optical output is considered due to the relaxed requirements of the C-band signal compared to other analyzed bands. Different EDFA solutions in the C-band from various providers can have significant variations in overall equipment power consumption, with one example consuming 10W in our lab. Therefore, focusing on the power consumption related to enabling the optical signal offers a more suitable comparison.

Photonic integration of key MB(oSDM) subsystems into a single chip or platform will minimize the need for discrete components and connections, reducing power consumption, signal losses, and physical footprint while potentially enhancing overall transceiver efficiency and reliability. Various standardized form factors could be envisioned, such as SFP28, QSFP28, QSFP-DD, OSFP, and CFP2 [Iso19]. For instance, the 400G ZR+ pluggables based on the QSFP-DD-DCO form factor, integrated within ADRENALINE, have a power consumption of less than 22.5W with uniform heat load distribution. This module not only implements the optoelectronic front-ends for converting electrical signals to the optical domain but also includes the relevant DSP associated with the modulation format used (up to 16QAM).

The performed transceiver power efficiency analysis/modelling paves the way for integration with a software-defined networking (SDN) control plane supported by energy-aware artificial intelligence (AI) and machine learning (ML) models, that will be performed in the framework of WP4. Initial integration work (WP3-WP4) has been performed and it will be reported in deliverable D5.1.

3.5 CAPACITY UPGRADE SCENARIOS WITH MB AND SDM TECHNOLOGIES

3.5.1 Comparison of available technologies

With the continuing demand for higher overall capacity and increasing connectivity requirements, the optical communication industry is looking for a successor of wavelength-division multiplexing (WDM), a technique that enabled in combination with coherent detection a dramatic capacity growth during the last decade but is now approaching the fundamental Shannon's limit. In this context, spatial division multiplexing (SDM) technology is a promising candidate to further substantially increase optical network capacity and density in the long-term. Using fiber bundles is the most straight forward implementation of SDM and a significant increase of capacity per cable duct has been achieved using fibers with reduced coating and diameters. This approach is of particular interest for submarine applications since cable redesign and cable manufacturing cost are minimized while increasing capacity by up to a factor of 1.5.

With an embodiment comprising multiple cores within a single fiber, SDM recently found further commercial application in data communication over submarine links. Using weakly-coupled multi-core fibers (WC-MCF) with two cores, waveguide density could be successfully doubled under strict constraints in view of cable diameter and optical repeater power. In turn, this allows increasing transmission capacity over a single cable by a factor of two without changing cable

construction. This aspect and the limited access to amplifiers sites along the transmission link make submarine communication the ideal application for the first commercial deployment of transmission over multi-core fibers (MCFs).

In contrast to this scenario, extending conventional C-band WDM systems by using additional wavelength bands offers a significant cost benefit over SDM in terrestrial links and networks, since this allows to further use the already deployed fiber infrastructure. This technology called multi-band (MB) transmission comes with significant cost benefits, since the major part of the cost for installation of new fiber links stems from labor cost associated with fiber deployment. Research directed to bandwidth expansion is ongoing with new record experiments being reported, and development of novel MB components including new types of amplifiers is being carried out. However, the need for installing additional MB in-line components, the inherent performance penalty due to wideband nonlinear effects such as stimulated Raman scattering (SRS), and the required system and network management and routing modification make the potential capacity gains of MB technology over brown-field links lower than theoretically possible. Furthermore, upgrading the capacity of already installed links by more than a factor of four will be difficult.

With the full utilization of deployed fiber cables allowing for error-free data transmission expected to happen during the next four to five years, SDM is an attractive and powerful technique whenever new fibers need to be installed (green-field installation), provided that this technology will deliver sublinear scaling of cost and power consumption per bit compared to using multiple independent single mode fibers (SMFs). Coming in a variety of implementations based on the underlying fiber technology, the most prominent embodiments of SDM are based on WC-MCFs, coupled-core multi-core fibers (CC-MCFs), and multi-mode fibers (MMFs). The first option enables coexistence with current SMF-compatible subsystems and routing schemes, but at the cost of additional fan-in fan-out (FIFO) devices and limited scalability in the spatial mode density. On the other hand, the latter two options require the development of multiple input multiple output (MIMO) digital signal processing (DSP), require high uniformity in the propagation loss and delay among modes, and may limit or require the re-design of channel routing with a given data rate granularity due to the strong coupling between groups of spatial modes during transmission.

The listed trade-offs make the optimum choice of the technology for future high-capacity applications still unclear and subject to extensive research effort. Recent developments in SDM fibers and subsystems with a focus on MCFs have been analyzed. The aim of the investigations has been to identify opportunities and to provide requirements and directions towards the commercial integration of SDM technology in optical networks considering also the commercial readiness of the ecosystems in different network segments.

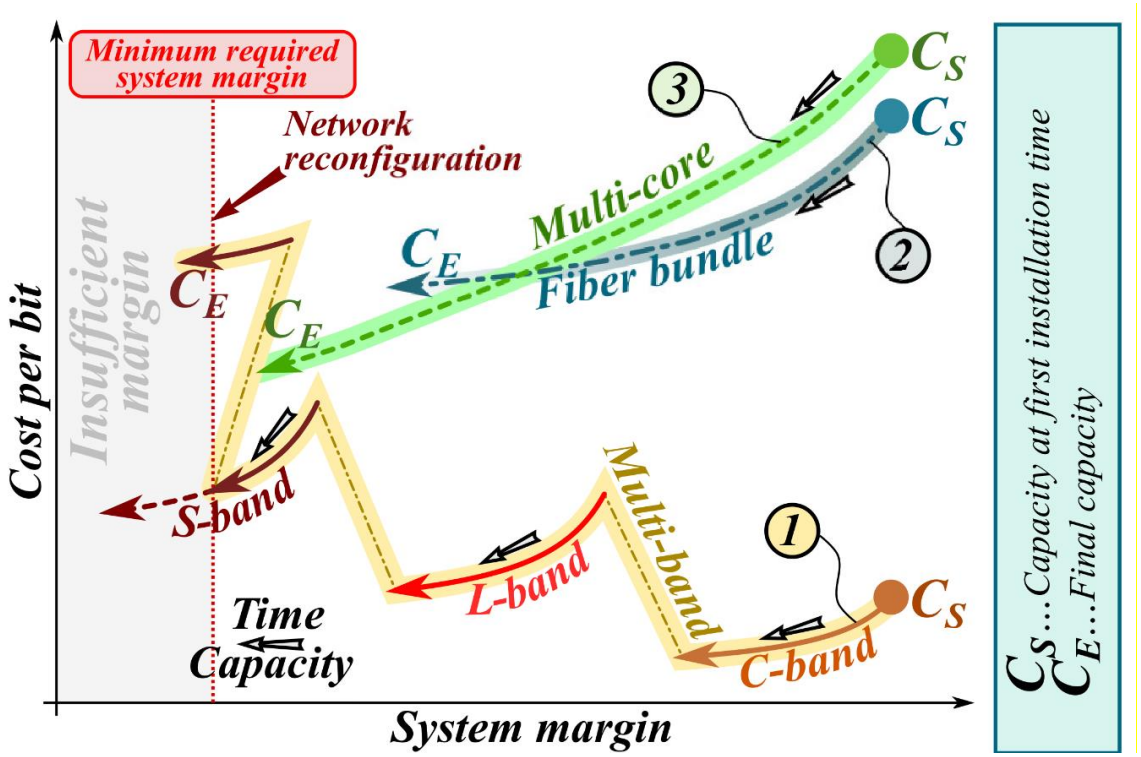

Figure 3.5-1: Parametric representation of an exemplary capacity upgrade scenario in a terrestrial network.

Multi-band transmission offers capacity upgrades over the already installed and depreciated fiber infrastructure at low cost if access to the amplification sites is ensured. This is the case in most terrestrial networks, and alternative techniques, such as SDM, are currently hardly able to compete. However, these advantages do not come into effect in submarine link since embedding new amplifiers across the link is almost impossible in this scenario. Here, reduced need for space per bit is more important. Not surprisingly, MCFs found their first application in this field. In the following considerations, it will be shown that MB transmission is nevertheless not forever the optimum solution in terrestrial networks based on an exemplary upgrade scenario sketched in Figure 3.5-1.

System margin is an important parameter for characterizing transmission performance, whereas cost per bit is a suitable parameter for assessing the economic potential of a transmission technology. Changes of these parameters are indicated by means of a parametric presentation, wherein time and capacity increase when following the curves in direction of the dark arrows. The task is to increase the capacity of an installed link with already depreciated fiber cables from capacity C_{start} at the time of first installation to the final capacity C_{end}. As indicated by curve (1), starting with filling up the C-band is the cheapest solution, but will also reduce system margin due to increased impact of nonlinear fiber effects. Opening the L-band leads to a sharp decrease of the system margin due to the installation of the band splitter followed by a further decrease with an increasing channel count. Furthermore, cost-per-bit increases since the amplifiers required for this wavelength band will come at higher cost as compared with the C-band. The same behavior is observed when introducing the S-band which leads to some further decrease of system margin and a further increase of cost per bit.

The decrease of system margin caused by populating the S-band with more and more channels may lead to a negative system margin such that error free data transmission is no longer feasible.

Possible measures of remedy are network reconfiguration and the installation of additional 3R regenerators performing reamplification, reshaping, and retiming. These measures help to increase margin again but cause a significant increase of cost per bit. On this point, using fiber bundles (see curve (2)) or MCFs (see curve (3)) may provide a more cost efficient solution, although both solutions suffer from increased cost-per-bit at smaller capacity due to cable installation cost. Whether MCFs will provide cost benefits compared with fiber bundles depends on the successful realization of above-described techniques operating simultaneously on several cores.

Link margin available in the considered exemplary link puts multiband transmission in a superior position as compared with SDM for channel upgrades up to around half of the S-band. In a link with larger margin, even deploying the E-band may still be useful. In contrast, only a C+L-band system may be beneficially used in a link with even smaller margin. To be economically successful, every system manufacturer needs to figure out whether the expected total sales volumes associated with the support of the different bands in its portfolio justifies the associated development cost based on the traffic patterns and margin distribution in the networks of its current or anticipated customers. The results may strongly differ from manufacturer to manufacturer.

A key question in view of the further development is if the relatively small volumes in the sub-marine market will be sufficient to efficiently bring down cost for MCFs and multi-core (MC) components such that entering the terrestrial market is achievable. A further cost factor is the labor cost for deploying such fibers which also depend on time required for joining two fibers. In fact, splicing cost is currently quite high since splicing two MCFs just takes as long as doing splices for an equivalent number of single-core fibers. Reducing the required time for connecting two fibers is therefore a prerequisite for improving cost position.

3.5.2 Modelling and Design of the Multi-Band over Space Division Multiplexing (MBoSDM) Optical Networks

MBoSDM elastic optical networks (MBoSDM-EONs) represent an ultra-wideband approach for next-generation optical backbone networks, especially as it is foreseen in core data centers which are expected to generate and exchange data at petabit-per-second.

However, the proximity of cores within the cladding of an MCF poses challenges, particularly inter-core crosstalk (ICXT). ICXT occurs when optical signals from one core couple into adjacent cores, causing interference and signal degradation. In addition, as MBoSDM systems seek to utilize a wider range of frequency bands, understanding and mitigating ICXT effects becomes crucial, especially in higher frequency bands such as the U-band, where ICXT tends to be more pronounced. Digital signal processing (DSP) techniques will also play a vital role in mitigating ICXT effects in MBoSDM systems. Advanced equalization techniques, such as multiple ICXT cancellation, can effectively compensate for ICXT and improve signal quality.

This section examines various strategies for implementing MBoSDM-EON technology and assesses the total network capacity expected from MBoSDM systems featuring four manufactured trench-assisted weakly coupled (TAWC) MCFs with four, seven, thirteen, and nineteen cores, designated as MC04, MC07, MC13, and MC19, respectively, based on a precise

quality of transmission estimator tailored for MBoSDM EONs. Figure 3.5-2 shows examples of MC07 and MC04 with different structures.

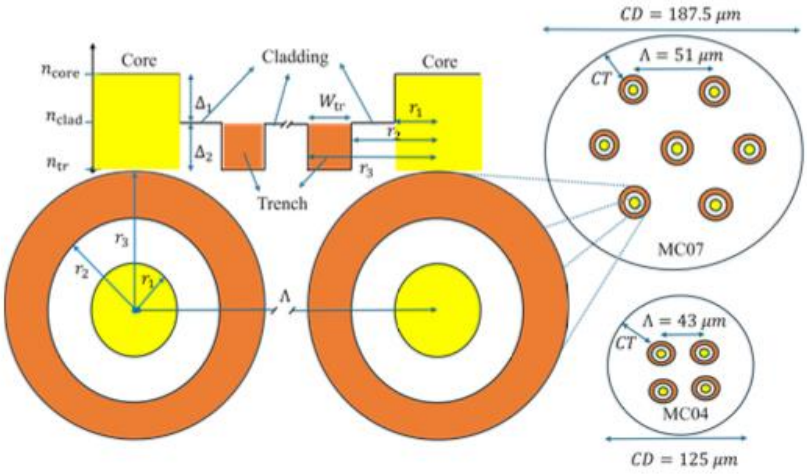

Figure 3.5-2: Trench-assisted multi-core fiber structure, 7-core fiber (MC07) (top-right) with cladding diameter 225 μm, and (bottom-right) 4-core fiber with cladding diameter 125 μm.

We consider a multi-layer optical transport network (OTN) switching-based MB-EON over MCFs or BuMFPs. We use C+L+S-band technology, providing approximately 20 THz of bandwidth. The modulation format of the line cards is adjusted based on a probabilistic constellation- shaping approach. Therefore, the modulation format of each LP depends on the channel and core used by the LP and the bit rate of each line card can be adaptively changed based on the generalized mutual information (GMI), which is a function of the signal-to-noise ratio [Bos19].

As depicted in Figure 3.5-2, a trench area with a lower relative refractive index (Δ2) compared to the cladding is considered around each core, with a width of Wtr. The ICXT in TA-MCFs depends on fiber parameters such as the relative refractive index difference between the trench and cladding, trench width, and center core-to-core distance, referred to as pitch (r1). It also depends on the frequency, which is negligible in C-band optical networks. However, this is not negligible in multi-band systems like the C+L+S-band technology, which is the considered system model in this work.

To estimate the ICXT of TA-MCFs several works proposed numerical simulations and experimental measurements [Tak11]. However, authors in [Ye14] proposed an analytical closed-form model for mode coupling coefficient of the TA-MCFs. In this context, the ICXT of a TA-MCF can be calculated from Eq. 4:

$$\mu_{ICXT} = \frac{N_{AC} - N_{AC}\exp\left[-(N_{AC}+1)\Omega\left(f^i\right)L\right]}{1 + N_{AC}\exp\left[-(N_{AC}+1)\Omega(f^i)L\right]} \quad \text{Eq. 4}$$

Furthermore, the power coupling coefficient (PCC), denoted as $\Omega(f^i)$, is calculated as in Eq. 5:

$$\Omega\left(f^i\right) = \frac{c\kappa^2 r_b n_{core}}{\pi f^i \Lambda} \quad \text{Eq. 5}$$

where κ, r_b, c, Λ, L, n_{core}, f^i and N_{AC} represent the mode coupling coefficient (MCC), bending radius, propagation velocity, the distance between the centers of two adjacent cores (or core pitch), transmission distance, effective refractive index of the core, channel's center frequency, and the number of lit adjacent cores of the channel under test, respectively.

Moreover, the mode coupling coefficient (MCC) is calculated as shown in Eq. 6:

$$\kappa \cong \frac{\sqrt{\Gamma\Delta_1}}{r_1}\frac{U_1^2(f^i)}{V_1^3(f^i)K_1^2(W_1)}\frac{\sqrt{\pi r_1}}{W_1\Lambda}\exp\left(-\frac{W_1\Lambda + 1.2\left(1+V_1(f^i)\right)w_{tr}}{r_1}\right) \quad \text{Eq. 6}$$

Where r1 is the core radius and the following variables (defined in equations Eq. 7, Eq.8, Eq.9, Eq.10 and Eq.11) are used:

$$\Gamma = \frac{W_1}{W_1 + \frac{1.2(1+V_1(f^i)w_{tr})}{\Lambda}} \quad \text{Eq. 7}$$

$$V_1(f^i) = \frac{2\pi f^i r_1 n_{core}\sqrt{2\Delta_1}}{c} \quad \text{Eq.8}$$

$$K_1(W_1) = \sqrt{\frac{\pi}{2W_1}}e^{-W_1} \quad \text{Eq.9}$$

$$W_1 \parallel_{\frac{\Delta_2}{\Delta_1}} = 1.143V_1(f^i) - 0.22 \quad \text{Eq.10}$$

$$U_1^2(f^i) = \left[\frac{2\pi f^i r_1}{n_{core}c}\right](n^4 - 1) \quad \text{Eq.11}$$

It should be noted that in many works within the literature of the optical network planning community, the authors did not consider the dependency of the PCC and MCC on frequency, which affects the ICXT analysis in SDM-EONs. They have only used the PCC at 1550 nm. For MBoSDM- EONs, the frequency dependency of the PCC and MCC is not negligible and must be taken into account. Therefore, the end-to-end QoT of an LP in terms of the generalized signal to the noise ratio (GSNR) at channel i is estimated inspired from the incoherent Gaussian noise (GN)/enhanced GN (EGN) model for multi-band systems proposed in [Zef20].

$$GSNR_{LP}^i = 10\log_{10}[(SNR_{ASE}^{-1} + SNR_{NLI}^{-1} + SNR_{ICXT}^{-1} + SNR_{TRX}^{-1})^{-1}] - \sigma_{Flt} - \sigma_{Age} \quad \text{Eq.12}$$

Hence, the GSNR for all potential connections from arbitrary sources to destinations in the network can be computed (see Eq.12). Subsequently, the GMI profiles of the K shortest (path, channel, core) tuples are pre-calculated, employing GSNR thresholds for each GMI.

The ICXT in MBoSDM EONs is frequency dependent as it can be shown from the analysis of the PCC and MCC based on the ratio of trench width to core radius. Figure 3.5-3 (a) illustrates the PCC in terms of frequency in the C+L+S-band. As shown in this figure, the PCC undergoes significant changes based on frequency. We can also see that the ICXT depends on the ratio of trench width to core radius, namely, when this ratio increases, the ICXT decreases. However, we cannot increase it indefinitely. The distance between two adjacent trenches must be less than 3 µm. For example, for MC04, this ratio cannot exceed 2. As expected, the PCC of the MC04 is higher than the MC07 because of the higher core pitch. To calculate the MCC, we apply Eq. 6. The MCC for different values of the ratio of trench width to core radius is illustrated in Figure 3.53 (b). The results show that by increasing the wtr/r1 from 1 to 1.5 in an MCF with a 125 µm cladding diameter, a significant decrease in MCC occurs. However, increasing it further does not result in any significant change. Regarding MC07, the results indicate that changes in wtr/r1 do not significantly affect the MCC.

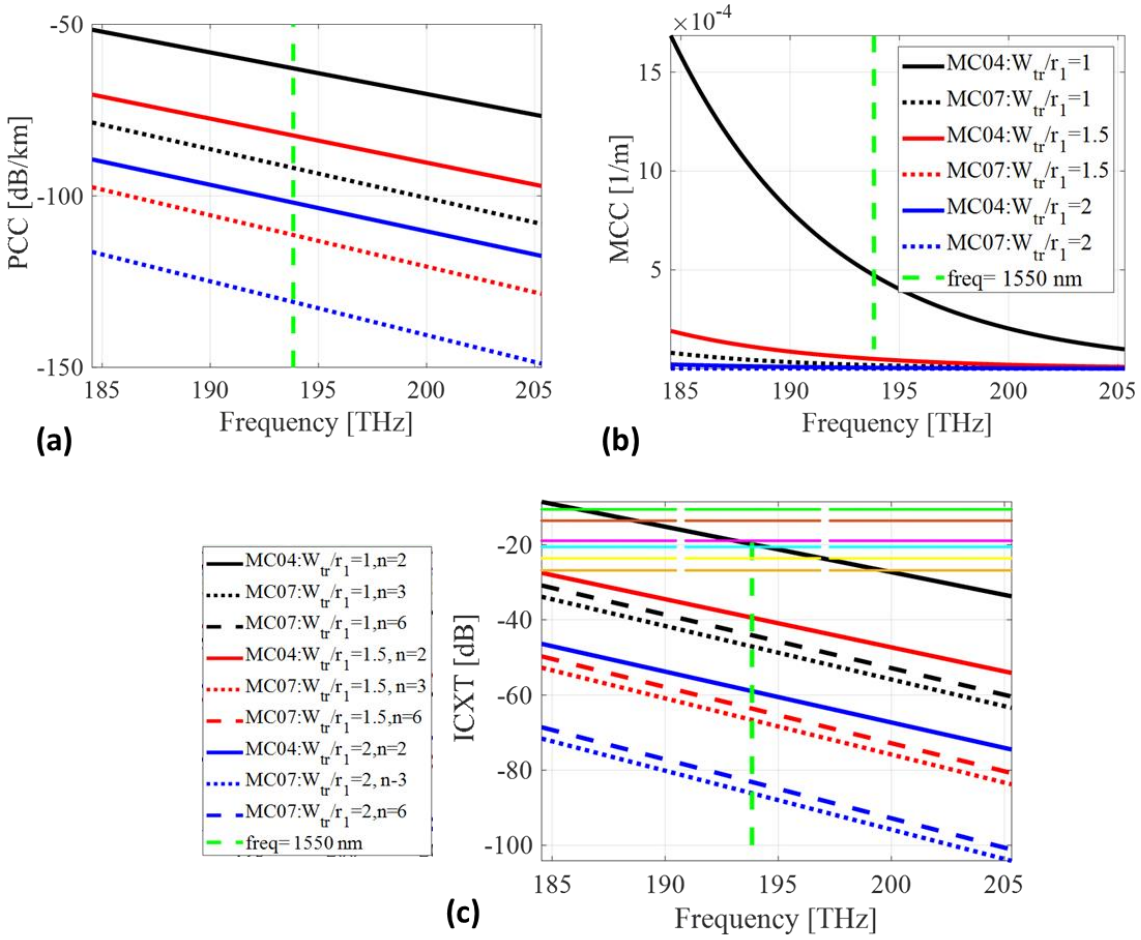

Figure 3.5-3: (a) Power coupling coefficient (PCC), (b) mode coupling coefficient (MCC), and (c) inter-core crosstalk (ICXT) versus frequency for different values of the ratio of trench width to core radius, i.e., wtr/r1 for seven-core MCF (MC07) and four-core MCF (MC04). For the legend of (a), please see (b).

As depicted in Figure 3.5-3 (c), we can conclude several findings. Firstly, the ICXT of a channel depends not only on the transmission reach but also on the frequency, physical structure of the MCF, number of adjacent cores, and core pitch. For example, in the MC04, as represented in Figure 3.5-2, each core has two adjacent cores and a core pitch of 43 µm. Despite this, the ICXT

in the MC07 cores is lower than in the MC04. Although the MC07 has two types of cores—the inner ones with 6 neighbors and the outer ones with 3 neighbors—the dominant effect on the ICXT is the core pitch, which is 51 µm in the MC07. Therefore, if we consider an MC07 with a smaller CD, we have to decrease the pitch, resulting in more ICXT.

It should be noted that because of fabrication restrictions, an MC07 with a standard CD of 125 µm and a core pitch of 43 µm is not possible. Furthermore, increasing the CD increases the effective area; for example, in the C-band, it is about 80 µm2 and 120 µm2 for MC04 and MC07, respectively. The primary challenge in designing MCFs is optimizing the number of cores within a limited cladding. Currently, there is no standard cladding size for MCFs, but a smaller cladding diameter is preferred to achieve high core density and ensure strong mechanical reliability when bending. To meet the failure probability limits, the cladding diameter should be less than 230 µm. Considering this fabrication restriction, the MC07 with a core pitch of 51 µm with CD = 187.5µm is an optimum choice for MCFs with a hexagonal close-packed structure.

Additionally, based on Figure 3.5-3 (c), the ICXT for all channels and cores is lower than the ICXT thresholds of the modulation format level with the highest GMI, even after a 10,000 km transmission reach. However, we do not have this situation for the MC04 with wtr/r1 = 1. For these types of MCFs, like the MC04 with wtr/r1 = 1, a complicated ICXT-aware algorithm for service provisioning and network planning is required. By increasing the wtr/r1 to 1.5, we achieve a good working zone for the MC04, where the ICXT for all channels in all cores is lower than -26.82 dB.

With this model for transmission over MCF with different numbers of cores and fiber characteristics, the next step is to evaluate its performance on a real network topology. To do this, the classical US backbone network with 60 nodes and 79 links, focusing on traffic exchange between the core nodes, i.e., only 14 nodes, as shown in Figure 3.5-4. The average nodal degree is 2.6, the average link distance is 447 km, and the average LP distance for the shortest path (k=5) is 9534 km. In the other nodes, we have only optical cross-connects, with add/drop functionality exclusively at the core nodes. This network is called USB6014.

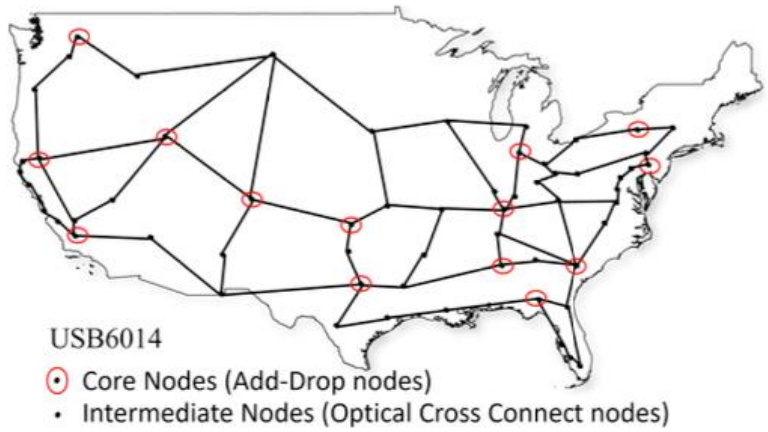

Figure 3.5-4: US network topology for evaluation.

All (path, channel, core) tuples' transmission bit rates for the USB6014 over a C+L+S-band with 268 channels of 75 GHz bandwidth are calculated for 92 connections in the network. The

maximum span length is 80 km in each link. The symbol rate of each channel is 64 GBaud, and the transmission bit rate varies between 100 Gbps and 600 Gbps based on the GSNR of each channel, calculated according to (4) for the k=1 shortest path of each connection. The noise figures of the DFA amplifiers are 4.5 dB, 5 dB, and 6 dB in the C-, L-, and S-band, respectively. The optimum pre-tilted launch power for each span is calculated based on the hyper-accelerated scheme introduced in [Arp24-2].

The cumulative throughput of all (path, channel, core) tuples for each connection is illustrated in Figure 3.5-5. The results reveal that the performance disparity between MFC and BuMFP. The main reason for this is that the loss coefficient of the MCFs is lower than that of the SSMF.

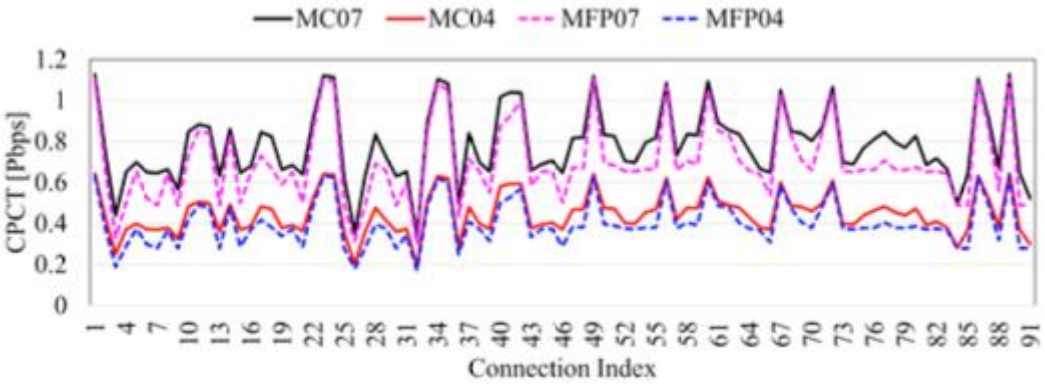

Figure 3.5-5: Cumulative path-channel throughput (CPCT) for each connection in USB60.

To gain a more insightful understanding, we calculate the total network throughput as illustrated in Figure 3.5-6. As shown in Figure 3.5-6, not only do the UL-IXCT MCFs have higher throughput (about 12%) compared to BuMFP, but the increased rate of throughput is proportional to the spatial lanes (cores/fiber pair) in both scenarios. For example, by increasing the core/fiber counts by 75%, the throughput also increases by 75%. A techno-economic study based on the pay-as-you-grow approach is suggested for the next study.

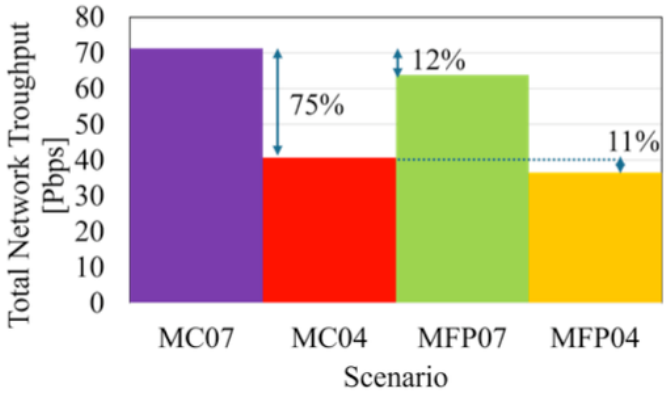

Figure 3.5-6: Cumulative path-connection throughput for each connection in USB60.

4 OPTICAL SUBSYSTEMS

4.1 ADVANCED OPTICAL TRANSCEIVER AND SWITCHING SOLUTIONS FOR NEXT-GENERATION OPTICAL NETWORKS

Within the SEASON project, CTTC has proposed and developed different multiband over spatial division multiplexing (MBoSDM) switching node (component C3.1- section 7.1) and transceiver (component C3.4 section 7.4) solutions to be adopted in future optical networks. The implemented prototypes and all the corresponding building blocks/architecture are described/detailed in section 7.1 and 7.4, respectively. Here, a proof-of-concept considering different target scenarios have been evaluated including the proposed node and transceiver prototypes (in Figure 4.1-1) and CTTC ADRENALINE testbed.

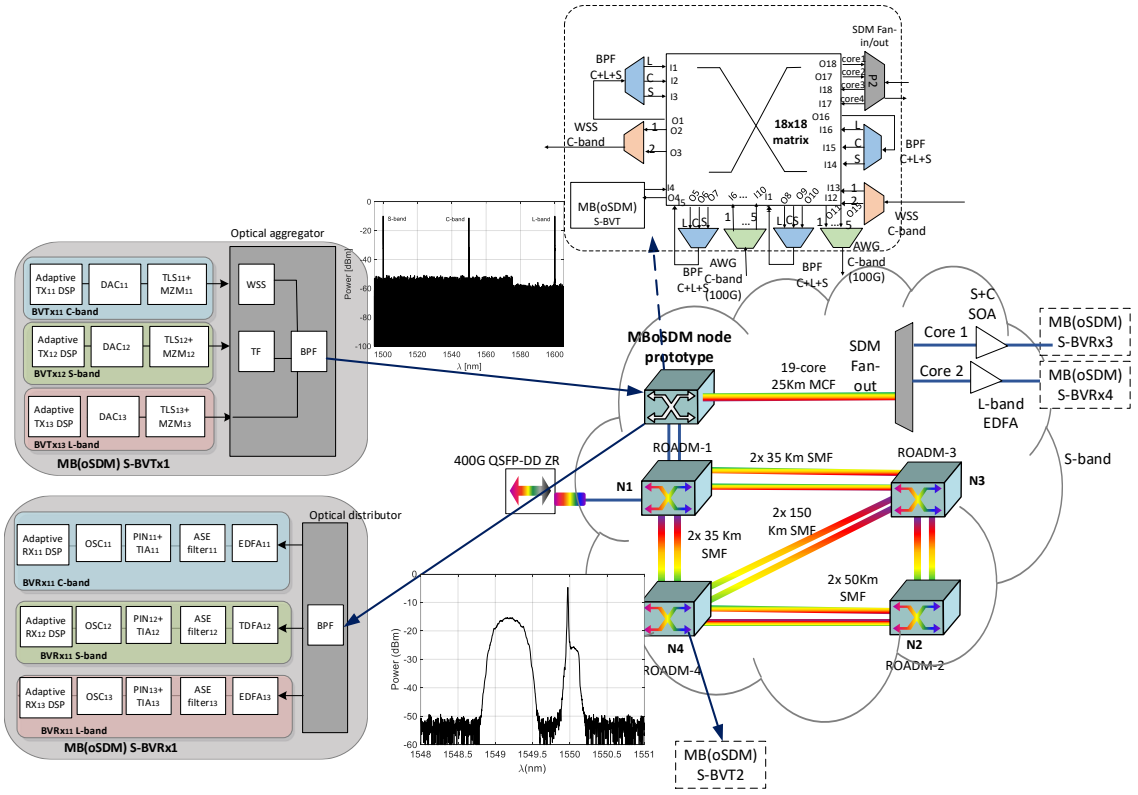

Figure 4.1-1: Experimental setup for the MBoSDM transceiver and switching node assessment including the ADRENALINE testbed.

The ADRENALINE testbed is an open-access infrastructure that integrates Software-Defined Networking (SDN) and Network Functions Virtualization (NFV), spanning packet/optical transport networks and edge/cloud computing capabilities. It supports advanced requirements of next-generation network services, including those anticipated for beyond 5G, 6G, and IoT/Vehicle-to-Everything (V2X) communications. The ADRENALINE photonic mesh network comprises four nodes, including two reconfigurable optical add-drop multiplexers (ROADMs) and two optical cross connects (OXCs). The network features five bidirectional flexi-/fixed-grid dense wavelength division multiplexed amplified optical links, each spanning up to 150 km, with

Dissemination Level	Public

a total coverage of 600 km of optical fiber. Additionally, the testbed includes an SDM domain with a 19-core 25.4 km MCF and a pair of open optical transponders equipped with pluggable optical transceivers, providing aggregated data rates of 400G to facilitate traffic flow between access and core network segments.

Three slices of the MB(oSDM) sliceable bandwidth/bit rate variable transceiver (S-BVT) based on intensity modulation (IM) with Mach-Zehnder Modulators (MZMs) and direct detection (DD) are enabled generating a S+C+L high-capacity flow. In particular, an external cavity laser (ECL) set to 1500 nm is employed for the S-band with a 150 kHz linewidth. Two tuneable laser sources (TLSes) at 1550.12 nm and 1600 nm are used for the C- and L-bands, respectively, with linewidth values below 100 kHz and equal to 500 kHz, respectively. The output power of the three contributions is fixed at 10 dBm. Single side band (SSB) modulation is implemented only within the C- and S-band slices, utilizing a wavelength-selective switch (WSS) with a 25 GHz bandwidth for the C-band and a tunable filter (TF) with a 30 GHz bandwidth for the S-band. However, due to laboratory and setup constraints, the L-band contribution is not filtered, resulting in a double sideband (DSB) signal being aggregated with the other contributions. Orthogonal frequency division multiplexing (OFDM) and adaptive modulation, implementing the Levin Campello (LC) loading algorithm, is executed at each transceiver building block to enhance overall performance [Nad23, Nad24]. Two band pass filters (BPFs) are used as optical aggregator/distributor at each S-BVT, as depicted in Figure 4.1-1. Different technology options are considered for each MB(oSDM) S-BVT building block, depending on the spectral band of operation. Specifically, for the C-band contribution, an EDFA operating in automatic power control mode and a WSS for amplified spontaneous emission (ASE) noise filtering (centered at 1550.12 nm with a 50 GHz bandwidth) are used at the receiver front-end. The S-band slice is amplified with a thulium-Doped Fiber Amplifier (TDFA) operating in automatic current control mode and filtered with a static filter. Meanwhile, the L-band utilizes an erbium-doped fiber amplifier (EDFA) operating in automatic current control mode and a static filter.

Regarding the target scenarios, the first scenario (scenario 1) addresses a back-to-back (B2B) configuration. Scenario 2 focuses on assessing wavelength division multiplexing (WDM) within the C-band, including co-propagation with a 400G QSFP-DD-DCO ZR+ pluggable module over a 35 km path of the ADRENALINE testbed (N1-N4 testbed path indicated in Figure 4.1-1). A flex-grid path is established by appropriately configuring the WSS integrated into the node and the corresponding switching matrix ports. This scenario also demonstrates point-to-multi point (PtMP) operation of the proposed transceiver solution, with the L- and S-band slices received at node N1, and the C-band slice transmitted to N4. Finally, scenarios 3 and 4 are assessed for multiband (MB) and MBoSDM operation by incorporating a BPF and spatial division multiplexing (SDM) fan-in elements of the MBoSDM node, see in Figure 4.1-1. In scenario 3, the MB flow is separated at O1 using a BPF, then aggregated again with the node BPFs (at I5) to be received at O4, where the MB(oSDM) sliceable bandwidth/bit rate variable receiver (S-BVRx) is connected. In scenario 4, the S+C+L flow generated at the S-BVT (I4) is separated at the node such that the S+C flow (I5) is connected to core 1 (O18) for joint MBoSDM transmission, while the L-band port (I1) is switched to core 2 (O17). These scenarios will demonstrate the adaptability and versatility of the proposed transceiver and switching solutions for adoption in next-generation optical networks.

A target bit error rate (BER) of 4.62e-3 is considered for a hard decision forward error correction (FEC) of 7% overhead. Firstly, scenario 1 involves a B2B configuration featuring the proposed

transceiver with capacities of 60.4 Gb/s (S-band), 60.5 Gb/s (C-band), and 60 Gb/s (L-band) at the target BER, with optical signal-to-noise ratio (OSNR) values of 40 dB, 39.6 dB, and 38.1 dB, respectively. These OSNR values were measured at 0.1 nm bandwidth using an optical spectrum analyzer positioned just after the x doped fiber amplifier (xDFA) modules of Figure 4.1-1. Similar performance is achieved across the three bands due to key technology and optimization of various device parameters for each band (such as MZM, working point, filter bandwidth/central wavelength, laser power/wavelength, EDFA/ TDFA output power/current).

In a second step, a PtMP WDM scenario (scenario 2) is experimentally assessed, considering both C-band transmission with the proposed MB(oSDM) S-BVT and the 400G ZR+ pluggable at maximum capacity. The S-band and L-band slices are disaggregated and re-aggregated at N1, and received at the MB(oSDM) S-BVRx1 of Figure 4.1-1, achieving 60 Gb/s and 58 Gb/s, respectively. The C-band slice is disaggregated and transmitted via a pluggable towards N4 over a 35 km flexi-grid path of the ADRENALINE testbed (N1-N4), as shown in Figure 4.1-1. The received spectra at ADRENALINE node N4 is depicted in the inset of Figure 4.1-1. The pluggable power at node N1 is fixed at around 11.5 dBm, with a maximum of 12.2 dBm. Alternatively, the MB(oSDM) S-BVT C-band contribution power at node N1 is varied using an optical equalizer integrated into the ADRENALINE node, affecting the achieved SNR and performance. Figure 4.1-2 shows the C-band slice results of the MB(oSDM) S-BVRx in terms of maximum capacity, highlighting performance degradation for output powers below 6.6 dBm. At −10 dBm optical power, the maximum capacity of the C-band contribution under test drops from 42.7 Gb/s to 15 Gb/s, showing a 27.7 Gb/s degradation.

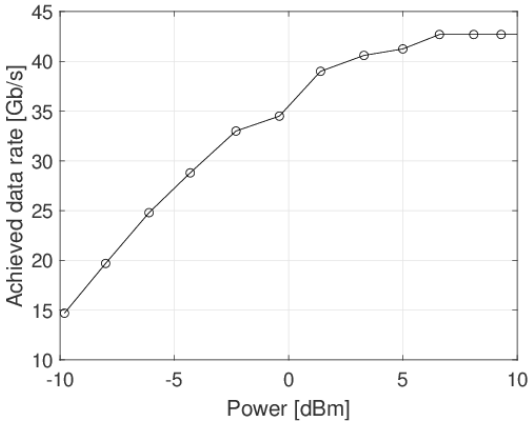

Figure 4.1-2: Achieved data rate for the C-band contribution at node N4 of the ADRENALINE testbed after transmission over the flexi-grid 35 km path co-propagated with a 400G ZR+ pluggable.

In scenario 3, the MB flow generated by the MB(oSDM) sliceable bandwidth/bit rate variable transmitter (SBVTx) is added to the MBoSDM node at input I4. The different band contributions are then separated and re-aggregated using BPFs integrated into the node. The output MB flow is received and dropped at node output O4. At this point, the achieved data rates are 58 Gb/s (S-band), 60 Gb/s (C-band), and 60 Gb/s (L-band) at the target BER with an OSNR of approximately 35 dB (see Figure 4.1-3). The achieved capacity is similar to B2B due to the primary influence of the insertion losses of the matrix (typically around 1.4 dB) and BPF losses (less than 0.5 dB).

Dissemination Level	Public

Finally, scenario 4 validates the MBoSDM capability by considering MB transmission over a 25.4 km, 19-core MCF. In this case, the MB flow generated by the proposed MB(oSDM) S-BVT is added to the MBoSDM node at input I4. Input I4 is then switched to output O1, where the different S-, C-, and L-band contributions are separated using an integrated BPF. The S+C signals are aggregated with another BPF, with the output switched to core 1 of the MCF (O18) and amplified with a C+S SOA for transmission over the 25.4 km SDM link. The L-band signal (I1) is directly switched to core 2 of the MCF (O17) and amplified before transmission over the fiber with an EDFA. The DSB L-band contribution is more affected by chromatic dispersion (CD) and has lower OSNR. Specifically, the L-band has higher CD coefficients of about 19.9 ps/km/nm when transmitting over the fiber, compared to 17.5 ps/km/nm in the C-band and 15.27 ps/km/nm in the S-band.

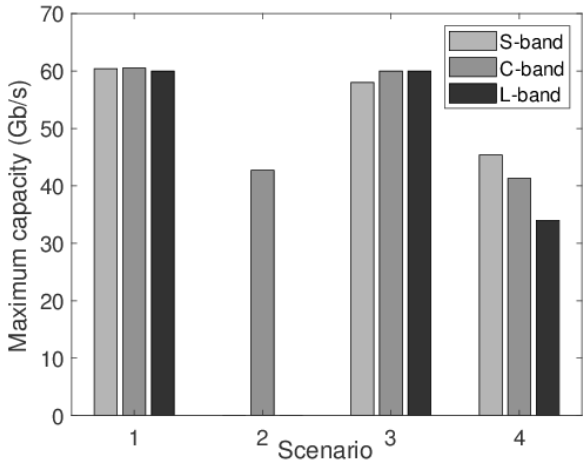

Figure 4.1-3: Achieved data rate per spectral band for the different assessed scenarios.

After MBoSDM transmission over the 25.4 km multi-core link, the data rate of the C-band slice is 41.3 Gb/s at 35 dB OSNR. The S-band and L-band contributions achieve maximum data rates of 45.4 Gb/s (31.8 dB OSNR) and 34 Gb/s (30.43 dB OSNR), respectively. These capacity results are depicted in Figure 4.1-3. This scenario is particularly relevant for scalability analysis, as considering the full population of the S+C+L band spectra and transmission over the 19-core MCF, the overall aggregated capacity can be significantly enhanced. Specifically, considering 350 channels of 25 GHz (S-band), 175 channels of 25 GHz (C-band), and 150 channels of 50 GHz (L-band), a 41 Tb/s transmission can be envisioned. This aggregated capacity increases to 0.5 Pb/s when including the MBoSDM assessment (scenario 4) with the 19-core MCF. However, when transmitting multiple channels within multiple cores, additional impairments such as stimulated Raman scattering (SRS) and crosstalk (XT) can limit the achievable aggregated capacity. A crosstalk analysis for the different analyzed bands, as presented in [Nad23, Nad23-2], shows low XT values below −18 dB (considering S-, C-, and L-bands) for the trench-assisted 19-core MCF over 25.4 km. Regarding SRS, the maximum impact appears at around 100 nm spacing, so different optimization strategies can be considered to maximize overall capacity and throughput [Fer20].

4.2 Node Architectures for High-Capacity Multi-band Over Space Division Multiplexed (MBoSDM) Optical Networks

In today's world, there is a critical need for networks that are not only highly adaptable and dynamic but also capable of supporting increased transport capacities [Gri10]. Multi-band transmission (MBT) technology has recently gained significant attention as a cost-effective means to boost network capacity. This technology extends beyond the conventional C band to incorporate unused bands like O, E, S, L and U, exploiting existing standard single-mode fibers. However, the adoption of additional transmission bands can lead to a decrease in the system's overall spectral efficiency [Sou22]. Spatial division multiplexing (SDM) offers a promising alternative for augmenting system capacity, which can be realized through various approaches, such as resorting to multiple fibers, cores, or modes. As the demand for data traffic continues to surge, a combination of these strategies will likely be employed, presenting new challenges in efficiently managing the switching of optical signals throughout the network.

In [Kaw20], a novel approach involving a multi-band (MB) switching node, which utilizes all-optical wavelength converters, is introduced and experimentally validated for systems operating across both C and L bands. This innovative solution employs a device that introduces an additional layer of versatility to MB systems through band-switching capabilities. Although this feature potentially boosts MBT system performance, it relies on technology that has not yet reached full commercial maturity. The work in [Iwa12] presents a streamlined design for reconfigurable optical add-drop multiplexers (ROADM) with a high nodal degree, utilizing wavelength-selective switches (WSS) with a limited port count. This design seeks to circumvent the complexities and insertion losses associated with fully contentionless cross-connects by allowing some contention within and between nodes. Furthermore, the authors suggest a dynamic network control algorithm tailored to the constraints of their proposed architecture. Numerical assessments indicate that this simplified architecture can achieve performance comparable to traditional large-scale cross-connect switches while significantly reducing the hardware footprint. Realizing the limitation in the port count of commercially available WSSs, the works reported in [Ped15] and [Ped17] describe heuristic and integer linear programming (ILP) strategies to optimize the internal WSS interconnection pattern of each ROADM as to mitigate the impact of blocking when the utilization of parallel fibers leads to nodal degrees that can exceed the number of WSS ports.

Our study explores multi-granular, modular, and adaptable switching frameworks with advanced capabilities, leveraging MB and SDM technologies. These frameworks are designed to meet the escalating traffic demands and the rigorous requirements of forthcoming optical networks. We introduce three nodal architecture solutions grounded on current technologies, which we believe present viable approaches for efficient multi-band switching over SDM systems (MBoSDM) for the next generation of optical networks.

This section begins by setting the stage for developing MBoSDM nodes in Section 4.2.1, projecting the future standardization of client data rates and their impact in line-interface capacity. Section 4.2.2 then offers an in-depth look at the proposed architectural solutions. Following this, Section 4.2.3 examines their optical performance.

4.2.1 Evolution of Channel Bandwidth and Implications on Node Requirements

This section explores the projected changes in channel characteristics over the forthcoming years and examines how these changes could affect the complexity of network nodes. The projections are detailed in Table 4.2-1.

Table 4.2-1: Estimation evolution of channel parameters.

Data Rate [Gb/s]	Year of Ethernet Standard	Year of Massive Adoption	Carriers	Symbol Rate [Gbd]	Frequency Slot [GHz]	Channels per fiber[1]	Total Fiber Capacity [Tb/s]
400	Dec-2017 [IEEE17]	2022	1	60.13	100	60	24
800	Mid 2024 [IEEE22]	2028	1	120.27	150	40	32
1600	2026 [IEEE23]	2030	1	240.53	300	20	32
3200	2030	2034	2	240.53	575	10	32
6400	2034	2038	4	240.53	1125	5	32

[1]*Considering a 6-THz transmission band*.

The discussion begins with 400G channels, assuming that standardized rates will double from their predecessors. The 400G standard received its approval from the IEEE and was published in December 2017 [IEEE17]. Projections based on the timelines of relevant task forces suggest that the standards for 800G and 1.6T will be approved in mid-2024 [IEEE22] and 2026 [IEEE23], respectively. Drawing from these approval timelines, it is estimated that introducing subsequent client rates will span four years. The widespread integration of 400G solutions into transport networks, making 400G the predominant data rate, was observed roughly four years post-standardization. It is presumed that similar timelines will apply to future client rates.

There is a broad consensus that achieving 800G and 1.6T rates will primarily involve doubling the symbol rate of the preceding data rate, given the limited scope for performance enhancements through DSP (Digital Signal Processing) technologies in the near term. For rates beyond these, however, the cost implications of further doubling the symbol rate may become prohibitive, and the power limitation of pluggables becomes a relevant issue [Shi20]. Consequently, the most straightforward approach is expected to involve aggregating additional carriers into a super-channel configuration.

As a result of doubling the spectral occupancy for 800G or higher rates, the number of channels will decrease proportionally to the rate increase. This reduction in available channels reduces the flexibility in establishing path connections between nodes and may lead to increased traffic blocking [Ped20]. With stagnant fiber capacity and the continuous surge in capacity demands, such constraints increase the appeal of alternative capacity-boosting solutions like SDM and MBT.

Furthermore, the likely scenario of having multiple fibers/cores connecting the same nodes and the diminished channel count in each fiber/core reduces the likelihood of requiring an add/drop (A/D) structure for every fiber/core at each network node. Hence, fiber/core- or band-switching strategies emerge as practical approaches to diminishing node complexity. The decreased

channel count also simplifies the node's A/D structure by reducing the dimensions of the required A/D WSSs.

4.2.2 Node Architectures

Various switching methods are anticipated to dynamically leverage multiple dimensions — namely, spectral (covering both wavelengths and bands) and spatial—tailored to specific network segments and application contexts. A hierarchical three-tier model (incorporating wavelength division multiplexing, MB, and SDM layers) integrating pivotal technologies at each layer offers various technological alternatives. This study primarily targets adopting a scalable strategy within the backbone network segment, which demands nodes with superior and rigorous bandwidth/capacity capabilities. The most direct and adaptable strategy employs a matrix-switch configuration to construct an MBoSDM node that capitalizes on this advanced capacity [Sah17], as depicted in Figure 4.2-1(a). The node structure is presented for a single amplification band, and identical schemes are used for the other bands. This reference architecture serves as a benchmark for subsequent comparisons.

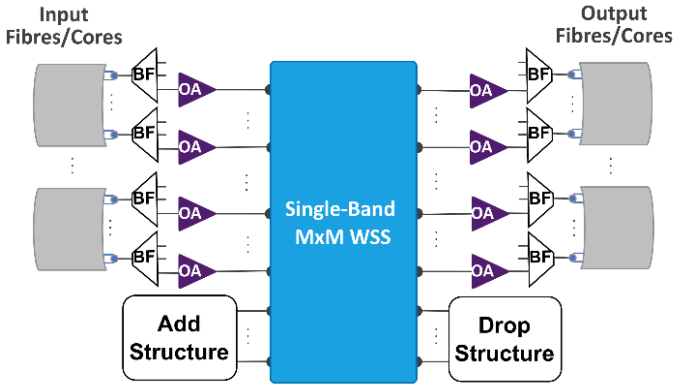

Figure 4.2-1: Reference architecture: single-band matrix-switch-based MBoSDM node. The node structure is presented for a single amplification band, and identical schemes are used for the other bands.

This architecture encompasses band filters (BF) at the ingress of the node, separating different spectral segments. These separated signals undergo amplification before entering an MxM WSS. We assume band-dedicated optical amplifiers (OA) and WSS units. The WSS can route incoming frequencies independently to the output cores of the node or its drop structures. Consequently, part of the M ports is linked to the egress cores, while the remainder is connected to A/D structures. Signals routed to the egress undergo amplification and are coupled with the remaining transmission bands using band filters. The node's A/D section may comprise optical amplifiers for the drop segment and WSSs, MCSs or splitters and couplers.

However, this design suffers from scalability issues concerning the increasing spectral and spatial dimensions. Given the likelihood of multiple parallel fibers/cores connecting the same nodes in the future, specific input and output fibers/cores may be directly interconnected (via core switching), bypassing the WSS and the A/D structure. This direct connection holds the potential to simplify the node by reducing the WSS port count and enhancing optical performance for signals bypassing the WSS, thereby minimizing additional losses.

The first proposed node architecture, illustrated in Figure 4.2-2(a) and labelled architecture #1, is a matrix-switch-based MBoSDM node with a spatial cross-connect (S-OXC). The node structure is only presented for a single amplification band since identical schemes are used for the other bands. The sole deviation from the reference design is the inclusion of an NxN spatial optical cross-connect. This S-OXC directs each amplification band towards an egress band filter or an MxM WSS. Whenever a channel needs to be dropped, or new channels need to be added, the WSS handles band processing at the channel level. We employ a spatial cross-connect to facilitate core switching of bands, ensuring rapid reconfiguration and heightened flexibility. Leveraging the programmability of the S-OXC enables optical band restoration for bands not processed by the MxM WSS. Additionally, it automates node reconfiguration to create new cross-connections or modify existing ones.

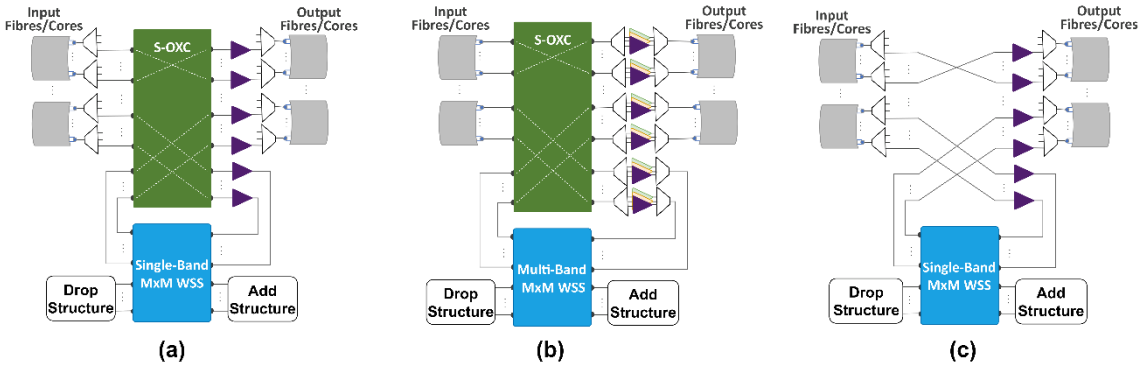

Figure 4.2-2: (a) Node architecture proposal #1: single-band matrix-switch-based MBoSDM node with a S-OXC. (b) Node architecture proposal #2: multi-band matrix-switch-based MBoSDM node with a S-OXC. (c) Node architecture proposal #3: single-band matrix-switch-based MBoSDM node without a S-OXC.

Alternatively, the architecture proposal #2 depicted in Figure 4.2-2(b) capitalizes on using wideband wavelength selective switches and A/D structures. Consequently, a single S-OXC, MxM WSS, and A/D structure serve all bands, eliminating the need for parallel structures for each band. On the other hand, this design has less flexibility regarding core switching than architecture #1 because core switching is simultaneously performed in all amplification bands.

However, both architectures #1 and #2 suffer from a potential single point of failure in the S-OXC, i.e., a failure in the S-OXC could lead to a node-wide failure. To mitigate this vulnerability and further reduce the node's complexity, we introduce a third design, illustrated in Figure 4.2-2(c). This design is a simplified version of proposal #1, employing fixed connections instead of an S-OXC. This design focuses on cost reduction and lacks the core switching programmability of the other two.

4.2.3 Analysis and Discussion

To provide a quantitative comparison of the proposed node architectures, we evaluate the optical performance using the estimated GSNR at the end of a lightpath of a Super-S+C+L-band system [Sou24] and a complexity comparison will be presented in Deliverable 2.2 [D2.2-25]. We select the longest lightpath of the Spanish (Telefónica) and the Italian national (Telecom Italia) reference networks available in the IDEALIST project [D1.1-13]. A single link and span length value are used in each network to simplify the analysis. The span and link lengths are the average values of the actual lightpaths. The Telefónica lightpath consists of ten links with three 75-km

spans each. The Telecom Italia lightpath consists of seven links with two 70-km spans each. We assume the transmission of 40 channels on a 150 GHz grid in each band (6 THz) and a 500 GHz gap between bands. Each channel consists of a 120 GBd signal with a 0.15 roll-off factor. The use of the ITU-T G652.D optical fiber modelled by a nonlinear coefficient of 1.27 W^{-1}/km, a dispersion parameter of 16.8 ps/nm/km at 1550 nm, and a dispersion slope of 0.058 ps/nm^2/km, is assumed. The frequency-dependent loss coefficient and the Raman gain profile of the optical fiber are the same as in [Sou24-2]. Additionally, we assume input and output connector losses of 0.25 dB and splice losses of 0.01 dB/km. The optical amplifiers are modelled by a constant noise figure of [5, 5, 6] dB for the L, C, and S bands. The insertion losses of the MxM WSSs, the S-OXC, and the band filter are equal to 14 dB, 2 dB and 1 dB, respectively. We assume a transmitter OSNR of 38 dB. The launch power is optimized to maximize the average GSNR and minimize the per-band GSNR variation [Sou24-2]. Table 4.2-2 presents the per band average GSNR and its variation within the frequency band for each lightpath. Two different scenarios are considered: 1) the signal passes through the WSS at every node (w/o core switching), i.e., considering the reference node architecture, 2) core switching is performed in every node (w/core switching) considering node architecture #2 or 3) considering architecture #3 (w/ fixed core connection). The optical performance when using node architecture #1 is like the one of #2.

Table 4.2-2: Per band average GSNR and GSNR variation within each band for each lightpath when considering the reference node architecture (w/o core switching), node architecture #2 (w/ core switching) or #3 (w/ fixed core connection).

Band	GSNR [dB] Telefónica			Telecom Italia		
	w/o Core Switching	w/ Core Switching	w/ Fixed Core Connection	w/o Core Switching	w/ Core Switching	w/ Fixed Core Connection
S	18.7 ± 0.4	18.2 ± 0.4	18.8 ± 0.4	22.6 ± 0.6	22.1 ± 0.5	22.8 ± 0.6
C	21.4 ± 0.8	21.2 ± 0.6	21.7 ± 0.6	24.8 ± 0.8	24.8 ± 0.5	25.4 ± 0.5
L	23.5 ± 0.4	23.8 ± 0.5	24.1 ± 0.5	26.6 ± 0.2	27.1 ± 0.4	27.5 ± 0.4

The generalized signal-to-noise ratio (GSNR) analysis presented in Table 4.2-2 shows that its behavior is similar in both lightpaths. The best-performing node architecture is the #3 because of the direct connection between the cores. In this case, the impact of the insertion loss of the S-OXC is avoided but at the cost of being unable to reconfigure core connections automatically. The reference node and architecture #2 show similar optical performance. The performance of the reference node is very similar to that of #3 in the S-band. This difference is small because of the increased attenuation the S-band experiences during fiber transmission (due to the combined effect of the higher fiber attenuation and stimulated Raman scattering). It needs a higher launch power and has a lower GSNR than the other two bands. Consequently, this band is less affected by the ASE noise of the extra amplifier in the reference node, i.e., the performance of the S-band is dominated by the noise added by the fiber and the in-line amplifiers. Therefore, the reference node has a higher GSNR than node #2 in the S-band because of the insertion loss of the S-OXC. On the other hand, the L-band is highly affected by this additional ASE noise and node #2 outperforms the reference node in this band. On the C-band, both architectures have similar performances.

4.3 APPROACHES TO THE NETWORK OPTIMIZATION USING P2MP DESIGN

Metro-aggregation networks connect access networks to metro-core networks and require specific characteristics like hub-and-spoke traffic, survivability, and intermediate capacity. Horseshoe topologies with coherent P2MP transceivers offer a solution to these requirements and can enable variable bandwidth configuration. Filterless architectures simplify network design by replacing active filter cards with passive devices. However, still there are some requirements and degrees of freedom that needs a careful assessment.

4.3.1 Filterless Node Architecture Simplification

Launch power is a crucial factor in optical transmission systems, but its increase is limited by non-linear effects and technological constraints. Previous research has explored optimizing launch power allocation in various scenarios, including ultra-wideband systems and metro-aggregation networks. In this section, we investigate the additional benefits of controlling launch power directly at P2MP transceivers within filterless horseshoe networks. The goal is to quantify the potential improvements in terms of amplifier reduction and SC power difference (which is only arising in P2MP transmission) minimization.

The launch power of transceivers has a minimum value of -21 dBm per SC and a maximum value of -12 dBm per SC with increments of 1 dBm between these two values. Figure below illustrates how the number of optical amplifiers and the SCs power difference change as launch power control increases from 0 dB to 9 dB in 1 dB increments. Notably, in both the "50/50" and "All" scenarios, most of the amplifier reduction is achieved within the first 4 dB of launch power control. However, the reduction in SCs power difference continues to improve with further increases in launch power control.

It's important to note that the fluctuations in SCs power difference are likely due to the optimization's primary focus on minimizing the total number of optical amplifiers. As a result, the SCs power difference may occasionally increase slightly, even though it is constrained within the set of feasible solutions.

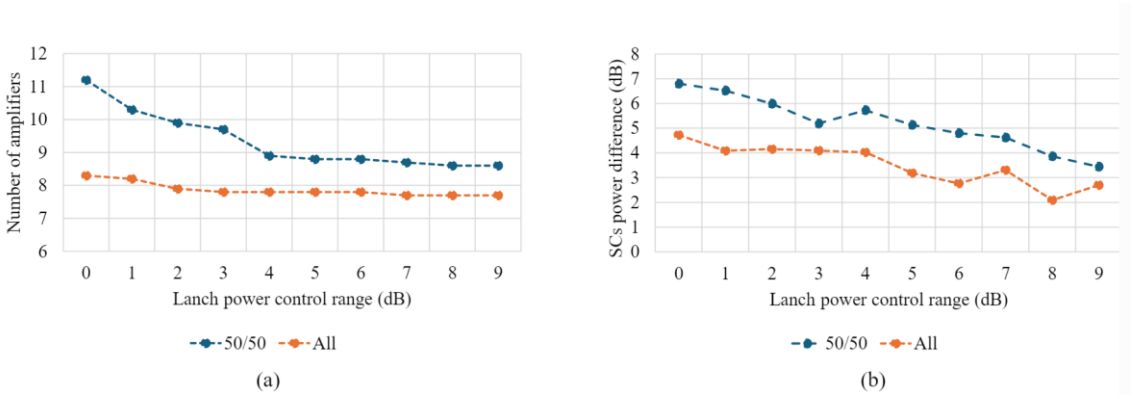

Figure 4.3-1: Average number of amplifiers and (b) SCs power difference for Extended horseshoes and "50/50" and "All" ratios versus the launch power range.

Dissemination Level	Public

4.3.2 Filterless Node Architecture Simplification

This section presents aims to minimize the number of amplifiers while meeting performance criteria. It compares node architecture realized by 2-by-2 couplers with the previously proposed 1-by-2 splitter/combiner-based architecture.

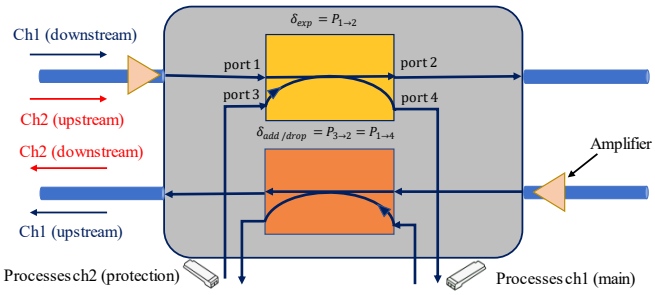

Figure 4.3-2: Two-by-two coupler-based node architecture.

The ILP model minimizes both the number of amplifiers and the SCs power difference at hub 2. It assigns losses to ports, models power levels, and enforces constraints on launch power, node configuration, amplifier selection, SC power levels, and receiver sensitivity. However, it cannot directly consider nonlinear constraints for ROSNR. The results evaluate the impact of coupler ratios on amplifier placement and SCs power difference for different node architectures and horseshoe sizes. In conclusion, the coupler-based architecture leads to a more compact node solution for horseshoe metro-aggregation networks leveraging P2MP transceivers with almost the same number of amplifiers (even lower if "50/50" ratio if enforced) despite higher SCs power difference ("90/10" ratio is an exception), when compared to the baseline solution that pairs splitters and combiners.

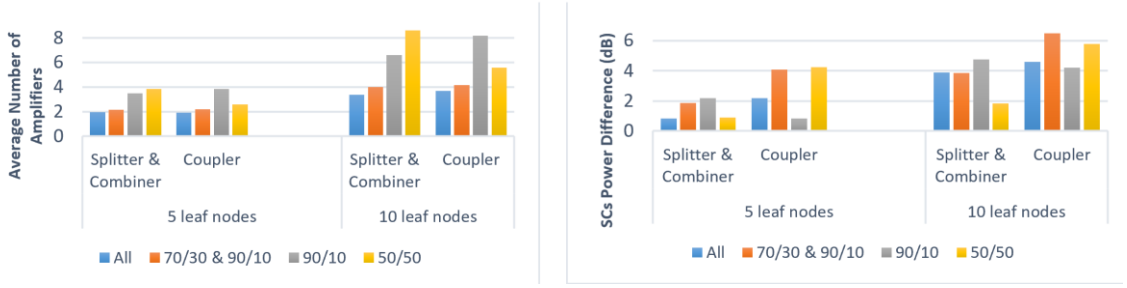

Figure 4.3-3: Average number of amplifiers and (b) average SCs power difference in 5-leaf and 10-leaf node horseshoe networks.

4.4 Efficient network design for power-optimized P2MP solutions in MBoSDM scenarios

In the modern era, networks are required to be not only flexible and dynamic but also equipped to handle growing transport demands [Gri10]. This work presents an efficient network design for power-optimized P2MP solutions in multi-band switching over space-division multiplexing systems (MBoSDM) for the next generation of optical networks. The next section (4.4.1) will

delve into the architectural details of each type of node. Then, Section 4.4.2 describes more efficient architectures for some nodes and presents a complexity analysis of the newly proposed architectures versus typical solutions currently deployed.

4.4.1 Network Architecture and Current Node Implementations

Take as an example the architecture of the Wavelength Division Multiplexing (WDM) transport network presented by TIM [D2.1-24]. The WDM network is segmented into Access, Metro-Regional Aggregation, Metro-Regional Core and Backbone. However, in this work, we focus on the Access and metro domains as shown in Figure 4.4-1.

Different levels of traffic exist in different regions of the network, with the lowest amount of traffic in the access domain, and progressively higher traffic when going to the metro regional aggregation, metro regional core and national core. This difference in supported traffic creates different requirements for each of the network nodes to maintain a cost-effective implementation of the network.

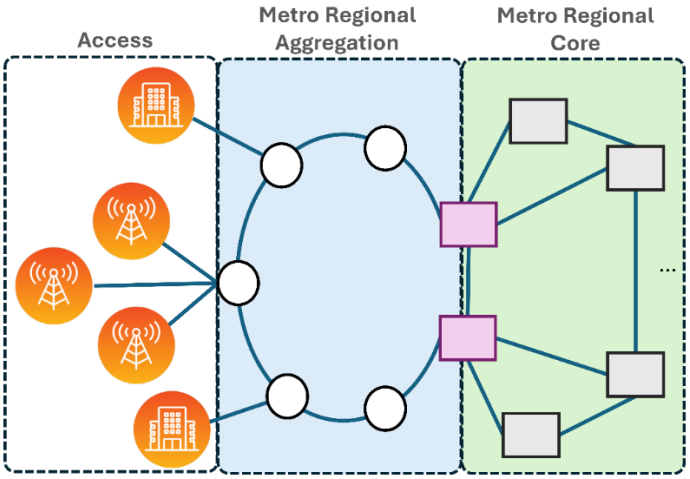

Figure 4.4-1: TIM access and Multi-MAN Metro Regional optical network level architecture.

Figure 4.4-1 presents three different node types in the metro regional domain:

The aggregation level node, between Access central offices (COs) and Regional COs, is represented by white circles. In the current deployment of the TIM network [D2.1-24], the aggregation node consists of a reconfigurable optical add-drop multiplexer (ROADM) and direct detection transponders at 10 Gb/s line rate and are connected in horseshoe topologies. The ROADM is connected to a router (aggregator) that aggregates/separates the information from/to the leaf nodes at the access domain of the network as shown in Figure 4.4-2.

The Interface node, serving as interface between the aggregation and core levels, is represented by purple rectangles. In the interface between the metro-aggregation and metro-core domains, the Interface node consists of two ROADMs connected to a single switch, as shown in Figure 4.4-2. Each ROADM is connected to one network domain (aggregation or core) and the router serves to interconnect them. Therefore, every signal that goes from one domain to the other must be converted to the electrical domain, processed by the router and then converted back to the optical domain.

The Metro-Core node, represented by grey rectangles. Due to the higher traffic demands, the Metro-Core level is realized by 100 Gb/s coherent transponders and ROADMs connected using a mesh topology. Each ROADM is connected to a router (feeder) to add/drop local traffic, as shown in Figure 4.4-2.

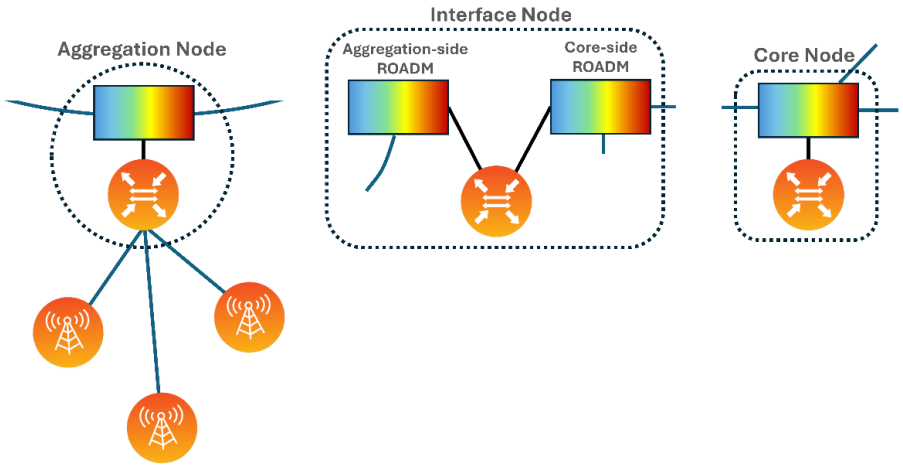

Figure 4.4-2: Diagrams of the current implementation of the different nodes of the network presented in Figure 4.4-1.

4.4.2 Complexity Analysis

The benefits of using a more cost-effective design for the high-capacity nodes in the metro-core domain of the network were analyzed in Section 4.2. Hence, here we focus the analysis on alternative and cost-effective designs of the Aggregation and Interface Node Architectures.

4.4.2.1 Aggregation node architecture proposal and benefits

Our design proposal for the aggregation node architecture relies on P2MP technology to reduce the cost of future networks. In the conventional architecture described in the previous section, the communication between the router on the aggregation node and the leaf nodes relies on an optical point-to-point technology, with each end required to operate at the same speed (1G, 10G, 25G, 100G, etc.), and two transceivers required for each connection, one at each end (as shown in Figure 4.4-3).

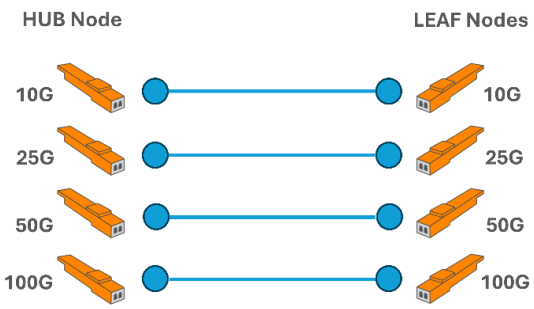

Figure 4.4-3 Diagram of optical connections between a hub and leaf nodes and required transceivers in a P2P architecture.

Dissemination Level	Public

In this case, for a hub router (on the Interface node) to communicate with N=4 access nodes at 100G via M=2 aggregation nodes, 16 100G pluggables are required (as shown in Figure 4.4-4). Four in the Interface node, (4+4) considering all aggregation nodes and one in each of the access nodes. Furthermore, the signals go through 3 RODAMs, one in the Interface node and one in each aggregation node. Table 4.4-1 presents the component count for a more generic case, with N 100G access nodes and M aggregation nodes.

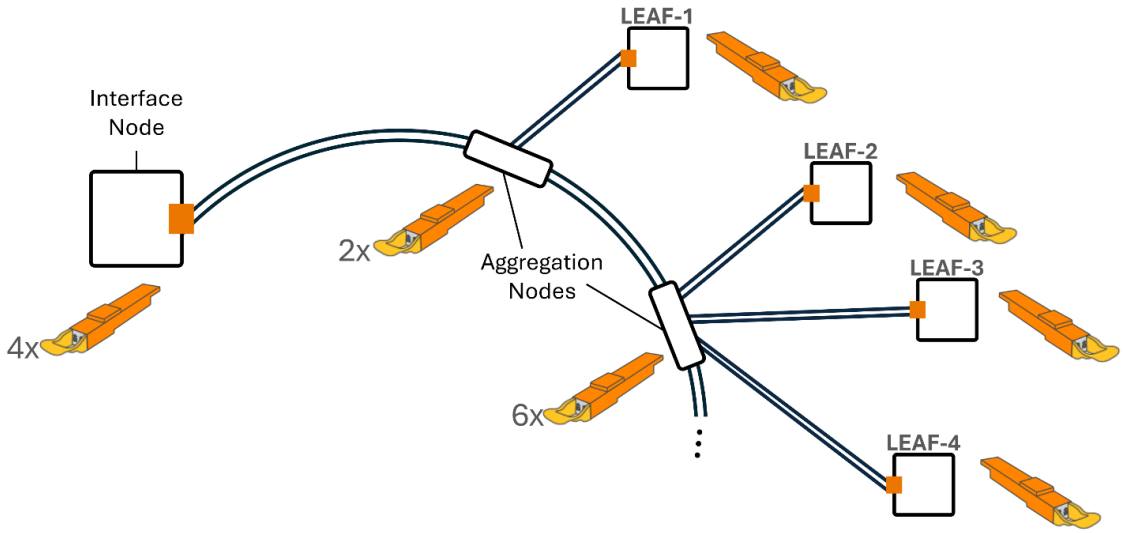

Figure 4.4-4: Representation of the number of required transceivers for the current node implementation using point-to-point solution to connect the interface node with four 100G leaf (access) nodes.

Digital subcarrier technology takes a single-carrier wavelength and divides it up into multiple lower-bandwidth subcarriers generated by a single coherent laser/transceiver leveraging advanced digital signal processing.

For example, a 16 GHz 100G wavelength could become four 25 Gb/s subcarriers, a 64 GHz 400G wavelength could become 16 x 25 Gb/s subcarriers, and a 128 GHz 800G wavelength could become 32 x 25 Gb/s subcarriers, with the 25 Gb/s subcarriers each having a symbol rate of 4 GBd with 16QAM modulation while occupying 4 GHz of spectrum. These subcarriers can now be routed to and from access transceivers in a variety of ways. A 400G hub transceiver could support 16 access nodes with a single 25 Gb/s subcarrier each, or four access nodes with four 25 Gb/s subcarriers each. It is also possible to have different numbers of subcarriers assigned to different access nodes depending on their bandwidth needs, as shown in Figure 4.4-5 [Inf22].

If P2MP transceivers are combined with filterless architectures of the aggregation nodes, the cost reduction is even bigger. This study focuses on a basic filterless node architecture for aggregation nodes using splitters/combiners as shown in Figure 3.2-2. The following complexity analysis consider the filterless aggregation node architecture that only uses 1-by-2 splitters combiners presented in section 3.2 (Figure 3.2-2(b)).

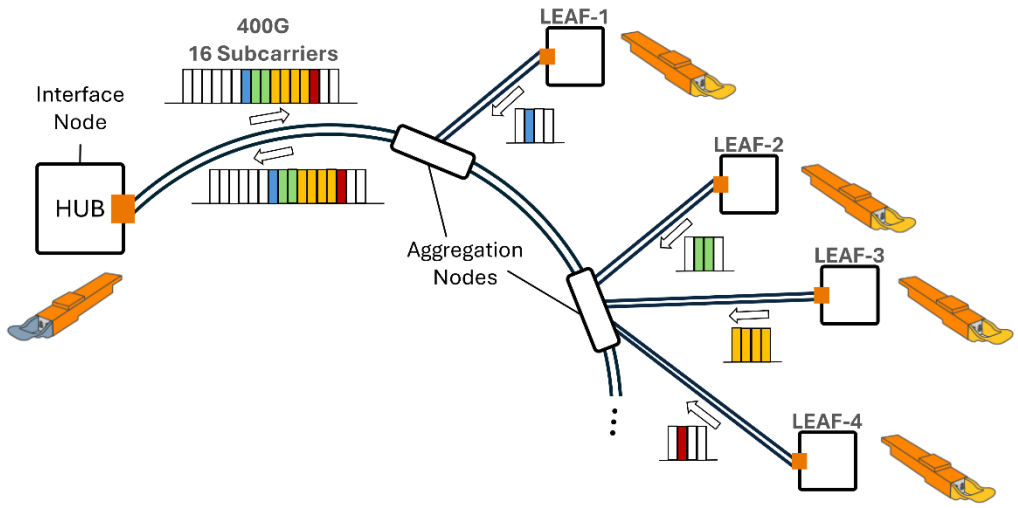

Figure 4.4-5: Representation of the number of required transceivers using the proposed Aggregation node and point-to-multipoint solution to connect the interface node (with a 400G transceiver) with four 100G leaf (access) nodes.

This way, for a hub router (on the Interface node) to communicate with N=4 access nodes at 100G via M=2 aggregation nodes (as shown in Figure 4.4-5), five pluggables are required, one 400G pluggable on the hub and four 100G pluggables in each of the access nodes. Furthermore, only the ROADM on the Interface node is required, and 12 1-by-2 splitters/combiners, assuming the filterless architecture of the aggregation nodes. Table 4.4-1 presents the component count for a more generic case, with N 100G access nodes and M aggregation nodes.

Table 4.4-1: Component count to connect the Interface node with N 100G leaf (access) nodes via M aggregation nodes using the current node implementation (point-to-point) and the proposed Aggregation node architecture with P2MP Agg.

	400G pluggables	100G pluggables	ROADMs	1-by-2 splitters/combiners
Point-to-point	0	4N	M+1	0
P2MP Agg	⌈N/4⌉	N	1	6M

By examining the component count in Table 4.4-1, deploying the proposed Aggregation node in combination with P2MP plugabbles reduces the number of 100G pluggables by 75% and ROADMs by M. On the other hand, the proposed solution requires $\lceil N/4 \rceil$ higher capacity (400G) pluggables and 6M splitters/combiners.

4.4.2.2 Interface node architecture proposal and benefits

Further simplification can be achieved in certain networks scenarios. For example, imagine that a datacenter located in one of the Core nodes needs to transmit data to the access nodes within the same horseshoe structure. Figure 4.4-6 shows the block diagram of the network. In this case, the design of the Interface node may be simplified to allow a direct optical connection between the data center and the aggregation nodes. In this way, the metro core node to which the datacenter is connected acts as a hub node in the P2MP scheme and the Interface node serves only as an optical pass-through of the optical signal to the aggregation nodes.

Given the different bandwidth requirements in the future, as already stated, we expect that MBoSDM transmission systems will be employed in the metropolitan core network. We expect that the node architecture used in the metro-core domain will be the same ones analyzed in Section 4.2. Due to the lower capacity requirement, we believe that a single band will be used to carry the P2MP signals in the metro regional aggregation and access domains.

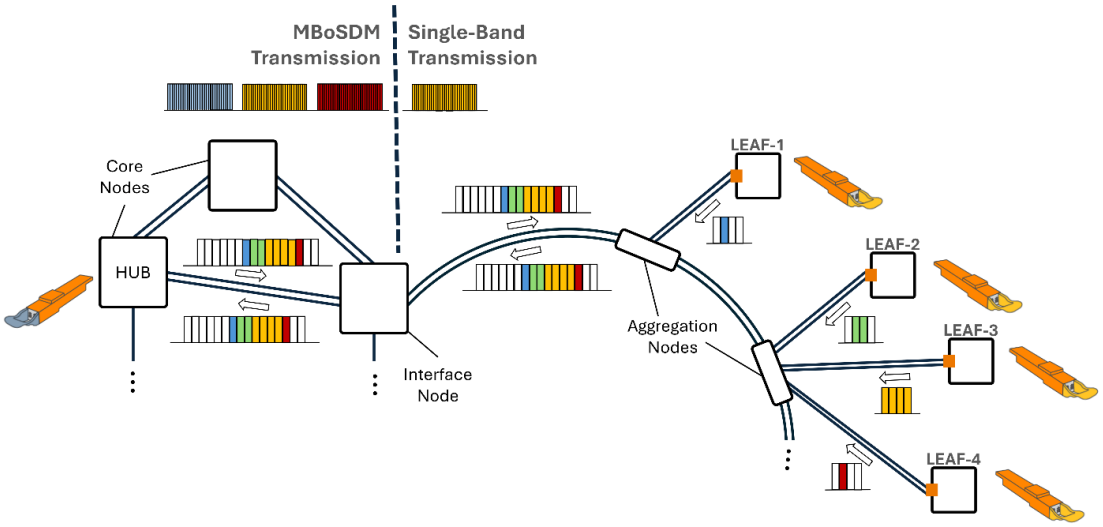

Figure 4.4-6: Representation of the number of required transceivers using the proposed Aggregation and Interface nodes and point-to-multipoint solution to connect a Core node (with a 400G transceiver) with four 100G leaf (access) nodes.

This way, the router in the Interface nodes only process data to be locally dropped and the number of transceivers required for the communication between the DC and the access nodes is reduced. For example, for the hub router (on a core node) to communicate with 4 access nodes at 100G in the same horseshoe structure via 2 aggregation nodes and 1 Interface node (as shown in Figure 4.4-6), 2 400G transceivers, 16 100G transceivers and 5 ROADMs are required using the current node architectures.

Table 4.4-2 Component count to connect a Core node with N 100G leaf (access) nodes via 1 Interface node, M aggregation nodes using the current node implementation (point-to-point), the proposed Aggregation node architecture with point-to-multipoint communications (P2MP Agg) and the proposed Interface and Aggregation node architectures with point-to-multipoint communications (P2MP Int+Agg).

	400G pluggables	100G pluggables	ROADMs	1-by-2 splitters/combiners
Point-to-point	2⌈N/4⌉	4N	M+3	0
P2MP Agg	3⌈N/4⌉	N	3	6M
P2MP Int+Agg	⌈N/4⌉	N	2	6M

In the same case, 3 400G transceivers, 4 100G transceivers, 3 ROADMS and 12 1-by-2 splitters/combiners are needed using the proposed filterless architecture of the Aggregation nodes. Lastly, using the proposed architectures of the Aggregation and Interface nodes, one 400G transceiver, N 100G transceivers, 1 ROADM and 12 1-by-2 splitters/combiners are required. Table 4.4-2 presents the component count for a more generic case, with N 100G access nodes and M aggregation nodes.

5 FRONT/MID-HAUL AND ACCESS BEYOND 5G

5.1 THE ROLE OF THE PHYSICAL LAYER IN RAN FRONTHAUL NETWORK

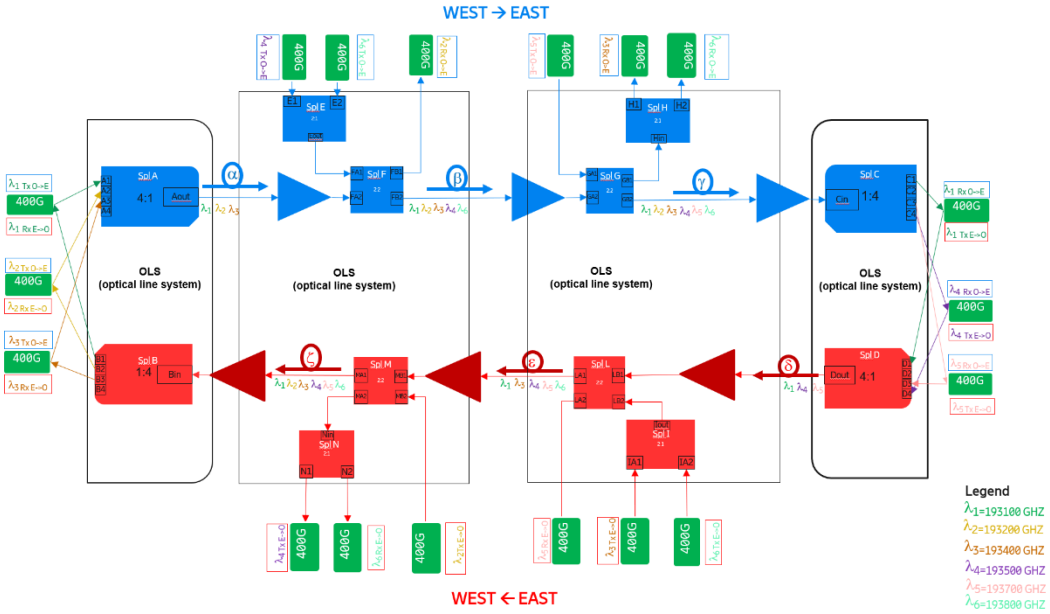

Figure 5.1-1: Optical network designed to handle the high-speed data transfer necessary for a RAN fronthaul.

The physical layer of RAN fronthaul plays an instrumental role in the deployment and efficiency of modern telecommunications infrastructure, especially with the emergence of 5G technologies. The fronthaul segment is the part of the network that connects baseband processing units, known as vDUs in a disaggregated RAN architecture, to the RRUs situated at the cell sites. Figure 5.1-1 provided a detailed depiction of an optical network designed to handle the high-speed data transfer necessary for a RAN fronthaul, highlighting the importance of the physical layer in such a system.

In the physical layer, the focus is on the hardware, transmission media, and fundamental networking functions that enable the transportation of bitstreams between network points. This layer includes cables, optical fibers, transceivers, splitters, and amplifiers—components that are essential for signal transmission. The image showcased an advanced optical networking system with OLS, high capacity 400G transceivers, and WDM techniques, reflecting the need for high throughput, low latency, and scalability.

As RAN fronthaul networks evolve to support a greater volume of data and more complex antenna systems, physical layer solutions must adapt to these expanding requirements. Technologies such as CPRI, eCPRI, SDN, and NFV are revolutionizing the physical layer by enabling more efficient bandwidth utilization, support for MIMO technologies, and dynamic resource allocation. These advancements are particularly relevant in light of the shift towards C-RAN and O-RAN architectures, which demand physical layer solutions capable of supporting different functional splits and high data rate transmission.

The illustrated network diagram underscores the significance of the physical layer in accommodating various wavelength channels and managing signal integrity within a RAN fronthaul network. It emphasizes innovations like tunable lasers in transceivers and the use of meshed optical networks to address challenges such as network synchronization, latency reduction, and the seamless integration of new and existing technologies. As the telecommunications industry advances towards more agile and high-performing RAN fronthaul networks, the physical layer will continue to be a cornerstone in achieving the full potential of 5G and future wireless communication standards.

Figure 5.1-1 depicts a detailed optical network diagram illustrating a bidirectional data flow within a system comprising multiple OLS. These OLS blocks are central to the network's operation, where signal processing and routing occur. The use of splitters, depicted as trapezoids, shows where the network's optical signals are either divided into multiple pathways or combined. Accompanying these splitters are green rectangles marked "400G," representing high-speed transceiver modules that handle data transmission at a rate of 400 gigabits per second. Each transceiver is connected to a specific wavelength channel, indicated by colored lines and associated with frequencies listed in the diagram's legend, ranging from 191300 GHz to 193800 GHz.

The network's directional flow is visually communicated with blue and red arrows, representing the west-to-east and east-to-west directions, respectively. Annotations along the data paths, such as "Tx-O-E" for transmission and "Rx-O-E" for reception, specify the direction and type of data being handled.

In general, the diagram portrays a complex optical communication system designed to manage multiple wavelength channels for the Fronthaul segment. The system efficiently transmits high-capacity data using a logical arrangement of splitters and couplers, ensuring that the optical network can handle the demands of high-speed data transfer.

5.2 COMPARISON OF DIFFERENT ALTERNATIVES FOR FH TRAFFIC TRANSPORTATION IN AN URBAN GEOTYPE SCENARIO

Considering the access scenarios and radio system requirements presented in D2.1 (section 5.1.3 for Geotypes, and section 3.3.3 for RU FH requirements) a comparison scenario of different transport solutions for FH connections has been defined. The scenarios presented in this paragraph will be analyzed in detail and evaluated from a technical and economic point of view, identifying the differences in terms of CAPEX and energy consumption, in WP2 and will be published in the deliverable D2.2 of WP2 (due for M24, December 2024).

The main assumptions for the fronthauling scenario under analysis are the following:

- The vDU are semi-centralized and placed at nearest CO reached from the radio unit (RU) site;
- The FH signals to be carried from RU site to nearest CO;
- For all RU sites at distance (L) compatible with latency constraint (e.g., split 7.2 requires L < 20 km):

Regarding the alternatives for transporting of FH traffic in Cloud RAN the following three have been identified for the comparison:

1. Cell Site Router aggregator at RU site and P2P connection on dark fiber to a router in the CO;
2. WDM between RU site and nearest CO. A small cheap router for low data rate flows aggregation is considered;
3. DSCM P2MP (e.g., XR transceivers: hub in CO and leaves in radio site) between RU site and nearest CO. As for WDM (point 2.) a small cheap router for low data rate flows aggregation is considered for lower bit rate FH flows aggregation.

To calculate the bandwidth requirements of the radio site, an urban geotype was considered with the radio layer configuration as in table 3-7 of D2.1 limiting the analysis to macro-type cells only. Numbers in table 3-7 of D2.1 are used with some adaptations and extension, as in the table, subcarriers with 10 MHz width and 4 MIMO layers are not included.

Both a medium term and a long term time periods are considered to set up the scenario analysis for the transport solutions comparison.

The medium-term scenario is characterized by system and requirement parameters of the RUs equipping each mobile radio site included in Table 5.2-1.

Table 5.2-1: RU parameters for the medium-term analysis. Values of FH capacity is per cell, each carrier has three cells in a site (three sectorial site assumed).

Carrier	Bands range	Carrier width	Mimo layers	FH capacity
C1	Sub GHz	10 MHz	2x2	0.54 Gb/s
C2	Sub GHz	10MHz	4x4	1.08 Gb/s
C3	1-3 GHz	20 MHz	4x4	2.16 Gb/s
C4	1-3 GHz	20 MHz	8x8	4.32 Gb/s
C5	3-7 GHz	100 MHz	8x8	21.6 Gb/s

A preliminary system high level view of the configuration of the scenario in the medium term that takes into account the site configuration and RU requirements specified in Table 5.2-1 is shown in Figure 5.2-1.

The three solutions shown on the same drawing are to be understood as alternatives used to transport the FH traffic from the RUs of the radio base station to the vDU function running on the servers in the relevant central offices.

The first solution (1. P2P) is the simplest one, it requires a pair for fibers used as dark fibers, for each connection; it needs a large capacity router capable of aggregate all the FH traffic of the site and does not optimize the interface capacity and the use of fiber in the access. The second solution (2. WDM) reduces the router capacity at the site because it carries the FH flows individually in WDM wavelengths, but it still requires a small packet router or switch device to consolidate the flows coming from the carriers at the lower frequency bands and with small channel width and low number of MIMO layers (Sub GHz and 1-3 GHz bands with 10 or 20 GHz of carrier width). The third solution (3. P2MP) is the one that potentially best exploits the capacity of the systems, being able to apply the 25 Gb/s modularity of the subcarriers. However, it also requires a small router (or switch) for the aggregation of the low bitrate flows coming

from the RU with minor FH requirements. Both WDM and P2MP can make better use of the access fiber by allowing a sharing of flows coming from different sites on fiber sections converging towards the CO. In the drawing this is highlighted only for the P2MP case in which simple passive splitters/combiners (filterless) can be sufficient, but it also applies to WDM with the needs of filters instead of splitters/combiners. In the latter case, i.e., WDM, if fiber sharing is implemented, a specific design of the transmission, filtering and an multiplexing system for the access trees is required.

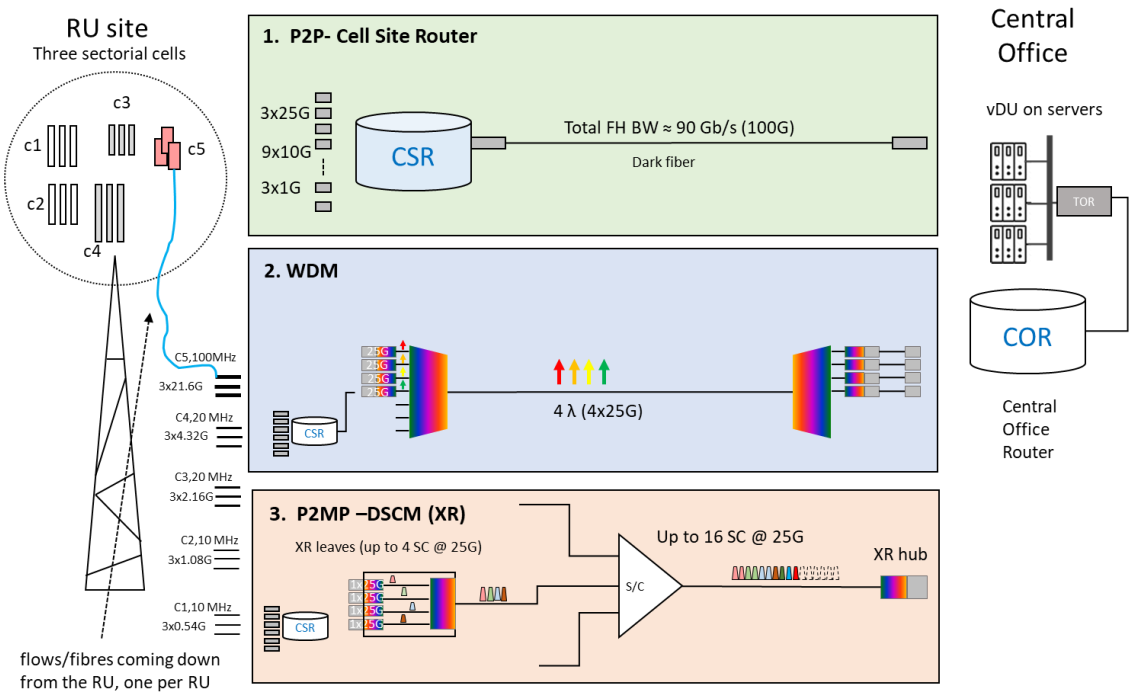

Figure 5.2-1 Scheme of the three FH transport solutions under analysis and comparison for the medium term period. The three solutions (P2P, VDM, DSCM P2MP) are to be considered alternatives for transporting FH flows from the radio base station to the nearest Central office (in any case less than 20 km away).

For long term the parameters of radio units of the radio base station site is given in Table 5.2-2.

Table 5.2-2: RU parameters for the long-term analysis. Values of FH capacity is per cell, each carrier has three cells in a site (three sectorial site assumed).

Carrier	Bands range	Carrier width	Mimo layers	FH capacity
C1	Sub GHz	10 MHz	2x2	0.54 Gb/s
C2.a	Sub GHz	10MHz	4x4	1.08 Gb/s
C2.b	Sub GHz	10 MHz	4x4	1.08 Gb/s
C3	1-3 GHz	20 MHz	4x4	2.16 GHz
C4.a	1-3 GHz	20 MHz	8x8	4.32 GHz
C4.b	1-3 GHz	20 MHz	8x8	4.32 GHz
C5	3-7 GHz	100 MHz	8x8	21.6 Ghz
C6	3-7 GHz	100 MHz	12x12	32.4 GHz

The number of carriers is increased, and the number of MIMO layers is higher in some cases, consequently the capacity for FH transport increases to the values shown in the table. An

example of mapping of the FH needs on the three transport solutions under comparison is given in Figure 5.2-2.

In the long-term example of Figure 5.2-2, two P2P systems on dark fiber are needed for scenario 1. P2P assuming the use of 100G transceivers (but one system with 200G or 400G grey transceivers would be enough). As for scenario 2. WDM and using a small router for aggregating low-bit rate flows, the lambdas and corresponding-coloured transceivers or responders needed are 7, part at 25 Gb/s and part at 50 Gb/s. For case 3. P2MP, still assuming the presence of a router aggregating small flows as in the case of WDM, 10 subcarriers at 25 Gb/s are necessary and therefore the leaves either have a capacity greater than 200 Gb/s (interworking with hub > 400G) or two leaves must be used (two at 200G or one at 100G in combination with a second at 200G). In this case, to exploit the potential of the DSCM systems, the HUB modules should manage at least 32 subcarriers at 25 Gb/s and therefore have a capacity greater than or equal to 800 Gb/s, a value perfectly compatible with the long-term scenario.

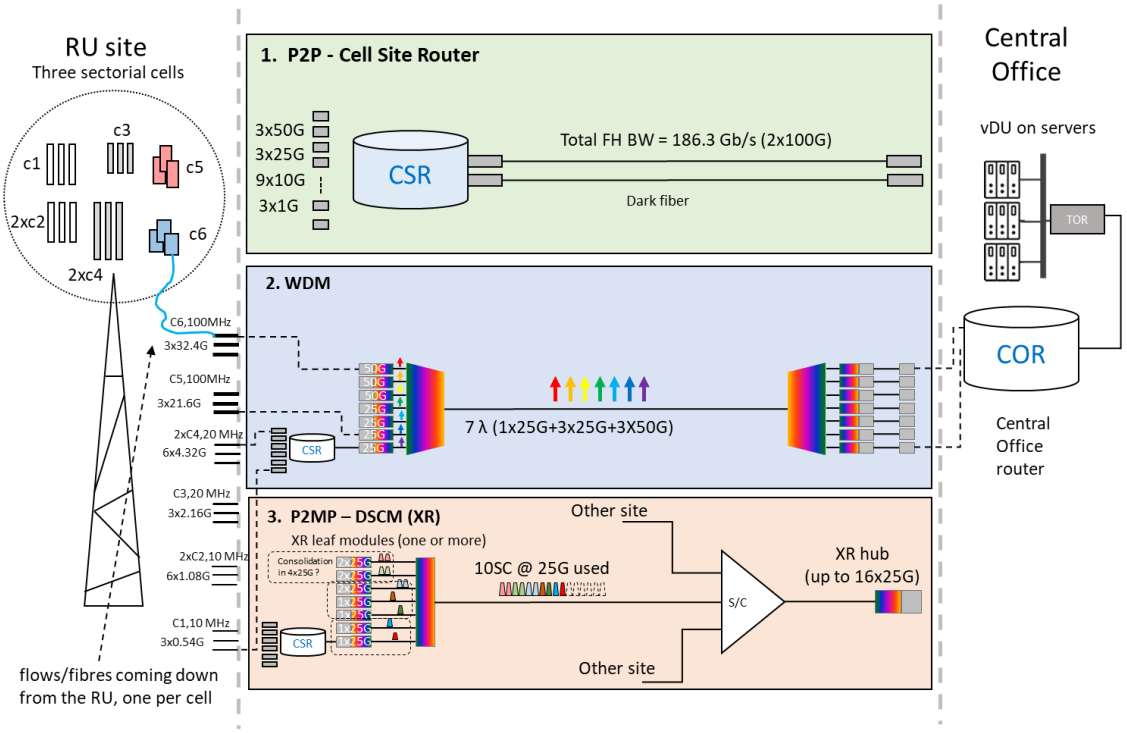

Figure 5.2-2 Scheme of the three FH transport solutions under analysis and comparison for the long term period.

The scenarios illustrated above have been presented as an anticipation of an ongoing technical-economic evaluation, the results of which will be published in deliverable D2.2 (WP2), which aims to report the first results obtained on technical-economic evaluations within the project. The hypotheses on the configurations of the radio base station and the three solutions identified for the transport of FH are subject to minor changes. Evaluations take into account both CAPEX and energy consumtion aspects. Please refer to deliverable D2.2 for the definitive description of the scenarios and the results of the tecno-economic analysis.

5.3 P2MP FOR NEXT GEN MOBILE TRANSPORT

This section reports on the ongoing experiments on metro-aggregation and single fiber bidirectional operation. The experiment is planned for next Q1 2025 in Genoa, between TEI and INF-G. A related techno-economic study is in progress within WP2. The experiment enhances the setup shown in Fig. 5-1-1, but updated with P2MP transceivers, thus reducing the total number of transceivers. We plan to first test the experiment in Munich and then reproduce it in Genoa. The work, as it is not completed in time for the submission of D3.2, will be reported on D3.3. Figure 5.3- illustrate the abstraction of Figure 5.1-1, where at least two 100G P2MP pluggable will be connected to the two 400G hubs so that the meshed networks can enables also P2MP transmission for next generation mobile transport networks.

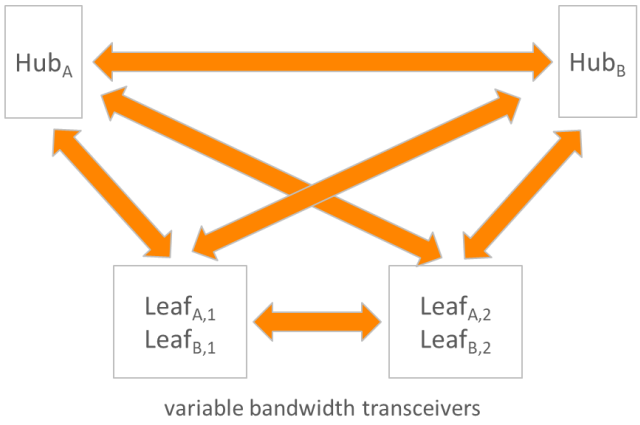

Figure 5.3-1 Simplification of Fig. 5-1-1 enabled by P2MP transceivers.

5.4 NODE DESIGN FOR PON SPATIAL AGGREGATION/DISAGGREGATION

The spatial PON architecture developed within SEASON leverages spatial switching to dynamically manage traffic, optimizing the utilization of OLT ports and spatial lanes. By enabling efficient aggregation of spatial lanes through the use of splitter/combiners, the architecture supports flexible, scalable, and cost-effective network designs that cater to various capacity requirements. This dynamic traffic management and aggregation mechanism ensures high performance, scalability, and energy efficiency, making it well-suited for next-generation optical networks. Figure 5.4-1 illustrates three configurations of a Spatial Passive Optical Network (PON) architecture, focusing on the node design for optimizing spatial lane aggregation and OLT port utilization. Each configuration showcases different ways to aggregate spatial lanes over OLT ports using a spatial switch and varying numbers of OLT ports and spatial lanes.

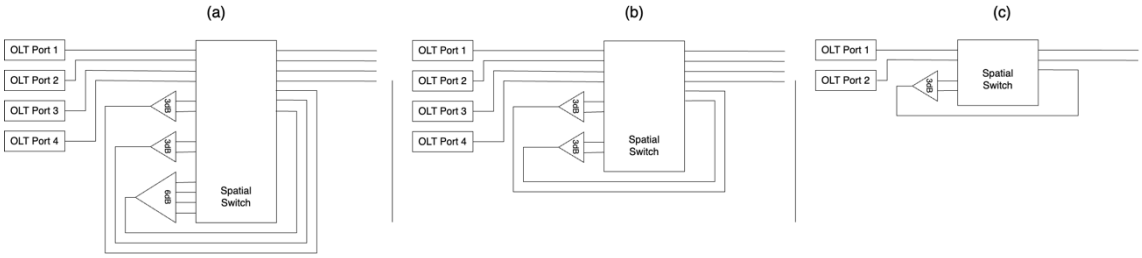

Figure 5.4-1: Spatial PON node architecture configurations: (a) 4x4; (b) 4x2; (c) 2x2.

In the 4x4 configuration (a), the architecture is designed to aggregate four spatial lanes over four OLT ports. There are four OLT ports labeled as OLT Port 1, OLT Port 2, OLT Port 3, and OLT Port 4. A central spatial switch is used to manage the aggregation of the spatial lanes. This switch facilitates the dynamic allocation of lanes to OLT ports based on the current network demands. The key components here are the splitter/combiners. The spatial switch can either direct the spatial lane to bypass directly to the corresponding OLT port or to the splitter/combiner to be aggregated.

In the 4x2 configuration (b), the architecture is designed to aggregate four spatial lanes over two OLT ports. The spatial switch facilitates the aggregation of the four spatial lanes over the two OLT ports, managing the dynamic allocation efficiently. Similar to the 4x4 configuration, the 1x2 splitter/combiners are used to realize spatial aggregation. The spatial switch can direct the spatial lane to either bypass directly to the OLT ports or to a specific splitter/combiner for aggregation.

In the 2x2 configuration (c), the architecture aggregates two spatial lanes over two OLT ports. This setup is useful for scenarios with lower capacity requirements or initial deployment stages. There are two OLT ports labelled as OLT Port 1 and OLT Port 2. The spatial switch manages the two spatial lanes over the two OLT ports. The splitter/combiner is used here to realize spatial aggregation. The spatial switch directs the spatial lanes to either bypass directly to the OLT ports or to the splitter/combiner for aggregation.

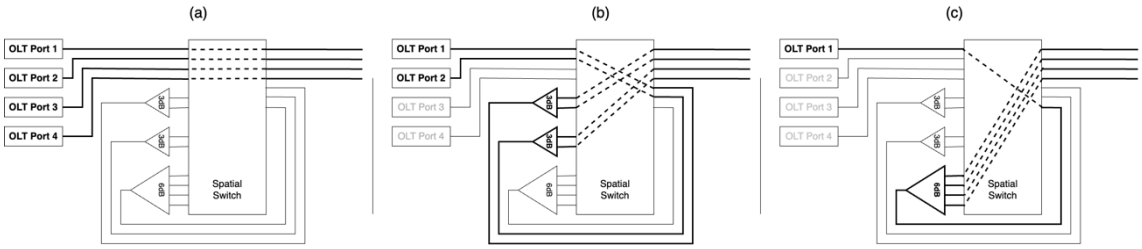

Figure 5.4-2: Spatial PON system 4x4 example.

Figure 5.4-2 showcases different aggregation configurations for the 4x4 architecture of the Spatial PON. The aggregation is driven by the control of the spatial switch, to manage the dynamic traffic demands efficiently. The following examples illustrate how the spatial switch can direct traffic through various aggregation configurations:

In the first configuration (a), all four spatial lanes are directly connected to their corresponding OLT ports (OLT Port 1 to OLT Port 4) without any aggregation. This setup is useful when the traffic demand is high, and each spatial lane requires dedicated bandwidth to maintain optimal

performance. The spatial switch bypasses the splitter/combiners, ensuring that each spatial lane is independently managed by its respective OLT port.

In the second configuration (b), the spatial switch aggregates four spatial lanes into two OLT ports (OLT Port 1 and OLT Port 2). Here, spatial lanes are combined through the splitter/combiners, specifically the 3dB splitters. This configuration is useful when there is moderate traffic, allowing the network to optimize the utilization of OLT ports by aggregating multiple spatial lanes, thereby reducing the number of active OLT ports and saving energy.

In the third configuration (c), the spatial switch aggregates all four spatial lanes into a single OLT port (OLT Port 1). This is achieved by directing all lanes through the 6dB splitter/combiner, combining them into a single lane for the OLT port. This setup is effective during low traffic periods, where the combined bandwidth of the four spatial lanes is sufficient to be managed by a single OLT port, leading to significant energy savings and efficient resource utilization.

Through these examples, the 4x4 architecture demonstrates the flexibility and dynamic capabilities of the spatial PON. The spatial switch plays a crucial role in managing traffic by directing spatial lanes to either bypass or aggregate through the splitter/combiners based on real-time network demands. This approach ensures high performance and scalability, making it well-suited for next-generation optical networks.

6 OPTICAL MONITORING AND POWER EFFICIENCY

6.1 PLUGGABLE TRANSCEIVERS TO REDUCE POWER CONSUMPTION

Within the framework of the SEASON project, the impact of pluggable transceivers into the energy consumption of optical networks has been investigated [Sam24].

In general, in optical networks, a relevant contribution to the energy requirements is given by transponders. As an example, transponders equipped with 600G transceiver cards may consume around 300 W [Rad24], with a contribution of 120 W due to the transponder board with inactive cards. Indeed, transponders include energy-hungry ASIC performing electronic processing, e.g., for equalization (linear dispersion compensation) and symbol decision. Actions in the transceiver components are required to reduce the energy consumption in optical networks. Recently, pluggable transceivers are penetrating the market. Pluggables permit to avoid transponders since they are directly installed in Layer-3 interfaces (e.g., routers). Moreover, their standardization is targeting low power consumption: e.g., 400ZR has a target maximum power consumption of 15 W, while 400ZR+ of 25 W. The main drawback of pluggables is the limited optical reach which can be in the order of 500 km. Moreover, to best of our knowledge, current pluggables operate in C-band only and they should be explored for other bands.

In this work, we carried on an analysis on the power consumption of networks equipped with pluggable transceivers, considering migration scenario to multi band and limited optical reach. Simulation results show how pluggable transceivers can strongly reduce the energy consumption of optical networks while traffic increases.

In traditional optical networks, routers are connected to transponders equipped with transceivers, as shown in Fig. 1a. On the contrary, pluggable transceivers are directly installed into routers (or Ethernet switches), thus avoiding the transponder (Fig. 1b). As mentioned above, given the target maximum power of pluggables, their main limitation is a shorter op- tical reach. According to these considerations, the following allocation strategy for pluggables or transponders is proposed with the aim of maximizing the use of pluggables while guaranteeing the proper network connectivity.

The proposed resource allocation strategy is summarized in the figure below:

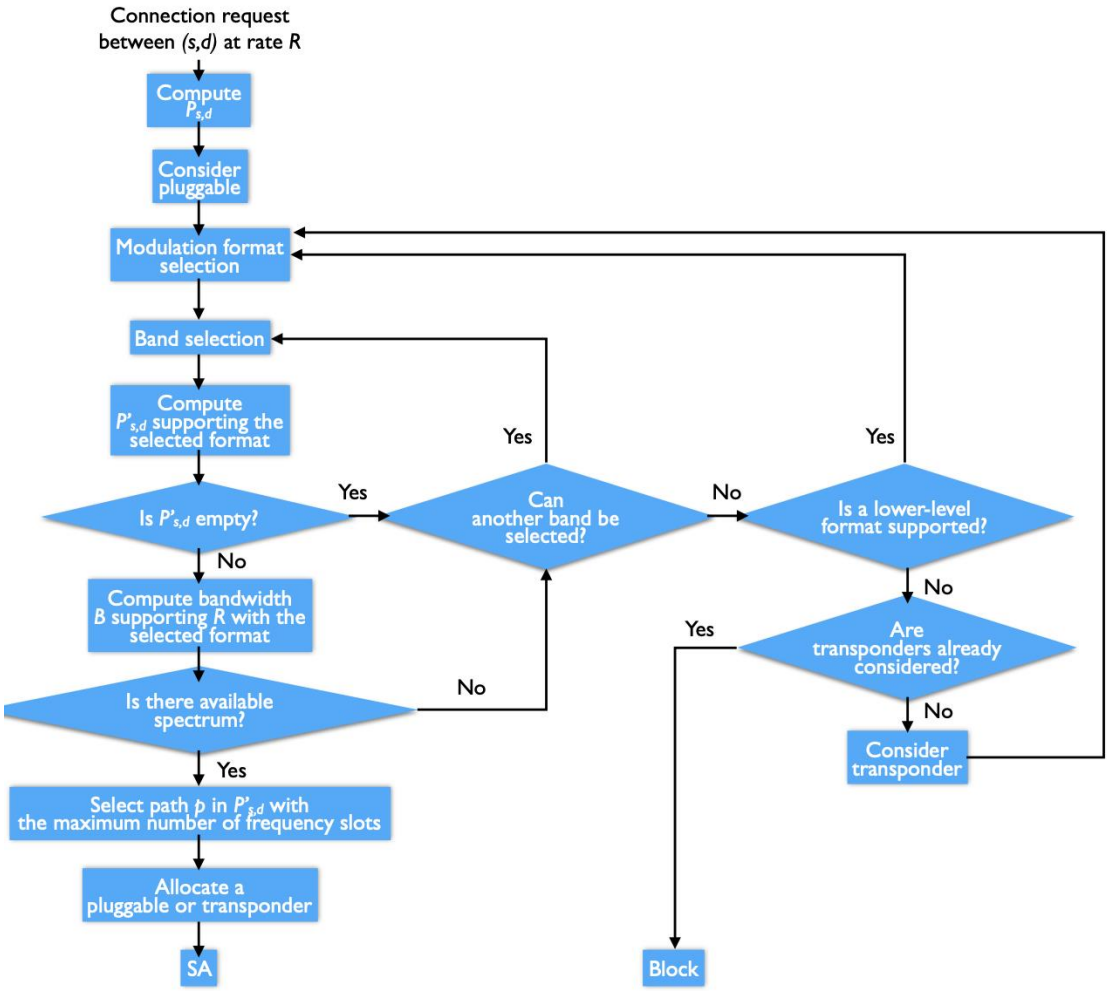

Figure 6.1-1: Flow-chart for resource allocation maximizing the use of pluggables.

A connection request at rate R between nodes pair (s, d) is assumed. The set of paths $P_{s,d}$ connecting (s,d) is computed (or, if pre-computed, is considered). The use of pluggables is preferred than the use of transponders. Then, the highest-level modulation format supported by the pluggable is assumed (e.g., DP-16QAM). After that, a band is selected; preference is given to the C-band, then to L-band, and finally to the S-band. Note that the bands present different transmission performance (e.g., due to different amplification technologies). Within $P_{s,d}$, the set $P'_{s,d}$ of paths supporting the maximum optical reach for that modulation format in the assumed band with the pluggable is computed. If $P'_{s,d}$ is empty, another band is attempted; if all the bands have been attempted, a lower-level modulation format is considered; if all the supported formats have been attempted, it means that (s,d) requires a longer optical reach to be connected and transponders are considered. If $P'_{s,d}$ is not empty, the bandwidth B required to meet the requested rate R with the selected modulation format is computed and the path in $P'_{s,d}$ maximizing the number of frequency slots satisfying s,d the continuity constraints is selected. Note that for frequency slot we mean a portion of spectrum of the ITU-T flex-grid including B. Finally, spectrum assignment (SA) is performed. In the case there is no available spectrum in $P'_{s,d}$, another band is attempted. Otherwise, the use of transponders may increase the number of paths in $P'_{s,d}$, given a larger optical reach supported. A connection is blocked when there is no

available spectrum and all the supported modulation formats and bands are considered with both pluggables and transponders.

A custom built event-driven C++ simulator has been used to evaluate the power consumption (due to transmitter and receiver sides) and the blocking probability of a network equipped with pluggables ("Pluggable preferred") and a network equipped with transponders only ("with Transponders"). Two multi-band scenarios are investigated: C+L and C+L+S. We tested the proposed scheme on a reference Spanish transport network with 30 nodes and 55 bi-directional links. The inter-arrival process of 200 Gb/s connection requests is assumed to be Poissonian. Requests are served with one DP-16QAM channel switched in 37.5 GHz, or with two DP-QPSK channels in 75 GHz. Inter-arrival and holding times are exponentially distributed with an average of $1/\lambda$ and $1/\mu$ = 500 s, respectively, with the connection requests uniformly distributed among all node pairs. Traffic load is expressed as λ/μ. $P_{s,d}$ is composed of shortest paths in terms of hops. The reach of pluggables in C+L with DP-16QAM and DP-QPSK is assumed 250 and 500 km, respectively, while in S-band it is assumed to be the half (e.g., 250 km for DP-QPSK). The reach of transponders is retrieved observing simulations of [Ter23]: with DP-16QAM it is 350 km in C+L and 235 in S, while DP-QPSK is assumed to connect each source-destination pair in the assumed topology.

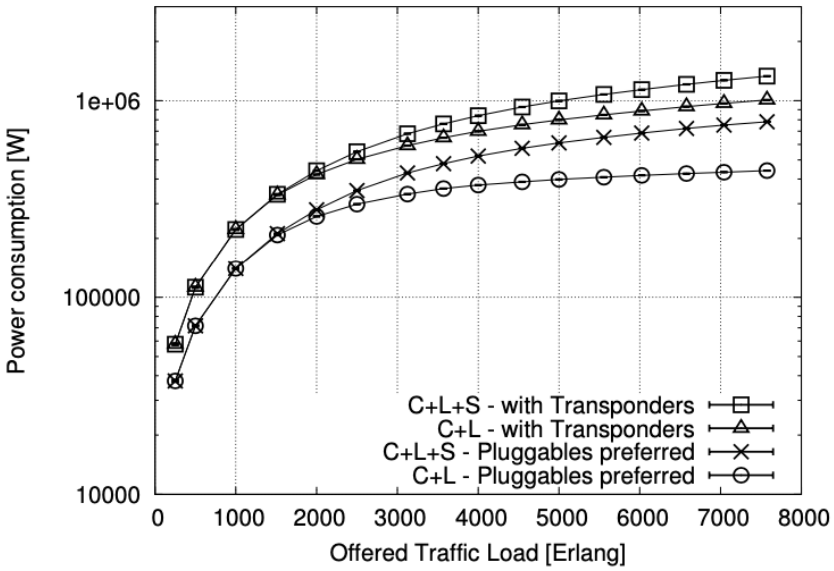

Figure 6.1-2: Power consumption vs. Traffic load.

Figure 6.1-2 shows the power consumption at varying the traffic load. As expected, power increases with traffic load given that an higher number of pluggables or transponders is required. The use of pluggables strongly decreases the power consumption on both C+L and C+L+S, thanks to source-destination pairs supporting the optical reach of pluggables. In general, in the C+L+S scenario, power consumption is higher than in the C+L scenario, because the availability of more spectrum permits to setup more connections activating more pluggables or transponders. As an example, focusing on "Pluggable preferred", the curves in C+L and C+L+S start to diverge around 1500 Erlang, which is a traffic load with non-zero blocking probability in C+L, thus where the S band starts to be exploited. The adoption of pluggables permits to reduce power consumption by around 50%.

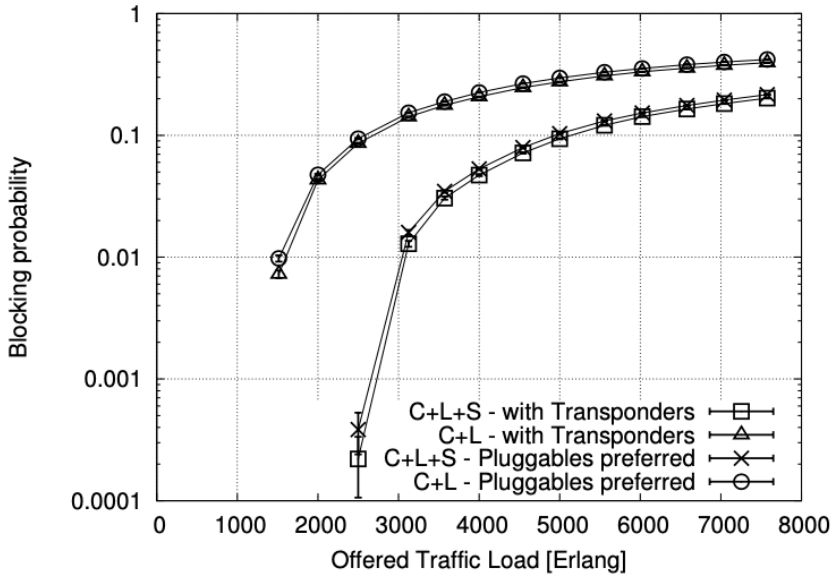

Figure 6.1-3: Blocking probability vs. Traffic load.

Figure 6.1-3 shows the blocking probability at varying the traffic load. As stated above, at 1500 Erlang, blocking probability of C+L is non zero, thus at that traffic load the S-band starts to be exploited in the C+L+S system. In general, the introduction of S strongly reduces blocking. Comparing "Pluggable preferred" with "with Transponders", the former experiences a slightly higher blocking probability. This is due to the shorter optical reach supported, thus shorter paths are more frequently used, limiting more the load balancing of routing and resulting in a faster saturation of shorter links/paths.

In conclusion, pluggables permit to avoid energy-hungry interfaces as transponders, thus reducing the power consumption of the network. However, the use of pluggables is limited by a shorter optical reach. Especially in a multi-band scenario, where bands present different transmission performance (e.g., different amplification technologies), and where the S band may present poorer performance (e.g., than C), it is fundamental to advance with this technology (still while limiting its power consumption to 15-25 W) so that even in the S band pluggables can be used for longer distances.

6.2 ENERGY EFFICIENCY ENABLED BY DSCM VIA TRAFFIC ADAPTATION

As modern network architectures are evaluated according to requirements related to flexible operation, scalability, and sustainability, their design and dimensioning have increased in importance when it comes to addressing traffic demands and traffic growth. Typically, networks have been constructed to provide connectivity based on peak traffic projection; for this reason, within the framework of SEASON, the dynamic behavior of network traffic (i.e., how there might be different peak times based on applications or traffic patterns depending on the day of the week or even on the season) has been investigated [Cas24].

By exploiting the flexibility offered by transceivers utilizing digital subcarrier multiplexing (DSCM) [Wel23], it is possible to enable new services such as point-to-multipoint communication

schemes and network slicing, which can potentially translate into spectral and/or energy savings.

In this regard, a study has been carried out focusing on network topologies inspired by Telecom Italia's real network; these networks are illustrated in Figure 6.2-1. In these topologies the leaf nodes (circles) are responsible for aggregating the traffic from the various connected users. From an operator's perspective, potential future traffic demands, and growth forecasts dictate the design of the network and the corresponding hardware deployment. For this analysis, Table 6.2-1 summarizes the peak traffic requirements of the networks considered. Since these values represent the highest amount of traffic for a given scenario, to emulate the time-dependent behavior of traffic, Telecom Italia has provided a set of traffic profiles for their fixed connectivity services, which can be used to establish a relation between time-of-day and amount of traffic.

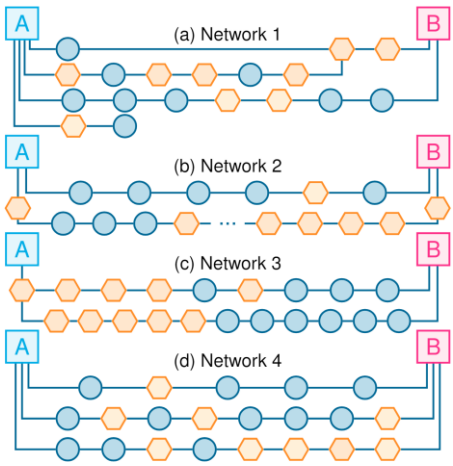

Figure 6.2-1: Considered metro-aggregation network topologies. Shapes indicate type of nodes: hub nodes (squares), leaf nodes (circles), transit nodes (hexagons).

Table 6.2-1 shows the peak traffic requirements per horseshoe for the networks in Figure 6.2-1.

Table 6.2-1: Peak traffic requirements per horseshoe for the networks in Figure 6.2-1. The overall peak traffic of the network is given in parentheses.

Network ID	Peak traffic (sublink 1, sublink 2, … N)
Network 1	10.7; 165.2; 498.1; 88.1 / (762.1) [Gbit/s]
Network 2	308.8; 118.5 / (427.3) [Gbit/s]
Network 3	255.0; 583.3 / (838.3) [Gbit/s]
Network 4	186.4; 120.0; 284.1 / (590.5) [Gbit/s]

Figure 6.2-2 depicts the traffic profiles that describe the ebb-and-flow of traffic during a normal day of operation for two slightly different costumers: large businesses and consumer/home office. In broad strokes, they both exhibit a similar behavior: low throughput late at night until the early morning, when activity starts ramping up, reaching full operation in the afternoon (Large Business) and in the evening (Consumer/Home office).

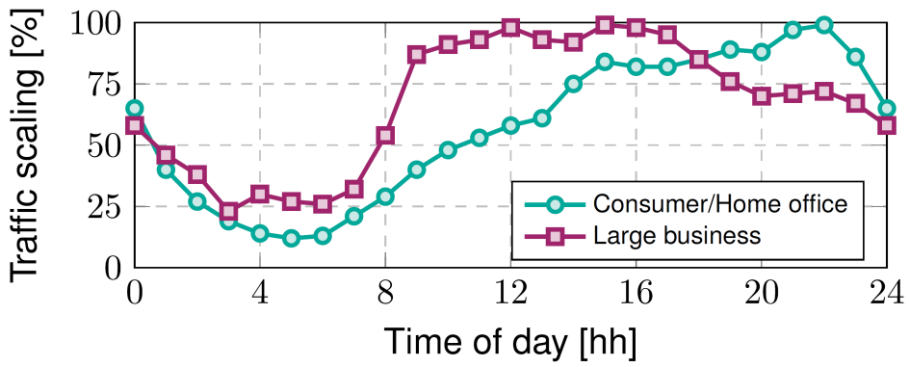

Figure 6.2-2: Time-dependent traffic profiles provided by Telecom Italia.

Knowing peak traffic conditions as well as how traffic fluctuates over a period of time, it is possible to estimate the resources (i.e., number of transceivers, number of subcarriers, etc.) that are needed to cope with the traffic demands at a given time. For example, Figure 6.2-2 clearly illustrates the contrast and relation between traffic, maximum resources, and software-powered hardware adjustments. By dimensioning the hardware (i.e., pluggable transceivers) to cover peak data demands, 12 units would have to be deployed and distributed among all possible leaf nodes. This is represented by the blue bars reaching an overall capacity –for the leaf nodes—of 1200 Gbit/s, assuming that all of the units are traditional single-channel 100 Gbit/s. Contrasting to this level of capacity is the dashed line, which describes the actual traffic demands of the network according to the network's peak traffic (Table 6.2-1) and traffic profiles (Figure 6.2-2). The red bars correspond to DSCM-powered optical transceiver, where it is possible to exploit digital subcarriers to adjust the throughput of a pluggable unit and have it work at a fraction of the total power consumption of the device depending on how many subcarriers are required. This adjustment to the operating conditions can be performed on the DSP at the transmitter, deactivating the 'unnecessary' subcarriers on the temporary demands of the network.

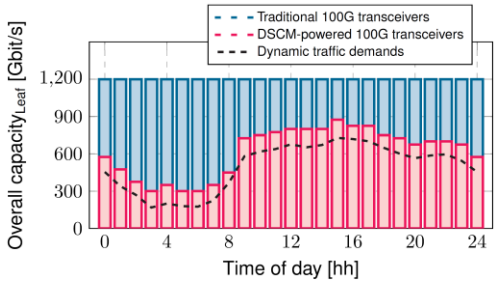

Figure 6.2-3: Time-dependent traffic estimation (dashed line) compared to the overall capacity of the leaf nodes in Network 1 (Figure 6.2-1). Blue bars represent traditional single-carrier 100 Gbit/s transceivers, while the red bars represent 100G (4 x 25 Gbit/s) DSCM transceivers.

By scaling down the operation of the transceivers across the network, it is possible to realize savings not only in terms of spectral flexibility (using fewer frequency slots), but also in terms of power consumption due to the reduced number of processes and computations required when operating the hardware. Figure 6.2-4 shows the normalized power consumed by the ASIC of a DSCM-transceiver for different capacity configurations (100 Gbit/s with 4 subcarriers and 400 Gbit/s with 16 subcarriers) as a function of the number of in-service subcarriers.

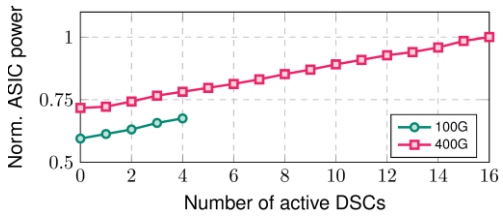

Figure 6.2-4: Normalized power consumption of the ASIC as a function of overall capacity and number of digital subcarriers.

While the total power of the ASIC consists of functional blocks that can be switched-off, some of them are shared and cannot be switched off; therefore, the total power of the ASIC will not tend to zero when all subcarriers are deactivated. Now, based on Figure 6.2-3 and Figure 6.2-4, in addition to considering traffic aggregation at the hub node (i.e., optical aggregation in filterless networks by means of passive elements [Cas23]), the corresponding type of hardware—and their capacity—and their throughput can be determined and used to calculate the overall consumption of the pluggable transceivers' ASICs across the network.

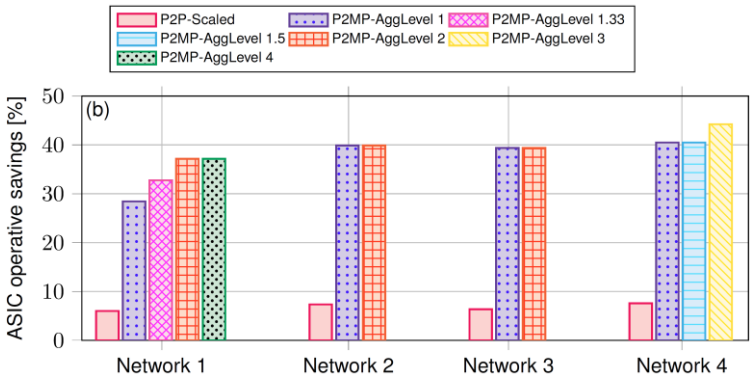

Figure 6.2-5: ASIC operative savings for the considered networks detailed in Figure 6.2-1.

Figure 6.2-5 summarizes the operative savings in terms of power consumption compared to a point-to-point scenario where the DSCM-transceivers are operated at full capacity (i.e., all subcarriers are activated). The results show that there is indeed a benefit in adjusting the settings of the DSCM-powered transceivers to match the traffic demands (P2P-Scaled). However, significantly larger benefits can be achieved by switching to a point-to-multipoint communication paradigm for the selection of networks, switching multiple low-speed transceiver units for fewer units at the hub nodes. According to Figure 6.2-5, savings larger than 25% can be realized. Furthermore, by increasing the level of aggregation, levels as high as 40%-44% could be achieved in some scenarios. Nevertheless, it must be kept in mind that the hardware configuration that is possible for a given network is strongly dependent on its design and high-speed traffic; for this reason, optical aggregation may or may not be possible, or there might be conditions that require a similar number of components and operating conditions, which could negate some of the savings. Ultimately, savings will depend on how the network can be provisioned and how effective the traffic allocation scheme is.

6.3 MONITORING OF CHROMATIC DISPERSION WITH MB TRANSCEIVERS

The MB(oSDN) transceiver developed in SEASON has been used in a joint project activity between B5G-OPEN (101016663) and SEASON to monitor the chromatic dispersion (CD) in MB optical networks [Boi24]. Three bandwidth/bitrate variable transceivers (BVTs)/S-BVT building blocks based on OFDM and DD are used working in the L+C+S-bands (SEASON prototype). The methodology considers the linear OFDM channel's transfer function which is analytically defined, according to [Bar18], in Eq.13:

$$\mathrm{H_{eq}} = \cos\left(\frac{\pi \cdot (f \cdot \lambda)^2 \cdot D(\lambda) \cdot L}{c}\right) \quad \text{Eq.13}$$

Here, f is the frequency, λ the channel central wavelength, $D(\lambda)$ is the dispersion parameter and L is the length of the lightpath. Equation Eq.13 describes a sinusoidal variation, with notches (zeros) dependent on the accumulated dispersion $D(\lambda) \cdot L$ (see Eq.14)

$$\frac{(f \cdot \lambda)^2 \cdot D(\lambda) \cdot L}{c} = \kappa + 1/2 \quad \text{Eq.14}$$

with κ is an integer. In our OFDM system, we monitor the power spectrum density (PSD) of the received signal in the positive frequency part of the received samples, which should match the square of the transfer function given by Eq.13. The estimation of the CD properties of a fiber link can be carried out as follows:

a) For each lightpath with central wavelength λ_j we record a 2048-point PSD versus frequency.

b) A moving average filter with a block size of 15 is used to smooth the monitored PSD.

c) The notches (zeros in the PSD versus frequency) are calculated using a least mean square approach, starting with the accumulated CD given by the datasheet fiber type and the measured fiber length.

d) Using Equation Eq.13, we compute the accumulated CD_j corresponding to the wavelength λ_j.

e) Each link dispersion is estimated by correlating the accumulated dispersions of lightpaths [Sev24]. f) From the measured curve of accumulated link CD versus frequency, the dispersion parameter D versus frequency curve, assuming perfect knowledge of the fiber length L, is computed.

g) Finally, we fit the curve D vs. λ (see Eq.15) using a derived three-term Sellmeier formula for the relative group delay [Coh85]:

$$D(\lambda) = \frac{S_0}{4}\left(\lambda - \frac{{\lambda_0}^4}{\lambda^3}\right) \quad \text{Eq.15}$$

where λ_0 is the zero-dispersion wavelength and S_0 is the dispersion slope at λ_0.

To establish the validity of the method, we first examine its accuracy on different fiber types, namely standard single mode fiber (SSMF) and Teralight (TL), with varying fiber lengths (50 and

75 km) across three optical bands: S, C, and L. Three building blocks of the SEASON transceiver described in section 7.4 are used. In this work, we focus on CD evaluation by including monitoring capabilities at the bandwidth/bit rate variable receiver (BVRx) without necessarily activating the receiver's OFDM-based DSP (see Figure 6.3-1). To evaluate the CD for the different bands, we vary the central wavelength of the TLS within each band before capturing data for different fiber types and lengths. For each acquisition, at the receiver DSP block, we perform a 2048-point PSD and adjust it by fitting with a function that accounts for the linear OFDM channel of Eq.13 and the scope bandwidth (20GHz). The PSD function is defined in Eq.16.

$$PSD(f) = P_0 \left|\cos\left((f\lambda)^2 \frac{D_\lambda * L}{c}\right)\right|^2 10^{\alpha * f} + N_0 \qquad \text{Eq.16}$$

where α is an attenuation coefficient related to the scope bandwidth, N_0 is accounting for multiple electrical and optical noise and is a background level, D_λ is the dispersion coefficient at the wavelength λ, L the fiber length. α is fixed for all the experiment 0.2 dB.GHz^{-1}. Figure 6.3-1 (a) shows a typical PSD (cross markers) with the fitted curve from Eq.16 in a dashed line.

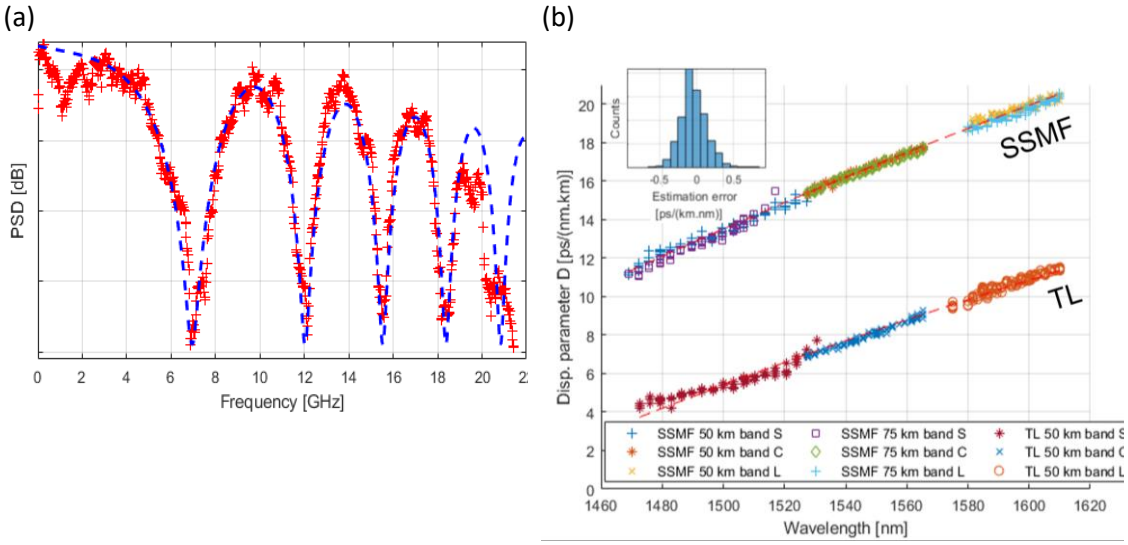

Figure 6.3-1: (a) PSD of detected signal after 75 km km of propagation in SSMF. Crosses are experimental points; dashed line is the fit based on Eq.16. (b) Dispersion parameter D as a function of the wavelength obtained from the fitting with Eq.16 for different fiber types and fiber lengths. Red dashed lines are the results of the fit with Eq.15 for each fiber type. Inset: histogram of the estimation error.

The results of this fit for all fiber types, lengths, and channel wavelengths are plotted in Figure 6.3-1 (b). For each fiber type, we perform a fit with Eq.15 by minimizing the root mean square error with the data to determine the fiber parameters λ_0 and S_0.

Table 6.3-1: Fiber type, length and fitted parameters.

Fiber	Length [km]	λ_0 [nm]	S_0 [ps/(km.nm2)]
SSMF	50	1335	0.0968
	75	1337	0.0966
TL	50	1416	0.0703

The resulting fit is plotted with a dashed red line in Figure 6.3-1 (b). The obtained parameters for each fiber type and length are displayed in Table 6.3-1. The curve fits well with the data for SSMF but deviates at low wavelengths for TL. This deviation is due to limited accuracy in the low accumulated dispersion area where the notch frequency approaches the signal bandwidth. Finally, the inset of Figure 6.3-1 (b) shows the histogram of the errors, illustrating overall good performance of the method with a standard deviation of 0.19 ps/(km·nm) and a mean value of -0.03 ps/(km·nm).

6.4 Complexity Analysis of Frequency Domain Group Velocity Dispersion Compensation

Coherent transceivers perform advanced signal processing and coding at ultra-high speeds while meeting strict requirements for performance and power efficiency. [Mor16] New generation coherent pluggable transceivers are expected to have bitrates up to 1600 Gbps or more. The discussions for the 1600ZR implementation agreement, have already started in the Optical Internetworking Forum (OIF). [OIF23] In the ASIC development of the energy efficient DSPs, computationally complex blocks can translate in higher power consumption and higher area utilization. Compensation for GVD in optical fiber is one of the most computational intense blocks and requires high amounts of resources on chip. Here we will discuss how this is expected to scale with higher symbol rates. In general power dissipation is one of the limiting factors of a coherent transceiver system efficiency and is directly related to the number of complex multiplications needed to processes the task on the digital signal. Figure 6.4-1 shows the block diagram of a finite impulse response (FIR) filter in the frequency domain (FD), which is most commonly used as an architecture for GVD compensation.

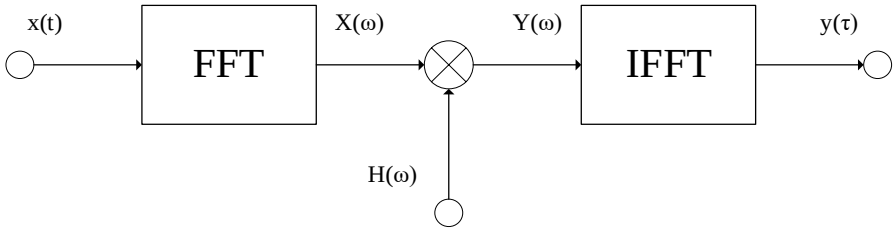

Figure 6.4-1: Block diagram of an FD filter

A fast Fourier transform (FFT) is used to convert the input symbols from the time domain (TD) to the frequency domain (FD), where signal processing, in this case a convolution with a filter, is more efficiently performed. Once the filtering operation is completed in the frequency domain, an inverse FFT (IFFT) is utilized to transform the processed signal back into the time domain, restoring the temporal characteristics of the signal. In an FD filter, the transform blocks account for most of the complexity because they usually involve a high number of operations. In order to calculate the appropriate size, we need to define the size of the input block x(t) as L_x see Eq.17.

$$L_x = \frac{Rs * OR}{R_C}, \quad \text{Eq.17}$$

where Rs is the symbol rate, R_C IS the internal clock rate and OR IS the oversampling ratio. The block size of the FFT is defined in Eq.18.

$$S_{FFT} = L_x + N, \quad \text{Eq.18}$$

ith N being the number of taps needed to compensate for a specific amount of residual GVD. The number of operations in a radix-2 FFT can be approximated, according to [Duh90], by Eq.19.

$$N_{FFT} = 2^{n+1} - 2n^2 + 4n - 8 \quad \text{Eq.19}$$

The number of complex multiplications per symbol is defined in Eq.20.

$$CC = OR \frac{S_{FFT} + 2N_{FFT}}{L_x} \quad \text{Eq.20}$$

given the above-mentioned conditions [Mor16]. The number of taps needed to compensate for GVD is defined in Eq.21.

$$N = 2\,OR \left\lfloor \frac{D\,\omega^2\,z\,B^2}{2\,c_0} \right\rfloor + 1 \quad \text{Eq.21}$$

where D is the GVD, ω the wavelength, z the distance, B the symbol rate and c_0 the speed of light. [Sav08]

We have evaluated Eq.20 for three different symbol rates, an oversampling ratio of 1.25, a clock rate of 1GHz and a center wavelength of 1550nm. The results can be seen in Figure 6.4-2.

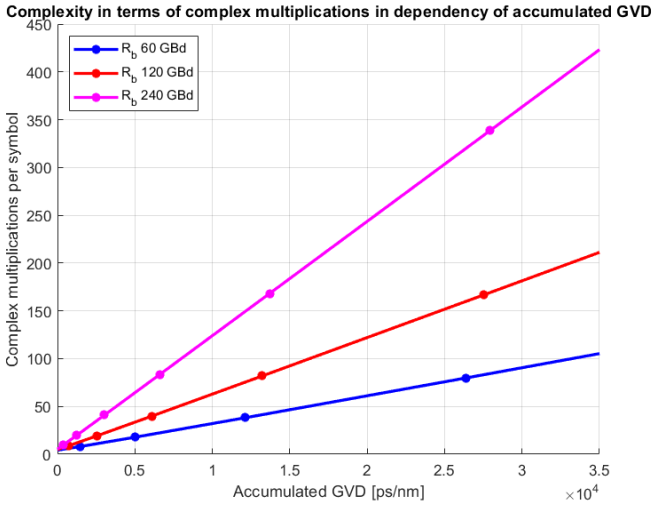

Figure 6.4-2: Complexity of GVD Compensation.

We see that for 120 and 240 GBd the complexity increases more drastically with respect to more accumulated GVD than in the case of 60 GBd and lower symbol rates. A SSMF with a dispersion parameter D = 17 ps/nm/km accumulates roughly 17e3 ps/nm for 1000 km of fiber. Given a higher symbol rate, a substantial increase in complexity is recognized from 100 km fiber lengths

onwards. We expect this to scale even further, when considering symbol rates higher than 240 GBd.

6.5 Digital Subcarrier Multiplexing Spectrum Optimization Techniques Towards Improved Power Efficiency

Digital Subcarrier Multiplexing (DSCM) is an advanced digital signal processing technique initially proposed for its propagation benefits, particularly in long-haul transmission [Wel23]. Instead of transmitting a single high-rate carrier, DSCM transmits multiple low-rate, digitally generated subcarriers. This approach offers several advantages, including increased robustness against chromatic dispersion [Sun20] and nonlinear fiber effects [Lia11]. Recently, DSCM has found a novel application in the coherent pluggable transceivers supporting point-to-multipoint transmission, allowing to simplify and reduce the cost of aggregation networks featuring a hub-and-spoke traffic pattern [Wel23].

Optical transceiver manufacturers continuously seek ways to enhance their products' capacity. However, current and next transceiver generations are nearing the Shannon limit, and fundamentally offer higher capacity (to reduce capital and operational expenditures per transmitted Gb/s) via increasing symbol rates, rather than significantly improving spectral efficiency (SE) [Zam24]. This trend of expanding channel bandwidth, coupled with limited fiber spectrum increases (e.g., Super C-band, C+L-band, Super C+L-band), will inevitably result in fewer available channels per fiber (as discussed earlier in Section 4.2.1). Consequently, despite higher capacity per transceiver, overall (usable) capacity in meshed core networks may decrease due to spectrum scarcity and underutilization of transceiver capacity [Zam24].

The obvious solution to accommodate the reduced number of channels per fiber is to adopt spatial division multiplexing (e.g., multi-core fibers, parallel fibers) or band division multiplexing (e.g., S-, E-band) solutions. However, except for parallel fibers in dark fiber-rich deployments, all these solutions are capital-intensive (e.g., rolling out new fibers) and/or rely on immature technology (e.g., new types of optical amplifiers). A short-term approach to enhance the spectral efficiency of deployed channels is to better adapt the transmitted signal bandwidth to the actual demand. However, the adaptability of existing coherent pluggable interfaces is limited, with multi-source agreements (MSAs) typically implementing only a few symbol rates [openROADM24]. Noteworthy, the OpenXR Optics forum MSA [openXR] specifies a coherent pluggable based on DSCM, which can dynamically adjust the number of subcarriers in use. Although this feature was originally intended for point-to-multipoint communication [Wel23], this work exploits the impact of using it to have a more granular adaptation of the optical signal bandwidth to the actual traffic requirements in core networks. Hence, we numerically compare the usable network capacity of a C-band system utilizing single- or multi-carrier (DSCM) coherent pluggable transceivers.

6.5.1 Simulation Setup

We perform network simulations of a C-band system employing either single-carrier (SC) or multi-carrier (MC) transceivers within the Spanish national backbone network, as provided by Telefónica in the IDEALIST project [D1.1-13], and the 48-node Japanese national backbone

network [IEICE22] (Figure 6.5-1). Two coherent pluggable transceiver types are considered, modeling the two next generations of these devices: (i) low rate and (ii) high rate. In the low-rate scenario, the single-carrier transceiver operates in three modes at 63 GBd and five modes at 126 GBd, as shown in Table 6.5-1. These values are derived from the OpenROADM agreement [openROADM24] for 200 Gb/s, 300 Gb/s, and 400 Gb/s formats (63 GBd), and scaled up to 126 GBd (800G transceivers), with the additional inclusion of 500 Gb/s and 700 Gb/s formats to allow fine-grained capacity increments of 100 Gb/s. In the high-rate scenario, the single-carrier transceiver operates in five modes at 126 GBd and another five modes at 252 GBd.

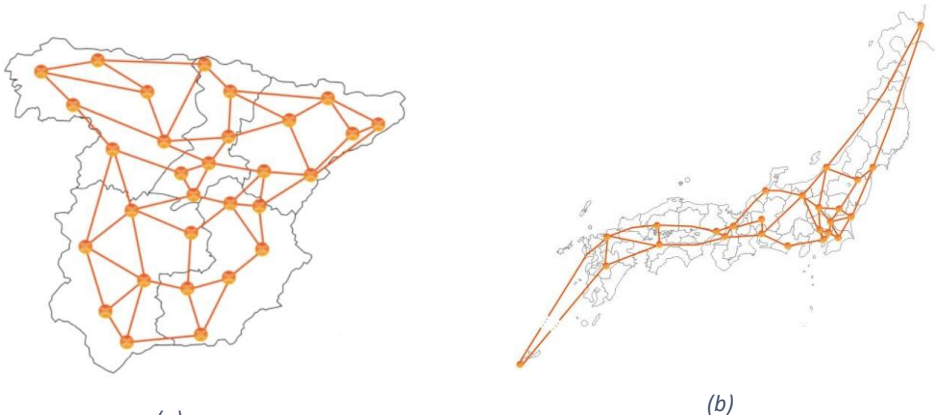

Figure 6.5-1: (a) Spanish and (b) Japanese national backbone network.

Despite the abovementioned potential performance advantages of DSCM, we adopt a conservative approach where the multi-carrier transceiver has 32 equal subcarriers (with the same symbol rate and modulation format) and its SNR requirements match those of the single-carrier transceiver at the highest symbol rate. The bit rate and required OSNR are calculated based on the number of subcarriers used. This approach guarantees that any observed capacity gains are not attributed to using better coherent pluggable specifications. The optical fiber characteristics and amplifier models follow that in [Sou22], with the C-band providing 6 THz of available bandwidth.

Table 6.5-1: Single-carrier transceiver characteristics.

Symbol Rate [Gbd]	Bit Rate [Gb/s]	OSNRreq[dB]	SNRreq [dB]
63	200	16.0	9.0
	300	21.0	14.0
	400	24.0	17.0
126	400	19.0	9.0
	500	21.5	11.5
	600	24.0	14.0
	700	25.5	15.5
	800	27.0	17.0
252	800	22.0	9.0
	1000	24.5	11.5
	1200	27.0	14.0
	1400	28.5	15.5

	1600	30.0	17.0

The amplifiers' operating points are optimized to maximize the average GSNR and minimize the GSNR ripple, following the methodology outlined in [Sou22]. For traffic provisioning, a sequential Routing and Spectrum Assignment (RSA) policy is implemented (Table 6.5-2). Traffic demands are uniformly generated, with payloads ranging from 400 to 1600 Gb/s in 100G increments for the high rate scenario, and from 200 to 800 Gb/s for the low rate scenario. Each demand is sequentially considered for routing over the shortest path, selecting the feasible modulation format and symbol rate/number of subcarriers that minimize the number of 25-GHz spectral slots required to carry the payload, provided there is no available capacity in already deployed channels.

Table 6.5-2: RSA algorithm description.

Inputs: demand rate (R), source (S), destination (D), set of deployed lightpaths (L), transceiver operating modes (T), spectral occupation of network links (S_{occ})
Outputs: Updated L and S_{occ}
1. Perform grooming and exit if there is available capacity for R in one of the deployed lightpaths between S and D. Continue otherwise
2. Calculate the shortest path between S and D
3. Check for available frequency slots in S_{occ} and calculate their required GSNR
4. Get the operating mode from T that minimizes the number of 25-GHz slots to transport R (multiple interfaces may be used). Exit if T is empty
4.1. if multiple combinations occupy the same number of slots, select the one with fewer interfaces
4.2. if multiple combinations still exist, select the one with the highest capacity
4.3. if multiple combinations still exist, select the one with the lowest GSNR margin
5. if the GSNR margin of the selected signal is positive, select the slots with the lowest positive margin and update S_{occ}, create a new lightpath in L and exit. If not, eliminate the operating mode from T and go to step 4

From the available and optically feasible spectrum slots, the algorithm selects those with the smallest positive residual margin to preserve the best frequencies for the most demanding paths. The number of 25-GHz spectral slots occupied by a channel is calculated including a total guard band of 25-GHz to ensure negligible filtering penalties.

6.5.2 Results and Discussion

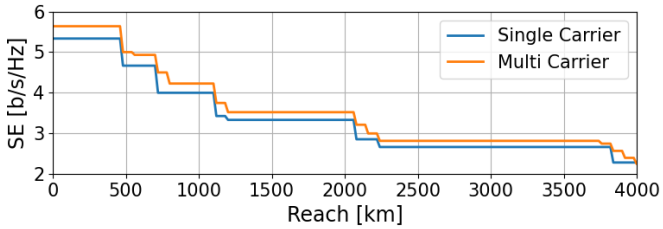

Figure 6.5-2: Maximum spectral efficiency versus reach on a point-to-point transmission with 80-km spans.

First, we examine the theoretical advantages of employing multi-carrier transceivers in a point-to-point link with N_S 80-km spans. Figure 6.5-2 illustrates the maximum spectral efficiency of each transceiver type relative to the link length. The results show that across almost all reach ranges there is a slight improvement in spectral efficiency with multi-carrier, which is exclusively due to the availability of a wider set of channel formats. Note that the additional formats (possible via controlling the number of active subcarriers) can feature a more optimal match between capacity and channel spectral occupation. Further evidence that this is the sole reason for the differences observed is that, although not shown here, a similar plot for maximum channel capacity versus link length yields the same values for both single- and multi-carrier transceivers.

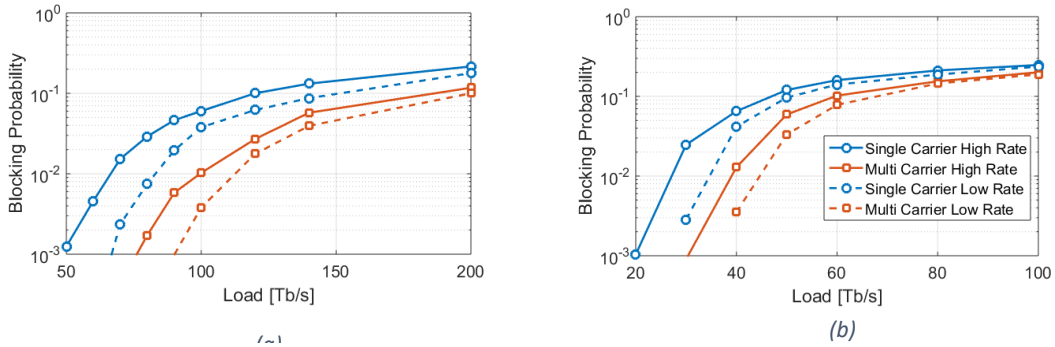

Figure 6.5-3: Total load for different blocking probabilities for the (a) Spanish and (b) Japanese networks.

Secondly, we run the network-wide simulation over the two reference core network topologies for a wide range of offered traffic load values assuming that either single-carrier or multi-carrier coherent pluggable transceivers are deployed. Figure 6.5-3(a) and Figure 6.5-3(b) plot the evolution of blocking probability versus network load for both transceiver types and rate scenarios, considering the Spanish and Japanese core networks, respectively. The most relevant observation is that a lower blocking probability is obtained by using MC transceivers for the same offered traffic load. This trend holds for both networks and when considering both low and high rate scenarios. Hence, always adapting the optical signal (number of active subcarriers) and channel (spectral width) characteristics to the traffic requirements can assist in augmenting the usable capacity of core networks. Moreover, given the significant blocking reduction observed with MC transceivers, these results suggest that the cumulative effect of exploiting this feature for every provisioned channel in core networks is higher than what the relatively

Dissemination Level	Public

modest spectral efficiency improvements observed in Figure 6.5-2 would suggest. Although not shown here, the number of required transceivers for the same carried traffic load is very similar for SC and MC.

Table 6.5-3: Load at a blocking probability of 1% and capacity gain by using a multi-carrier transceiver.

	Spanish Network				Japanese Network			
	Low Rate		High Rate		Low Rate		High Rate	
	SC	MC	SC	MC	SC	MC	SC	MC
Load@ 1% BP	83	113	66	100	35	45	27	39
MC gain [%]	36		52		29		44	

To gain further insight into the network capacity improvements, consider the results in Table 6.5-3, which summarize the average offered traffic load that leads to a blocking probability of 1\%. For both transceiver types, higher loads can be reached in the low rate scenario with traffic flows limited to 800 Gb/s, which is expected, since doubling the traffic flow size and transceiver baud rate, leads to faster exhaustion of spectrum as a result of the smaller number of channels. More importantly, in both networks and for both rate scenarios, the utilization of multi-carrier transceivers always results in a significant increase in traffic load when compared to using single-carrier devices. The gain values range from 29 to 52% and provide evidence of the effectiveness of adapting the signal and channel properties to the exact traffic requirements to improve the utilization of spectrum resources in mesh core networks. Another relevant observation is that the gain from using multi-carrier transceivers is consistently larger in the high rate scenario than in the low rate one (e.g., 52% vs. 36% in the Spanish network and 44% vs. 29% in the Japanese network). This highlights that using multi-carrier transceivers, or more generically solutions to better match signal/channel properties and traffic payload, will become increasingly critical when deploying in mesh core networks the next generations of coherent transceivers, featuring even higher symbol rates.

6.6 Optical Monitoring in Edge Computing

Edge computing, as outlined in D3.1, facilitates stakeholders in managing IT infrastructures, AI processing, and service operations closer to where data is generated and utilized. Achieving this requires edge computing resources to offer advanced networking features with extremely high bandwidth connections. Data Processing Units (DPUs), also known as Smart Network Interface Cards (SmartNICs), originally designed for use within data centers, are emerging as a promising solution for providing edge computing infrastructures with robust networking capabilities. These DPUs, now reaching speeds of up to 400 Gbps and incorporating embedded GPUs, have the potential to support coherent pluggable transceivers. This development makes DPUs a cost-efficient technology that integrates packet, optical, and edge computing resources within a single networking unit, paving the way for new applications in programmable optical networking.

In the SEASON project, we propose utilizing DPUs equipped with point-to-point (P2P) and point-to-multipoint (P2MP) coherent transceivers as a novel, cost-effective edge solution that combines packet, optical, and computing capabilities on a single platform.

A DPU is a specialized hardware component designed for high-speed data processing. While DPUs are commonly used in data centers, servers, and supercomputing environments, there is increasing interest in their application within edge networking due to their ability to handle data

movement, storage, and processing for large datasets. This allows for rapid computation, enabling real-time analysis and the acceleration of data-intensive tasks. Unlike traditional NICs, which focus primarily on accelerating low-level protocols such as Ethernet and depend on server CPUs for other network-related functions, DPUs provide programmability at higher layers, allowing them to perform advanced in-network functions directly. This helps to free up CPU resources for tenant and application-level tasks. Modern DPUs feature up to four interfaces operating at speeds up to 400 Gbps, advanced timing and synchronization, hardware-based encryption, and embedded security mechanisms. They also include up to 16 ARM CPUs to manage embedded computing tasks, with the latest models incorporating embedded GPU resources. Traditionally, DPUs use flat-top connectors (e.g., OSFP, QSFP112/56/28) but have yet to fully adopt the QSFP-DD form factor found in packet-optical switches with coherent pluggable modules. However, a new generation of coherent transceivers is now available for 100 Gbps, and future DPU models are expected to support QSFP-DD for rates of 400 Gbps and beyond. This advancement will bring two significant benefits to optical metro and edge network infrastructures.

The first benefit is a reduction in the number of active standalone nodes and the need for Optical-Electrical-Optical (OEO) conversions. SEASON explores an innovative scenario for optical metro networks that includes edge computing nodes with DPUs equipped with coherent transceivers, allowing for the integration of optical, packet, and computational resources on a single platform.

The second benefit concerns a reduction in latency, achieved by combining computing and optical network resources into a single platform, thus reducing the need for OEO conversions and minimizing end-to-end latency.

Moreover, the use of high-speed transceivers directly integrated into DPUs will greatly enhance the support for ultra-low latency services, particularly for access networks, while leveraging hardware-accelerated network functions in DPUs (such as encryption). These advancements are expected to improve performance for both low-latency user applications and Telco infrastructure components.

In the SEASON project, two main use cases are considered for edge computing encompassing coherent pluggable modules.

The first use case refers to the deployment of 5G functions (e.g., DU) closer to the cell site and deployed on powerful edge nodes. Such use case is investigated by effectively combining SEASON hardware technologies investigated in WP3 (i.e., DPU equipped with coherent transceivers including PTMP openXR pluggable modules) and innovative software components by WP4 (5G software modules, AI decentralized intelligence, SD Agents, etc). To avoid duplications, this use case is entirely addressed in WP4 deliverables.

The second use case refers to monitoring. The availability of DPUs equipped with coherent transceivers enables effective monitoring and correlation features directly at the network card. Received packet and optical data can be processed locally also leveraging powerful GPU resources. In D3.1 we reported on the design, implementation, and preliminary proof of concept validation, published in [Cas24-2], of an optical monitoring solution deployed in the DPU with coherent receiver. In particular, N optical RX parameters were elaborated by a DPU to detect critical anomalies like soft failures. Results reported in D3.1 showed inference time of around 50-70ms in the case of N=30 and up to 360ms in the case of a very large number of parameters (N=5000).

In this document we report on the significant enhancements applied to the optical monitoring solution deployed in the DPU of edge computing nodes. In particular, we introduced the use of hardware-accelerated Deep Packet Inspection (DPI) technology combined with enhanced AI processing. DPI is used to extract, in-network, monitoring packets originated by different nodes

and encompassing monitored parameters such as Bit Error Rate (BER) and fiber power in optical networks, targeting scalable deployments of proactive maintenance and failure prediction.

Traditionally, optical RX monitoring data are locally retrieved from the optical components, processed by the CPU of the host network element, encapsulated in network packets, and delivered to telemetry collectors. Here, those network packets are first retrieved from the network interface, then processed by the host CPU and stored in external time-series databases where AI processing can take place with global visibility. No direct exchange of monitored data among network elements is typically implemented. As a consequence, complex network operations requiring such as correlations or soft failure detection are demanded to centralized elements, with increased delay.

The introduction of edge computing nodes with DPU encompassing embedded GPU and coherent transceivers has the potential to significantly improve the efficiency of this procedure, limiting the intervention of centralized elements thus improving the overall network reaction time. Indeed, the optical RX monitoring data retrieved from the plugged transceiver can be locally processed by the DPU. Furthermore, as key innovation, remote optical devices can also stream their extracted telemetry data to other edge nodes, where hardware-offloaded DPI can be used to extract packet network information in a scalable way, avoiding the interaction with the CPU of the host system. Finally, the local GPU in the DPU can directly perform AI processing, guaranteeing fast reaction time and forecasting capabilities. This way, accurate awareness of the surrounding network area can be achieved by each edge node. In this work, a specific innovative DPI component has been developed for extracting optical monitoring data from custom-built UDP packets containing payload information about selected monitoring parameters, such as BER and power levels of optical fiber devices. Then, the hardware-accelerated DPI system continuously inspects these payloads, comparing against predefined thresholds directly configured within the DPU pipes. If the monitored parameters exceed these thresholds, indicating a potential failure, the system is able to react efficiently, performing further elaborations (e.g., exploiting the embedded GPU and/or sending automated warning/alarm messages possibly leading to traffic reroute even before the link fails. This proactive approach ensures continuous network reliability and operational efficiency also in case of soft-failures. Figure 6.6-1 shows the proposed innovative architecture using a combination of DPI and deep learning techniques. The system, specifically designed for DPU execution, allows to support other use cases, such as embedded cyber security (e.g., in-network detection and mitigation of DDoS attacks). The DPI Module handles packet inspection of monitoring packets at wire speed, identifying optical parameters for failure detection. Only packets flagged by the DPI are forwarded and process by the CNN model running on the DPU with embedded GPU. This way, only resources within the network card are utilized for monitoring purposes, not requiring CPU/GPU resources of edge computing node which can be fully dedicated to edge application and Telco services. The metrics extracted from DPI are provided as input features to the CNN. We use standard CNNs to analyze data collected from optical networks and make real-time predictions about potential optical failures based on the latest network conditions. The CNN model is trained to detect both gradual and sudden degradations of critical parameters. The system utilizes both historical data and latest monitoring metrics. By forecasting potential failures, the system can trigger preventive recovery and maintenance actions before actual failures occur, thus enhancing network reliability and minimizing downtime.

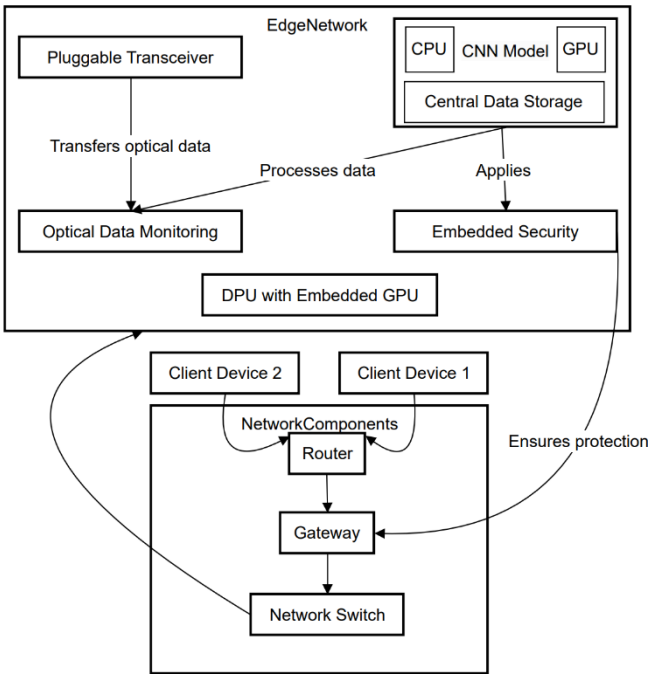

Figure 6.6-1: Proposed Edge Network Architecture.

The proposed solution has been validated considering the network testbed reported in D3.1. It includes two DELL PowerEdge Servers with NVIDIA Bluefield2 DPU with GPU. Due to the current lack of support for coherent transceivers in these DPU, we depend on Edgecore switches that are equipped with 400ZR+ coherent transceivers. Nevertheless, the DPU manages the transceivers using a Rest interface rather than relying on an SDN Controller. This allows the transceivers to be controlled as if they were physically integrated into the DPU. Subsequently, the two transceivers are joined by three optically amplified spans, each spanning a distance of 80 km.

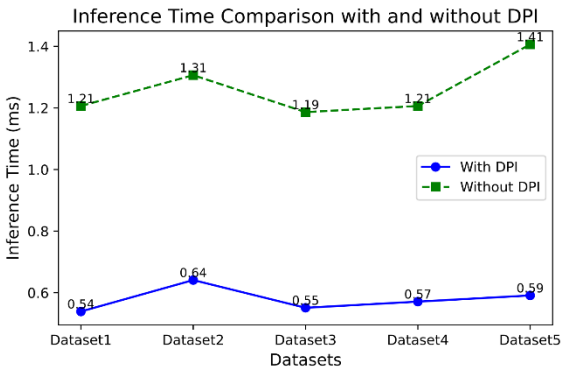

Figure 6.6-2: Inference Time.

Figure 6.2-2 shows the inference time comparison for optical failure monitoring with and without DPI. Data was collected from five different datasets representing various network environments. The results indicate that the DPI-based solution has a significantly lower inference time due to its real-time packet inspection capabilities. Each dataset consists of 30 optical parameters. These parameters simulate a single received signal event.

The inference times represent the duration taken to analyze the received monitoring packet data and predict potential optical failures. The DPI system inspects UDP packets carrying payload information about pre-FEC BER and power levels from optical devices. As anticipated, these values are processed in real-time to identify any threshold breaches that indicate potential optical failures. The processed BER values and power levels are passed to the CNN model. The CNN model compares the real-time data against learned patterns to predict potential failures. With DPI, the average inference time across all datasets is around 0.54 ms. In the absence of DPI, the system directly processes packet attributes for anomaly detection without the initial inspection and preprocessing by DPI.

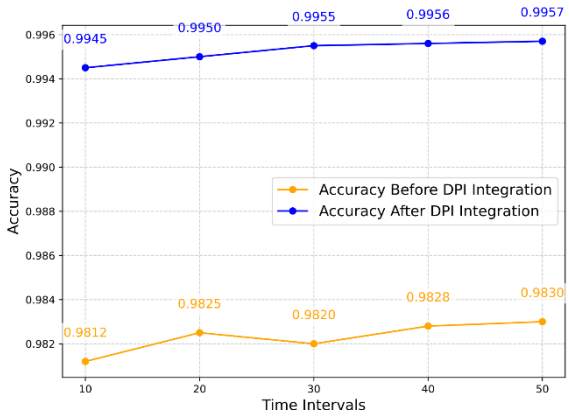

Figure 6.6-3: Accuracy Over Time.

Figure 6.6-3 shows the accuracy of optical failure monitoring over time with and without DPI integration, exceeding 99%. This indicates that combining DPI metrics with deep learning enhances the system's ability to monitor and predict optical failures effectively and in a scalable way.

6.7 FAILURE IDENTIFICATION: MODEL VS. DATA CENTRIC TECHNIQUES

Within the framework of the SEASON project, ML techniques have been investigated for failure identification, i.e., a classification problem, where each type of failure is associated to a class [Kha24].

In a live network, some failures occur more frequently than others, resulting in an uneven distribution of samples among different failure types. If ML is applied to a failure identification problem, such an imbalance among different failure classes compromises the training phase of a ML model, resulting in performance degradation during the inference phase (i.e., the estimation of the type of failure). Such a trend is visible on least represented failure classes in [Tre23], where field data collected for seven months have been utilized for ML-based failure identification

In SEASON, we investigated a direct and comprehensive comparison between different ***model-centric*** and ***data-centric*** **ML approaches** for dealing with the imbalanced training problem in ML-based failure management, with failure identification as the considered use-case and NN as the employed ML model. The model-centric approaches investigated in this work focus on modification of the standard loss function of NN, as well as changing the sampling strategy of

batches within a training epoch of NN to account for the imbalanced distribution of failure samples in the training dataset. To that end while modifying loss function, the contribution of different failure classes to the overall training loss has been re-weighted based on the extent of their representation in the training dataset. With focal loss, this approach has been extended to the sample level, further reducing the contribution of correct classifications to the overall loss so that NN could focus more on misclassifications, which are typically from less frequent failure classes. The combined performance of re-weighting of failure classes as well as samples has also been investigated to address the imbalanced training problem. As for sampling strategy during training, a balanced mini-batch training approach has been studied that samples imbalanced training data in a balanced manner for each batch within a training epoch.

On the data-centric side, the objective is to improve the data quality, and a typical approach is data augmentation. SMOTE-TOMEK and generative and adversarial networks (GANs)-based techniques have been used to augment data of under-represented failures by generating synthetic samples to reduce their scarcity. A balanced mini-batch training approach, which can be considered as a hybrid of model-centric and data-centric approaches, has also been studied in the scope of this work. All these techniques have been individually applied to an optimized baseline NN, and the resultant performance has been compared in terms of classification accuracy (i.e., F1-score) and computational complexity (i.e., sum of the training time of the employed NN-based failure identifier and additional time required for processing of the training data).

For more technical details on the techniques investigated, the reader can refer to [Kha24], while here the performance comparison is reported. The following model-centric techniques have been considered: weighted categorical cross entropy (WCCE) loss, focal loss, weighted focal loss, and Balanced mini-batch training (BmBT). Regarding data-centric approaches, SMOTE-TOMEK and CT-GAN have been considered.

Performance comparison will show that an improvement of data quality (i.e., achieved through data-centric techniques) has a more relevant impact on ML performance.

Data has been collected from an experimental testbed shown in the figure below:

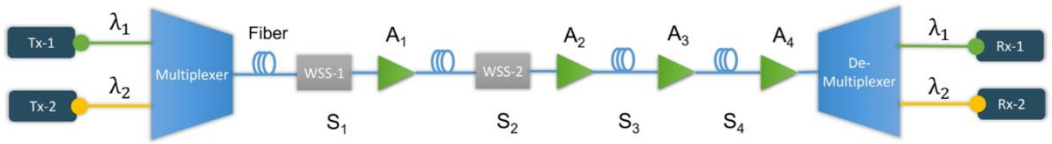

Figure 6.7-1: Experimental testbed.

The considered testbed includes two Ericsson SPO 1400 optical devices, SPO-1 and SPO-2. Each SPO is equipped with OTN muxponder, exploiting an optical tunable coherent transceiver at 100 Gb/s with dual polarization quadrature phase shift keying (DP-QPKSK) modulation format. Each transceiver is composed of a transmitter (Tx) and a receiver (Rx). Two channels i.e., channel-1 and channel-2, with around 37.5 GHz of spectrum width, central frequencies λ1 = 194.1 THz and λ2 = 194.2 THz, respectively, have been set up in the testbed for this study. Two arrayed waveguide gratings (AWGs) have been used at Tx side and Rx side for multiplexing and de-multiplexing the optical signals. The optical link is composed of four spans, labeled S1, S2, S3,

and S4. Each span consists of a single mode fiber spool with length of approximately 80 km, and a fiber attenuation co-efficient of 0.2 dB/km. The attenuation of optical signals along the optical link has been compensated using a series of erbium doped fiber amplifiers (EDFAs) denoted by A1, A2, A3, and A4, configured in a fixed gain mode. To artificially generate failures in the network, two wavelength selective switches (WSSs), namely WSS-1 and WSS- 2, have been placed at the end of S1 and S2, respectively. Four failure conditions on both channels have been considered i.e., attenuation, filter tightening, filter tightening + attenuation, and filter shift + attenuation. The bit error rate (BER) and optical signal-to-noise ratio (OSNR) values have been collected from the two receivers with a sampling interval of approximately 4 seconds. A total of 2000 samples have been collected for each failure per channel and then, after removing duplicates with the removal of duplicates followed by the manual removal of samples, an imbalance to in the dataset has been created to mimic the real network scenario where higher frequency of occurrence of some failures results in sufficiently well-representation of those failures and under-representation of other failures in the training dataset. The Table 6.7-1 shows the imbalanced distribution of samples among the considered failures in our case:

Table 6.7-1: Data distribution.

Failure type	Number of samples in overall dataset		Number of samples in training dataset	
	Channel-1	Channel-2	Channel-1	Channel-2
Attenuation	1124	1205	717	773
Filter tightening	869	981	552	632
Fight tightening + attenuation	526	601	328	394
Filter shift + attenuation	360	289	231	184

From this imbalanced dataset, 20% of the data has been kept as a test dataset for the final model evaluation after training, and the remaining 80% has been split into training and validation datasets using an 80-20% split ratio. That validation dataset has been used during the training phase to ensure that the NN is not overfitting.

The performance of considered model-centric and data-centric approaches has been compared with each other against a base- line NN. Optuna, a Bayesian optimization-based tool, has been used to tune the hyperparameters of baseline NN. The resultant baseline NN (i.e., with tuned hyperparameters) contained 3 neurons in the input layer, 189 neurons in the first hidden layer, 220 neurons in the second, and 4 neurons in the output layer. The dropout regularization rate has been 0.159 to prevent over-fitting, with the learning rate of 8.25×10^{-4} and batch size of 64. Tanh has been used as the activation function for the hidden layers, while SoftMax has been used for the output layer. All the afore described techniques have been applied to this optimized baseline NN, and the performance has been evaluated in terms of computational cost and F1-score for both the channels. F1-score is one of the appropriate metrics to evaluate classification performance in case of class imbalance because it takes into account both precision (i.e., the ratio of true positives to the sum of true positives and false positives, measuring the model's ability to avoid false positive errors) and recall (i.e., the ratio of true positives to the sum of true positives and false negatives, quantifying the model's ability to avoid false negative errors). Figure 6.7-2 shows the results on channel-1 in terms of the obtained F1-score on the unmodified and imbalanced test dataset for all the considered failures.

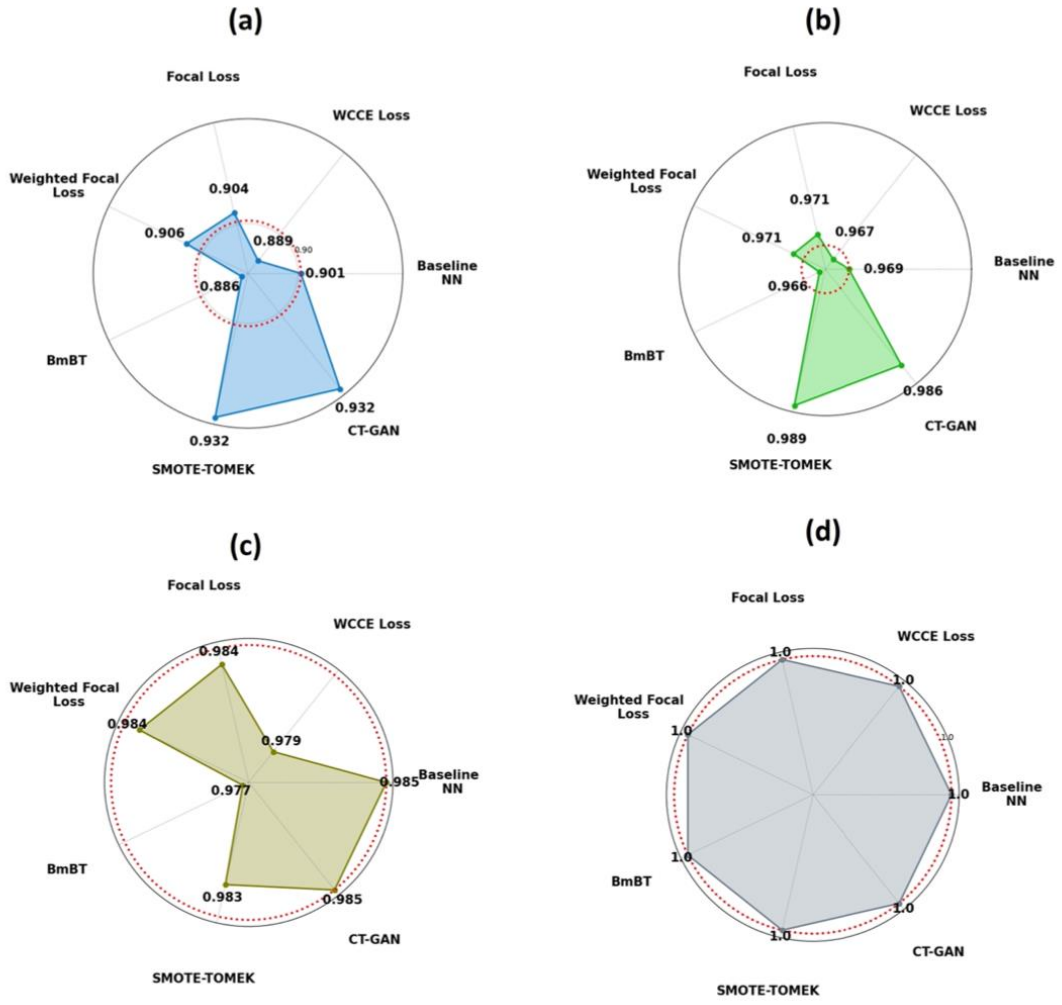

Figure 6.7-2: F1-score comparison of all considered techniques on channel-1 for (a) Filter shift + attenuation, (b) Filter tightening + attenuation, (c) Attenuation and, (d) Filter tightening.

Since filter shift + attenuation has been the failure with the fewest samples in the training dataset, we can see that the F1-scores obtained on it are on the lower side as compared to other failures with more samples. The red dotted circle represents the reference score i.e., score on the baseline NN. As shown in Figure 6.7-2 (a), data-centric approaches outperformed model-centric approaches on this under-represented failure, with an improvement of 3.1% being observed in this case. For filter tightening + attenuation, Figure 6.7-2 (b), i.e., the second least represented failure class in the training dataset, we observed a similar tendency that data-centric techniques perform better, with up to 2% improvement observed. Few of the model-centric approaches (i.e., focal loss and weighted focal loss) achieved similar performance as data- centric approaches for attenuation, Figure 6.7-2 (c), i.e., one of the well-represented failure classes in the training dataset, however, none of the approaches could outperform baseline NN, which classified this failure extremely well with an F1-score of 0.985. For filter tightening Figure 6.7-2 (d), the other well-represented failure class, also having slightly disjoint BER and OSNR values from other failures, the employed NN-based failure identifier learnt the underlying pattern extremely well in all scenarios, resulting in its perfect classification.

Figure 6.7-3 shows the averaged computational time for each approach in terms of training time of the employed NN for failure identification after the application of each technique, as well as the additional processing time (applicable only to data-centric techniques) for training dataset. Additional processing time includes training time of ML models, i.e., in case of CT-GAN, and/or time taken to generate synthetic samples for training dataset. These times have been monitored on an Intel(R) Core(TM) i7-12700H @ 2.30 GHz with NVIDIA GeForce RTX 3060 Laptop GPU.

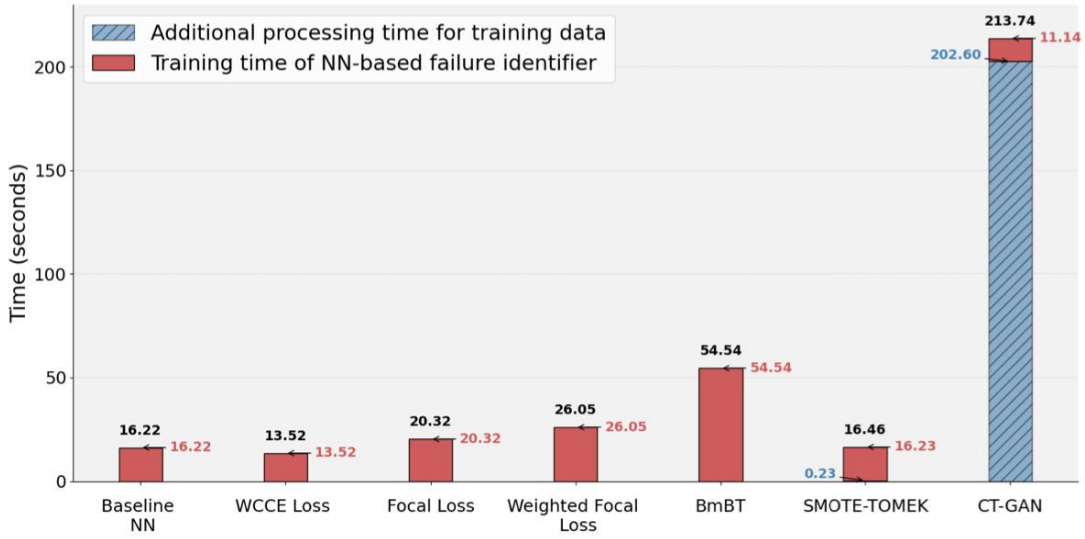

Figure 6.7-3: Computational costs.

As can be seen, with BmBT approach, the NN-based failure identifier takes the longest training time. The possible reason for this is that in our implementation of this technique, random sampling of training data has been performed for each batch within an epoch to select an equal number of samples from each failure class, which prolonged the training process. On the other hand, training time of NN-based failure identifier, with CT-GAN additional synthetic samples in training dataset generated using CT-GAN, has been the shortest because the addition of high-quality synthetic samples to the under-represented failure classes increased their overall representation in the training dataset which resulted in faster NN convergence. However, this has been achieved at the cost of high additional processing time for training data as training of CT-GAN itself takes long because of its inherent adversarial nature. SMOTE-TOMEK, the other considered data-centric approach, generates synthetic samples through linear interpolation, so there is no ML model involved for data augmentation and thus no significant additional processing time.

In conclusion, based on these results, it can be inferred that the data-centric approaches tend to be more effective in handling imbalanced scenarios because the addition of synthetic samples diversifies the training dataset, allowing the model to better learn and recognize different patterns in the dataset and, as a result, improve performance on the test dataset. However, some data-centric approaches may require significant additional processing time. When training of the employed NN for failure identification has to be performed offline and the availability of computational resources such as GPUs is not an issue, GAN-based approaches such as CT-GAN can be used. However, if computational resources are very limited then data-centric approaches such as SMOTE-TOMEK can be used to augment training data.

6.8 SENSING

6.8.1 High-precise position localization

At the time of writing, we are investigating different machine learning (ML) techniques for detecting various types of vibrations/movement around an optical fiber. We achieved high accuracy in classifying and identifying anomalies in relation to KPI 5.3, i.e., achieving position measurement within 4 ns and < 1 meter accuracy.

The experimental setup, reported in Figure 6.8-1 involves monitoring the fluctuations of the state of polarization (SOP) to detect and localize anomalies around the fiber with high precision. We employed a Novoptel PM1000 polarimeter and an active laser source that ensures accurate measurement of SOP changes. These changes can be correlated to specific positions along the fiber. The ML model enhances detection accuracy, achieving 95% accuracy even in noisy environments as shown in Figure 6.8. This approach ensures timely detection and mitigation of potential threats, maintaining network stability and resilience. These results have been submitted to OFC 2025.

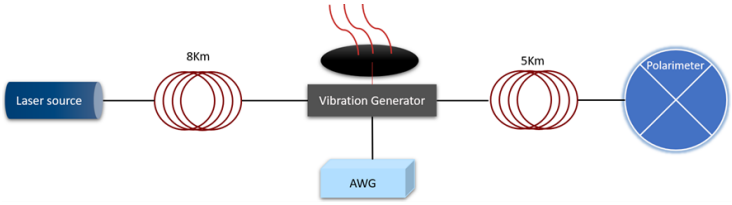

Figure 6.8-1: Experimental setup for measuring vibrations.

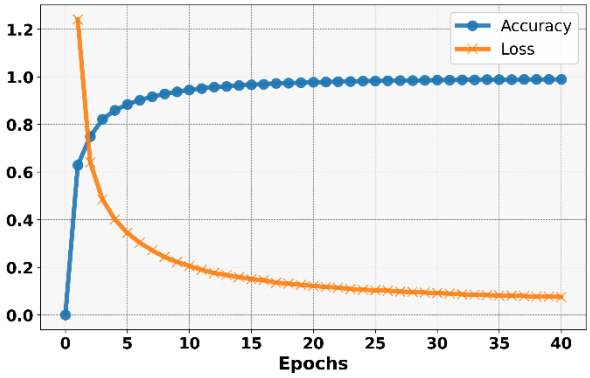

Figure 6.8-2: ML model training accuracy and loss.

Building on this, we applied ML for detecting and classifying multiple types of mechanical events, such as small hits, vertical displacements, and shaking. These events are characterized by unique polarization signatures, which are captured and analyzed using the polarimeter. The experimental setup involves generating these events using an Arduino-controlled robotic arm, which manipulates the fiber to create specific disturbances as illustrated in Figure 6.8-3.

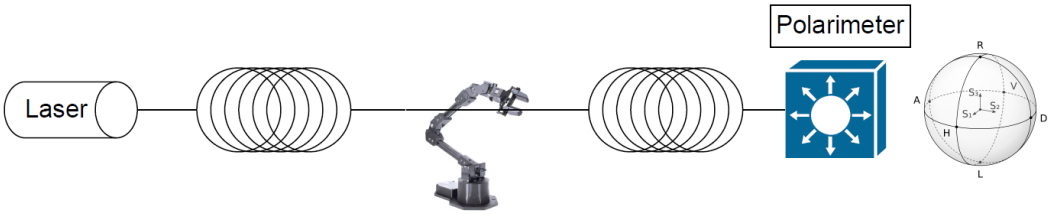

Figure 6.8-3: Proposed setup for events generation and robotic arm.

The data collected from these experiments is then processed and used to train various ML models, including Random Forest, Support Vector Machine (SVM), Logistic Regression, and Extreme Gradient Boosting (XGBoost). Among these, Random Forest and XGBoost showed superior performance, achieving high accuracy and efficiency in detecting and classifying anomalies. The integration of ML with SOP monitoring allows for real-time detection and early identification of potential threats. The ML models not only enhance detection accuracy but also enable proactive maintenance by predicting and mitigating potential fiber damage before it occurs. This approach ensures timely interventions, reducing the risk of network disruptions and improving overall network resilience. Furthermore, the use of a Weighted Performance Metric (WPM) to evaluate the ML models highlights the balance between accuracy and training time, ensuring that the chosen models are both effective and efficient. The study's findings underscore the transformative potential of ML in enhancing the reliability and stability of optical communication systems, making it a valuable tool for achieving the high precision required by KPI 5.3. This last investigation has been submitted to IEEE ICMLCN 2025.

7 DATA PLANE PROTOTYPES – STATE OF THE ART / INNOVATIVE ASPECTS OF THE COMPONENTS TO BE DEVELOPED

This section introduces the different WP3 components developed and proposed within SEASON project, focusing on innovations in the data plane that support high-capacity, scalable, and energy-efficient networks. Key challenges in MBoSDM optical networks are addressed towards enhancing performance, power efficiency and flexibility. The prototypes/components and research activities include advanced optical transceivers, amplifiers, switching solutions, and monitoring systems designed to enable efficient MBoSDM operations. Each component is described also presenting technical specifications, interfaces, and projected roadmap for future development, contributing to SEASON's goal of developing sustainable, high-capacity optical infrastructure from access to cloud.

7.1 MBOSDM NODE PROTOTYPE (C3.1)

7.1.1 Description

In the framework of SEASON project, CTTC has developed a multiband (MB) over spatial division multiplexing (SDM) switching node prototype to advance the capabilities of current node options. The architecture is designed to support both spectral (band and wavelength) and spatial granularities to meet the capacity scaling and traffic demands of next-generation optical networks. It ensures a highly adaptable, modular, and flexible switching paradigm with advanced capabilities suitable for evolving network environments. Spectral granularity, in terms of wavelength, is achieved using fixed- and flex-grid wavelength division multiplexing (WDM) technology, utilizing C-band 100 GHz AWG and programmable WSS devices, respectively. The WSS bandwidth and central wavelength can be adjusted with 12.5 GHz granularity within the C-band. The design includes two WSS units with 1x2 ports and two AWG units with 1x5 ports on fixed 100 GHz ITU-T C31-C35 channels to leverage WDM [8]. MB dimension is addressed by incorporating four 1x3 MB filters operating within the S-, C-, and L-bands (two units per direction for bidirectional MB transmission). SDM is achieved by utilizing distinct spatial paths, enhancing switching capabilities and network throughput. To this end, fan-in/-out devices are included, enabling efficient core switching with a 19-core multi-core fiber (MCF) of 25.4 km (two cores per direction). This setup ensures bidirectional SDM transmission, providing bidirectional core availability. The prototype supports core switching across four cores within the available MCF and facilitates add/drop operations. The core structure is built with an 18x18 optical matrix switch, offering multiple and dynamic switching configurations.

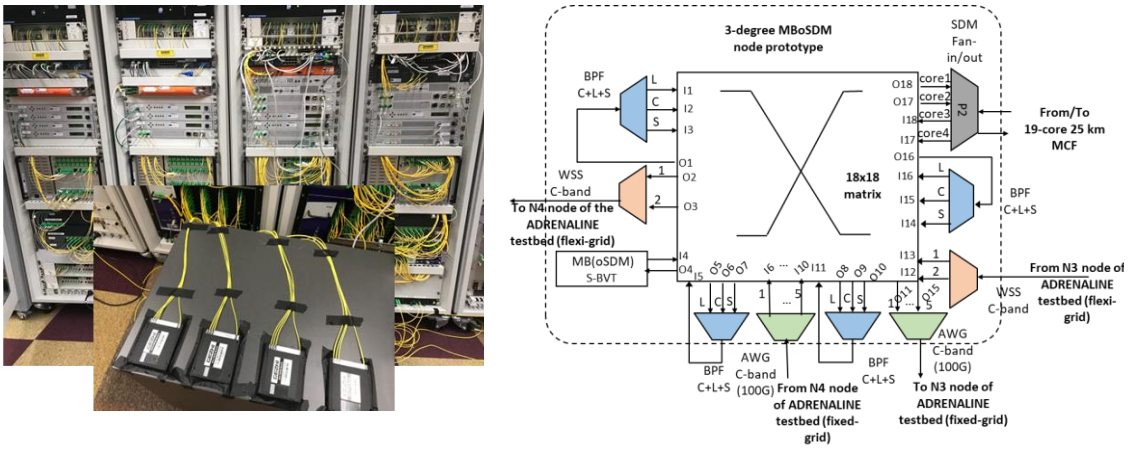

Figure 7.1-1: MBoSDM switching (a) prototype integrated in the ADRENALINE testbed and (b) architecture with the main building blocks.

The node prototype is integrated within the ADRENALINE testbed, establishing different path connections to two network nodes. Node programmability and flexibility are achieved using WSS devices, which allow full reconfiguration within the C-band for flex-grid operation and optimized resource utilization, as seen in Figure 7.1-1 (b). This design also ensures flexibility and versatility regarding exploited granularities and available resources (both spectral and spatial). Broader spectrum coverage and the use of spatial channels significantly enhance overall network capacity, flexibility, and efficiency. The node solution can be scaled to meet target capacity requirements by increasing the number of ports in the matrix and WSS modules. These capabilities create a switching solution that aligns with the anticipated demands of high-capacity and dynamic network environments.

Table 7.1-1: MBoSDM switching node prototype parameters and key features.

Parameter	Specifications
Operation bands	S-band (1460-1530 nm) C-band (1530-1565 nm) L-band (1565-1625 nm)
Operation cores	2 cores per direction
Insertion loss	< 3.2 dB
Optical power	< 20 dBm
PDL	< 0.1 dB
Switching speed	20 ms

Table 7.1-2: MBoSDM switching node key features.

Key features	Specifications
Scalability	Limited to the matrix and filters port count
Flexibility	WSS (flex- grid operation) Enhanced resources and bandwidth
Programmability	WSS central wavelength, port attenuation and bandwidth
Operation	MB, WDM and SDM

Table 7.1-1 and Table 7.1-2 specifies the node parameters, including main bands and cores of operation, insertion loss (IL), maximum optical power allowed, polarization-dependent loss (PDL), and switching speed.

7.1.2 Interfaces

The proposed MBoSDM node prototype can be controlled by means of SDN agents. This activity has not yet started and will be planned in the following months. A set of control operations will be specified towards enabling SDN control of the node prototype. Additional key programmable parameters will be identified to implement low level interfaces that will enable the reconfiguration of specific node building blocks.

S.No	Interface	Description
1	SDN control	SDN agent implementation for node reconfiguration and programmability.
2	Identification of node control operations	A set of node control operations will be identified to enable suitable SDN control integration.

7.1.3 Status and Roadmap

S.No	Status and Roadmap	
1	Status	▪ Currently, a first version of the node prototype has been developed. ▪ Initial proof-of concept assessment has been implemented targeting different scenarios of interest.
2	Roadmap	▪ Initial integration with SDN control plane Q2 2025. ▪ Node optimization Q2 2025. ▪ Integration with transceiver prototype and control Q4 2025.

7.1.4 Assessment

Here we have evaluated the IL of the matrix included in the proposed MBoSDM node prototype [Nad24-2]. For this analysis, we used a tunable laser source injected at the I4 input node, operating within the S, C, and L range of 1500-1610 nm in order to assess the node performance. We have considered the switching operations from input I1 to all available node outputs (see Figure 7.1-1), evaluating multiple wavelengths within the S, C, and L bands. This evaluation allowed us to assess the performance and consistency of the switching matrix across a broad spectrum, ensuring that it can handle a variety of MB channels efficiently. As shown in Figure 7.1-2, the measured IL values remain consistent across different wavelengths for the various switching analyzed connections. The achieved results indicate robust performance across a wide spectral range, ensuring efficient and reliable switching operations.

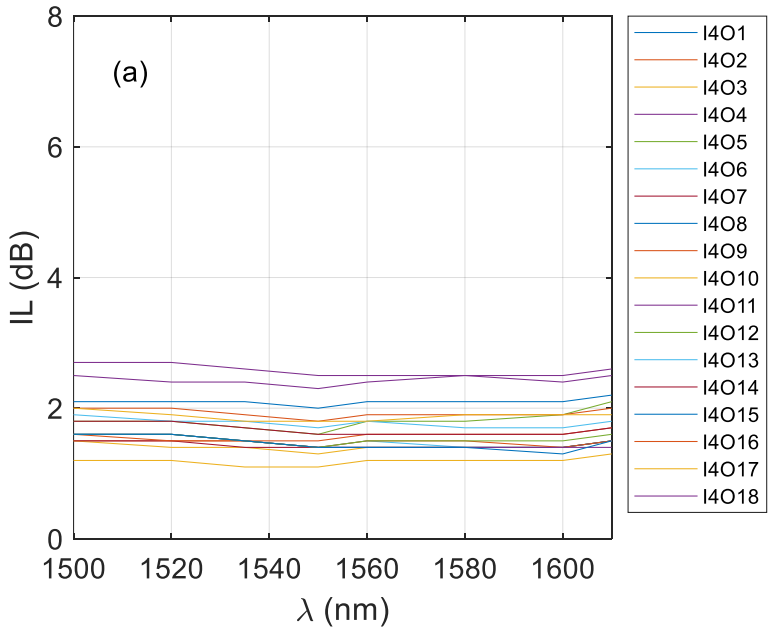

Figure 7.1-2: IL at different wavelengths due to switching from input I1 to all the available outputs of the proposed MBoSDM node architecture.

7.2 MULTI-GRANULAR OPTICAL NODE PROTOTYPE (C3.2)

7.2.1 Description

Within the scope of B5G-OPEN, a multiband (semi-) filter-less add/drop node prototype was designed. In SEASON, the prototype was extended into a MBoSDM multi-granular switching node, enabling fiber switching for SDM (i.e., switching the entire spectrum range among fibers/cores) and enabling band switching (i.e., switching one entire band among fibers). The prototype is cost effective, consisting of four bundles containing two SMF, eight multiband (S + C + L) multiplexers (MB Mux and MB Demux) and an optical matrix switch responsible for routing the bands accordingly. Monitor couplers are also introduced for effective monitoring of the ports during the validation and the operation of the prototype. The prototype architecture is shown in Figure 7.2-1.

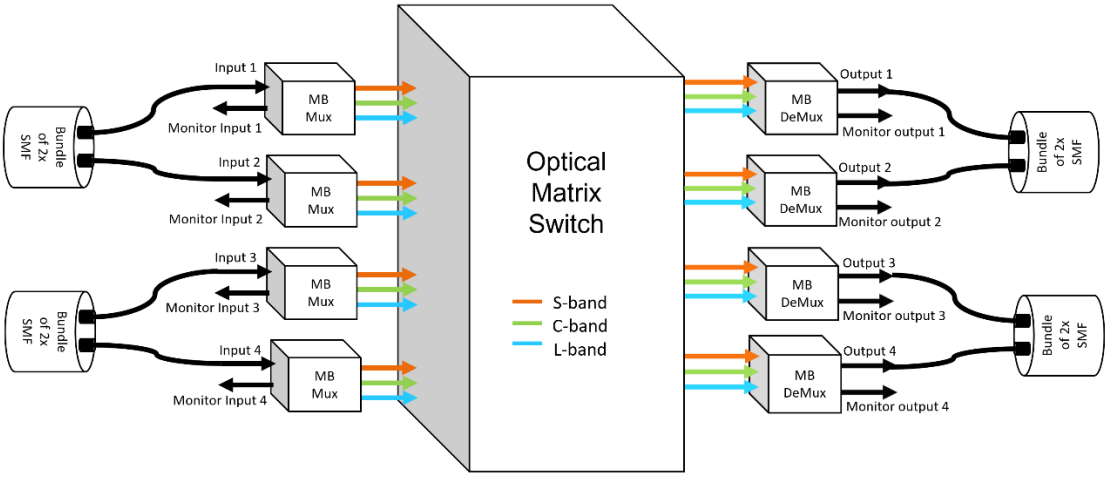

Figure 7.2-1: Multi-granular Optical Node Prototype Architecture.

7.2.2 Interfaces

The switch is fully programmable, allowing for remote operations between the multiple inputs and outputs.

S.No	Interface	Description
1	SDN Control	SDN agent implementation for node reconfiguration and programmability.

7.2.3 Status and Roadmap

In the assembly process, each four multiplexers and four monitor couplers are integrated in a single box or chassis, so we end up with two chassis and the optical matrix switch, the assembled prototype is present in HHI laboratory and shown in Figure 7.2-1.

S.No	Status and Roadmap	
1	Status	An initial version of the node prototype is being assembled The software control agent and the corresponding software code is finished
2	Roadmap	A proof of concept testing and initial result of the node prototype and assembly with the control agent in Q4 2024 & Q1 2025 Integrated in the MB (S+C+L) testbed for the Demos in Q2 2025

7.2.4 Assessment

The prototype was characterized using a polarization-dependent loss analyzer (PDLA) to verify insertion loss (IL) and PDL of the multiple paths. An example of the characterization curves can be observed in Figure 7.2-2 (b), where it is possible to note an average IL below 3 dB and a PDL below 0.1 dB across all bands for all pathing possibilities of the prototype. These values are also presented in Table 7.2-1, where the specifications of the device are summarized. The gaps

observed in the transitions of the bands occur due to the overlap of the distinct transfer functions of the band-specific filters that compose the MB Mux and MB Demux. Thus, these transitional regions are out of the specification of operation of the device.

Table 7.2-1: Prototype specifications.

Parameter	Specification
Operation Bands	S-band: 1460-1522 nm C-band: 1527-1565 nm L-band: 1574-1640 nm
Insertion Loss	< 3.0 dB
PDL	< 0.1 dB

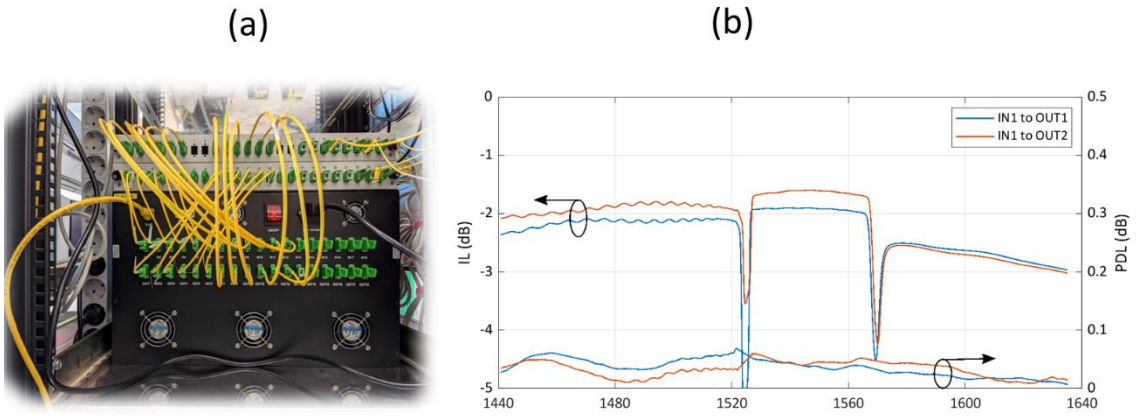

Figure 7.2-2: a) One of the Chassis and the Optical Matrix Switch b) Example of the Prototype Characteristics.

7.3 SPATIAL PON NODE (C3.3)

7.3.1 Description

In the framework of the SEASON project, a prototype of a Multicore Passive Optical Network (PON) node has been developed, showcasing an innovative and flexible architecture designed to optimize the use of multicore fiber (MCF) technology in access networks. This prototype enables efficient management of spatial lanes within the MCF, supporting dynamic traffic adaptation and energy efficiency while maintaining high network performance.

The Multicore PON node prototype supports multiple spatial lanes that can be dynamically aggregated or bypassed using a spatial switch, as depicted in the architecture diagram (Figure 7.3-1 (a,b,c)). The prototype architecture follows a 2 lanes configuration, where two spatial lanes can be aggregated/disaggregated over two OLT ports. The spatial switch in the architecture plays a crucial role, either bypassing the spatial lanes directly to their corresponding OLT ports (2x2 configuration, Figure 7.3-1 (b)) or directing them to a splitter/combiner for

aggregation (2x1 configuration, Figure 7.3-1 (c)). The splitter/combiners are essential for realizing spatial aggregation, allowing multiple spatial lanes to be combined and efficiently transmitted over the available OLT ports.

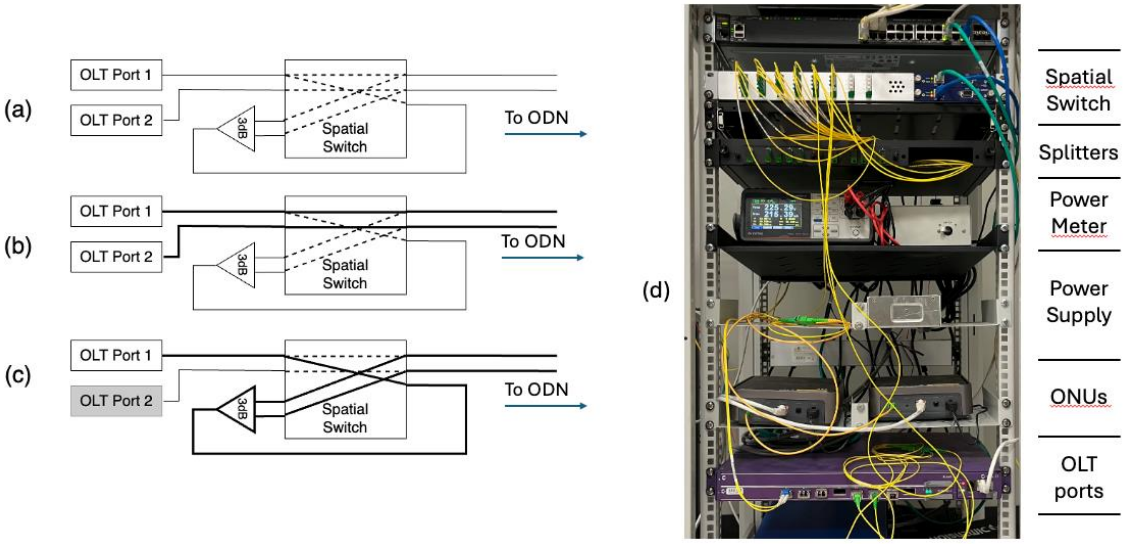

Figure 7.3-1: (a) 2 lanes spatial PON architecture; (b) 2x2 configuration; (c) 2x1 configuration; (d) Spatial PON Prototype

In practice, the prototype is implemented with a compact and modular design, as shown in the photo of the physical setup (Figure 7.3-1 (d)). The prototype shown in the photo includes an end-to-end spatial PON system comprising several functional layers: an ONU layer, a splitting layer for realizing the ODNs and spatial aggregation, a switching layer to control spatial aggregation, and an OLT ports layer for the activation and deactivation of transceivers. Additionally, the photo shows an energy consumption measurement device that will be used in the ongoing project for the assessment of energy savings. The prototype's modularity allows for flexible deployment in various network scenarios, accommodating different traffic demands and network configurations.

7.3.2 Interfaces

The table below outlines the key interfaces supported by the Multicore PON node prototype, each playing a crucial role in the management and operation of the system. These interfaces facilitate communication between the prototype and higher-level network management systems, allowing for efficient service setup and dynamic control of network elements. The REST interface provides a north-bound communication channel for the transport orchestrator, enabling the configuration of services with specific requirements such as VLAN characterization, bandwidth allocation, and prioritization of traffic. The NETCONF PON interface allows direct interaction with the OLT ports, managing the activation and deactivation of transceivers. Additionally, the NETCONF SWITCH interface is used to control the spatial switch, handling the physical aggregation and disaggregation of spatial lanes. Each of these interfaces is integral to the prototype's functionality, ensuring flexibility and control in a complex network environment.

S.No	Interface	Description
1	REST	This high level north-boud interface allows transport orchestrator to setup a service with specific requirementes in terms of vlan characterization, bandwidth assignment, time prioritization.
2	NETCONF PON	The prototype supports NETCONF to interact with OLT ports and control port activation/deactivation.
3	NETCONF SWITCH	The prototype supports NETCONF to interact with the spatial switch and control physical aggregation/disaggrgation of spatial lanes.

7.3.3 Status and Roadmap

S.No	Status and Roadmap	
1	Status	Realized physical prototype of node for PON spatial aggragation/disaggregation Realized control of the node for realization of 2x2 and 2x1 configurations
2	Roadmap	Implement dynamic logical association of users to different OLT ports to be operated in conjunction with physical aggregation/disaggregation, expected in Q1 2025

7.3.4 Assessment

The Multicore PON node prototype's capabilities have been evaluated by assessing its performance in different configuration settings using a controller and the management interface of the Polatis switch. These evaluations are crucial to demonstrate the dynamic adaptability of the system in managing spatial lanes and OLT ports.

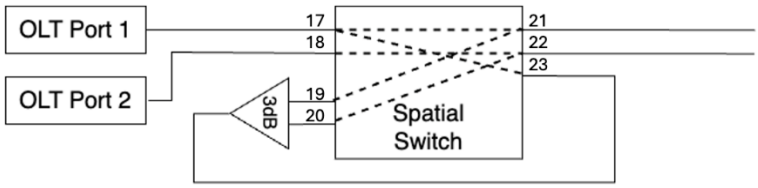

Figure 7.3-2: Two lanes setup adopted for testing.

Figure 7.3-2 shows the adopted setup for testing purpose. In the figure, port identifiers of the spatial switch are reported.

Figure 7.3-3 presents the configuration of the node in a 2x2 setting. On the left side of the figure, the controller interface is shown, which is responsible for setting and managing the configuration. It displays the commands and status outputs as the 2x2 configuration is implemented. On the right side, the management interface of the Polatis switch provides a visual representation of the cross-connects, confirming that the spatial lanes are correctly routed and aggregated according to the 2x2 configuration settings. This demonstrates the successful application of the controller's commands and the switch's ability to manage the spatial lanes effectively.

Figure 7.3-3: 2x1 configuration demonstration.

Figure 7.3-4 illustrates the node configuration in a 2x1 setting. Similar to the first figure, the left side shows the controller interface managing the configuration process, while the right side displays the Polatis switch's management interface. In this scenario, the 2x1 configuration involves aggregating two spatial lanes into a single output, demonstrating the system's flexibility in adapting to different network demands. The visual feedback from the switch's interface confirms that the configuration is applied correctly, with the spatial lanes being managed and routed as intended.

These assessments highlight the prototype's capability to dynamically adjust to different configurations, ensuring optimal network performance. The real-time monitoring and control provided by the integrated interfaces are critical for maintaining the efficiency and reliability of the system, showcasing its potential for deployment in advanced optical networks.

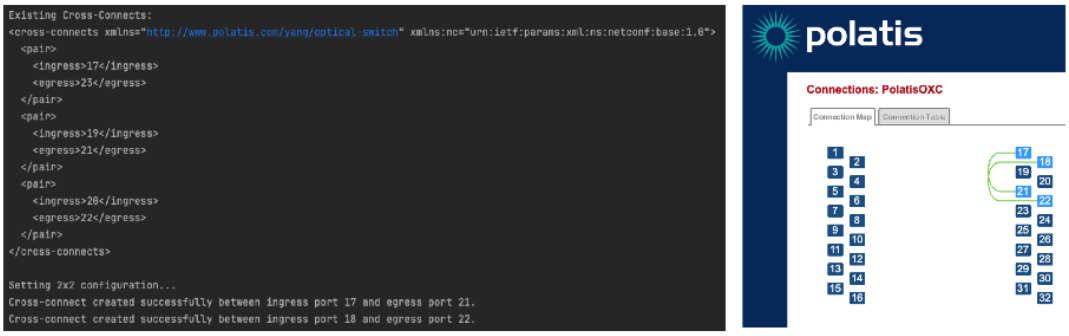

Figure 7.3-4: 2x2 configuration demonstration.

7.4 MB(oSDM) S-BVT PROTOTYPE (C3.4)

7.4.1 Description

A MB(oSDM) S-BVT prototype has been proposed and developed in the framework of SEASON project. This versatile and innovative solution enables us to enhance network efficiency, resilience, and sustainability [Nad23]. This transceiver prototype supports MB operation within the S, C, and L bands, offering capacity scalability. It features a flexible and adaptable structure composed of various bandwidth/bit rate variable transceivers (BVTs), which can be based on different technologies, operate beyond the C-band, and be activated or deactivated according

to traffic demands and network requirements. The proposed transceiver architecture is shown in Figure 7.4-1Figure 7.4-1. A high-capacity flow is generated and distributed over the network using an optical aggregator/distributor with band-pass filters (BPFs). Additionally, programmable filters such as wavelength selective switches (WSSes) or tunable filters (TFs) can be included to perform SSB modulation, enhancing resilience against chromatic dispersion. Thanks to its modular architecture, both point-to-point (P2P) and point-to-multi-point (P2MP) connectivity are supported, reducing cost and complexity while enhancing efficiency. The sliceable architecture allows for the dynamic allocation of available MB bandwidth into smaller, manageable portions that can also be transmitted through different fiber spatial channels.

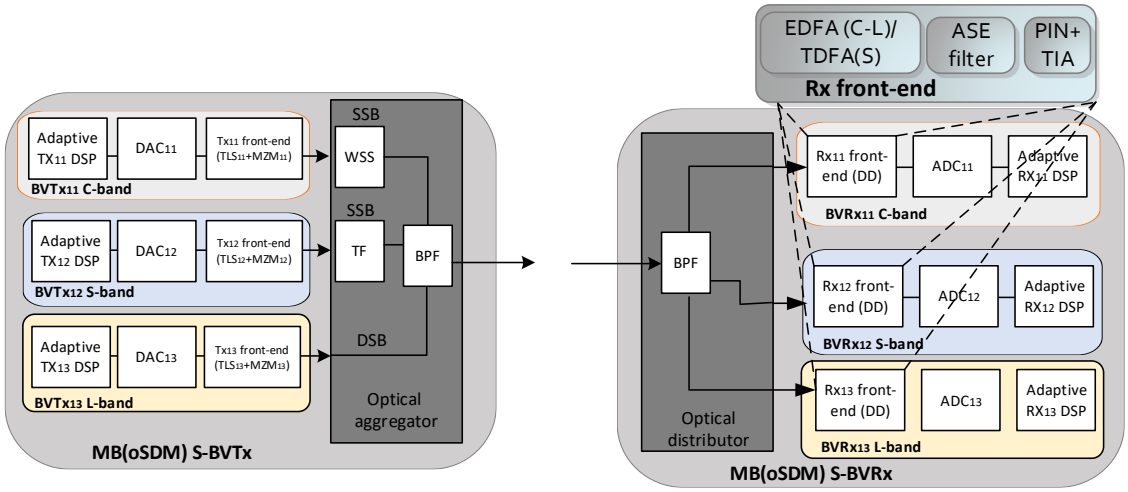

Figure 7.4-1: MB(oSDM) S-BVT prototype architecture.

The developed prototype (Figure 7.4-1) leverages advanced modulation formats, such as orthogonal frequency division multiplexing (OFDM), and is based on intensity modulation (IM) and direct detection (DD). Adaptive loading is implemented to further enhance overall flexibility and performance [Nad23-2]. Digital-to-analog conversion is performed using a digital-to-analog converter (DAC) operating at 64 GSa/s. Details on the implemented adaptive digital signal processing (DSP) can be found in [Nad23]. At the transmitter side, external modulation with Mach-Zehnder modulators (MZMs) and tunable laser sources (TLS) per band are adopted. An external cavity laser (ECL) is used for the S-band contribution. At the receiver side, suitable amplification options are targeted for each band based on doped fiber amplifier (xDFA) technology. Specifically, erbium DFA (EDFA) is used for the C and L bands, while thulium DFA (TDFA) is considered for the S-band. The receiver front-end also includes a filtering stage for amplified spontaneous emission (ASE) noise removal and simple PIN photodiodes. An oscilloscope operating at 100 GSa/s is used for analog-to-digital (ADC) conversion.

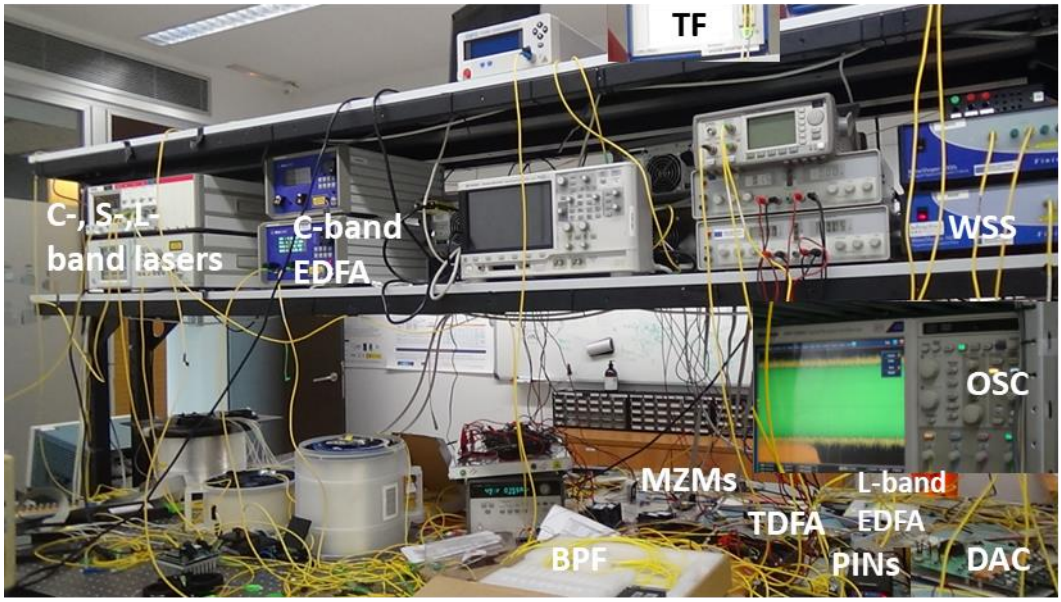

Figure 7.4-2: MB(oSDM) S-BVT prototype at CTTC premises.

7.4.2 Interfaces

The programmability and interoperability of the proposed MB(oSDM) transceiver can be facilitated by the effective implementation of open SDN agents [Nad23]. These agents reconfigure various system parameters and optical elements according to the network requirements. The SDN paradigm provides the flexibility needed to automatically satisfy the stringent and varying demands of the network. This is achieved by dynamically adjusting the transceiver components and their parameters appropriately. Specifically, the OpenConfig open data model can be implemented to suitably reconfigure the transceiver [OpenConfig24]. Various programmable transceiver parameters and elements have been identified for the effective configuration and modification of the proposed MB(oSDM) S-BVT. Primarily on the transmitter side, it is possible to adjust the central frequency and power of the TLS, as well as the DAC channels. On the receiver side, the OSC can be reconfigured. Additionally, an activity related to energy-aware routing computation has started including specific and relevant power consumption attributes of the underlying transport devices (S-BVT) to extend the current TAPI Context information (see section 3.4) [Nad24].

S.No	Interface	Description
1	SDN agents	Implementation of SDN agents, based on OpenConfig, to suitable program the MB(oSDM) S-BVT.
2	Energy-aware routing computation	Extend current TAPI Context information to include specific and relevant power consumption attributes of the MB(oSDM) S-BVT.

7.4.3 Status and Roadmap

S.No	Status and Roadmap	
1	Status	A first version of the MB(oSDM) S-BVT working within S+C+L-bands have been implemented and experimentally validated. Initial proof-of-concept validations considering different scenarios of interest (i.e., back-to-back, B2B, SSMF up to 75 km and MCF transmission, network scenario including CTTC ADRENALINE testbed). Initial energy-aware routing computation activity started including the power consumption values of the MB(oSDM) S-BVT.
2	Roadmap	Optimization of the transceiver in Q2 2025. Assessing additional scenarios in Q2 2025. Integration with the control plane and CTTC MBoSDM switching node prototype in Q4 2025.

7.4.4 Assessment

The MB(oSDM) transceiver solution has been experimentally assessed in an initial proof-of-concept. Specifically, different scenarios have been considered including: i) B2B configuration; ii) MB transmission after up to 75 km of standard single mode fiber (SSMF) and iii) MBoSDM transmission after 19-cores MCF of 25.4 km. The signal-to-noise ratio (SNR) profiles in a B2B configuration are depicted in Figure 7.4-3. The figure illustrates that the three slices operating in different bands exhibit similar performance in terms of SNR per subcarrier. The main factor contributing to the degradation at higher frequencies, associated with higher subcarrier numbers, is the limited bandwidth of the DAC, which is approximately 13 GHz. Specifically, the electrical OFDM signal spans a 20 GHz bandwidth, with 512 subcarriers. In the B2B configuration, an aggregated capacity of 212 Gb/s (S+C+L) is achieved ensuring a target BER of 4.62e-3, as seen in Figure 7.4-3.

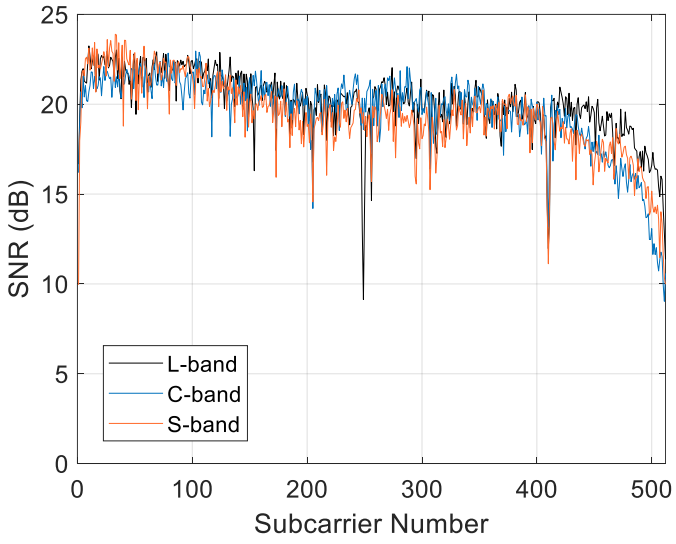

Figure 7.4-3: B2B SNR profile of the S-, C- and L-band slices generated with the MB(oSDM) prototype.

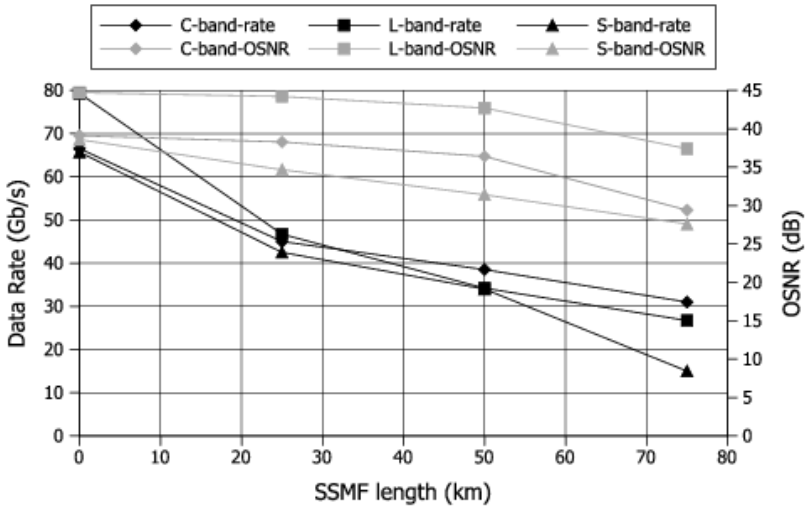

Figure 7.4-4: Achieved data rate and OSNR per slice/band considering different fiber paths of up to 75 km of SSMF.

After 25 km of SSMF, the aggregated data rate drops to 134 Gb/s, but thanks to the implementation of adaptive loading algorithms, the three contributions still exhibit similar performance (see Figure 7.4-4). The received amplified spectra after 25 km of SSMF and with adaptive loading are depicted in Figure 7.4-5. From the DSB L-band spectrum, shown in Figure 7.4-5 (c), it could be seen that the implemented adaptive loading algorithm has set to 0 the subcarriers with lower SNR.

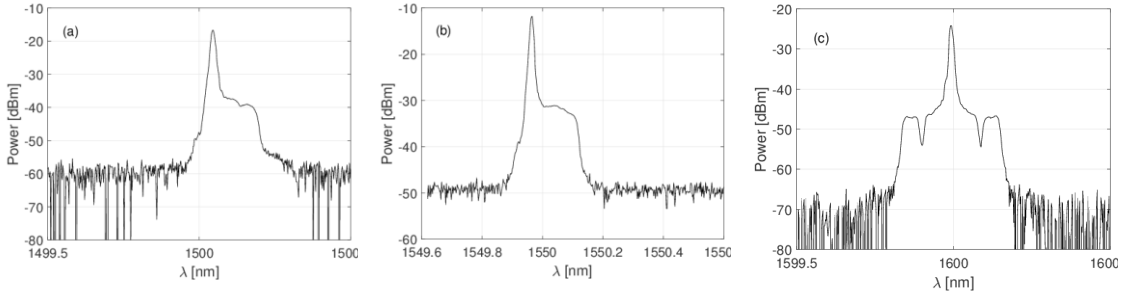

Figure 7.4-5: OSA captures applying adaptive loading after 25 km of SSMF of the (a) SSB S-band, (b) SSB C-band and (c) DSB L-band signals generated with the MB(oSDM) S-BVT prototype.

After 50 km and 75 km, the aggregated capacity further decreases to 107 Gb/s and 73 Gb/s, respectively. Due to setup implementations, the L-band contribution achieves higher optical signal-to-noise ratio (OSNR) values. However, the DSB transmission is more affected by CD. This effect is illustrated in Figure 7.4-4, where the C-band contributions outperform the L-band contributions after transmission over the fiber, despite having lower OSNR values.

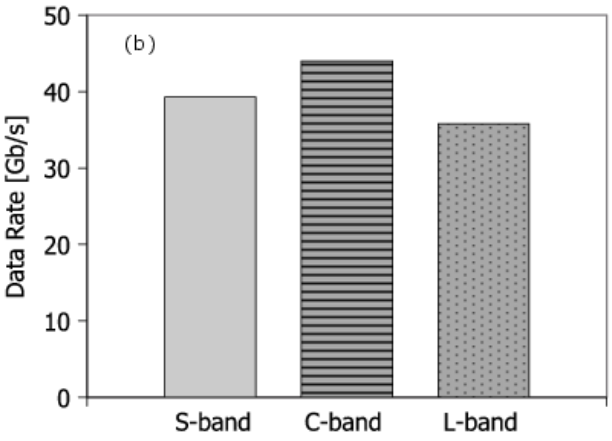

Figure 7.4-6: Achieved data rate per band after 19-cores MCF of 25.4 km.

Finally, transmission over a 19-cores MCF of 25.4 km has been assessed without considering crosstalk (XT). A XT analysis has been presented in SEASON deliverable [D3.1-24]. Figure 7.4-6 shows that the C-band contribution achieves the highest data rate of 44 Gb/s at the target BER and an OSNR of 36 dB. The L-band achieves a capacity of 35.8 Gb/s at 37.8 dB OSNR, while the S-band reaches 39.3 Gb/s at 31.7 dB OSNR. This variation in performance across different bands when transmitting over the MCF is due to the wavelength dependence of fiber properties such as effective area, CD, and fiber attenuation/loss.

By leveraging SDM, the spatial dimension can also be utilized, providing new resources to further increase overall network capacity. Using a single core of the 19-core MCF and fully populating the S, C, and L bands, data rates of 13.8 Tb/s for the S-band (350 channels), 7.7 Tb/s for the C-band (175 channels), and 5.5 Tb/s for the L-band (150 channels) can be achieved. The envisioned capacity would be doubled considering two different polarization states by exploiting polarization division multiplexing (PDM) [Nad17]. Therefore, considering the S, C, and L bands across all 19 cores, the aggregated capacity can scale up to 500 Tb/s (19×27 Tb/s). However, transmission impairments such as Raman scattering (SRS) and XT can limit the overall achieved capacity.

7.5 DSP RX-BASED MONITORING (C3.5)

7.5.1 Description

A key interest in optical networks nowadays is to largely increase the monitoring capabilities of optical equipment to leverage the collected data into insightful explanations. Massive monitoring can be implemented either with dedicated low-cost hardware or more interestingly via the coherent transponders. The latter area of research has attracted significant research works in the last years. Among these, a very promising technique is longitudinal power profile estimation which offers an estimate of power but also a localization of anomalies along the link.

In previous projects (B5G-OPEN), the relevance of the technique based on correlation method was validated by utilizing the proposed link tomography for two different use-cases: longitudinal power profile monitoring and anomaly detection [Sen22, Sen22-2]. The first use-case utilizes the

power profile to infer amplifier characteristics, such as gain and tilt within the system. The second use-case studies anomaly detection, in which optical amplifier anomalies, such as, gain, tilt and narrowband gain compression are observed. In SEASON, the goal is to implement the Linear Least Squares (LLS) approach version of the scheme to have a better accuracy in anomalies detection and localization. The technique promises a better resolution, the work is ongoing regarding this section. More details, verification and assessment of the scheme will be provided in D3.3.

7.5.2 Interfaces

S.No	Interface	Description
1	Correlation Method	Old interface was based on the correlation method with lower resolution
2	LL**S**	New interface will use LLS technique pursuing a higher resolution accuracy.

7.5.3 Status and Roadmap

S.No	Status and Roadmap	
1	Status	Current DSP RX-based transceivers is based on correlation method. New implementation will consider LLS to enhance resolution of anomalies localization.
2	Roadmap	By the end of 2024, the first version of the LLS approach will be completed. Further adjustment and trials will be addressed in Q2, Q3 2025 frame Testing measurements are to be conducted in Q2, Q3 2025 frame.

7.6 MULTIBAND AMPLIFIER (C3.6) - ENSURING AVAILABILITY BY PREDICTIVE MAINTENANCE APPLIED TO OPTICAL AMPLIFIERS

7.6.1 Description

In today's digitalized society, communication is essential for various forms of communication, including messaging and social media. Telecommunication networks, such as access networks and datacenter interconnections, use long-haul optical transmission links with optical fiber amplifiers for repeatedly restoring signal power. Performance of these amplifiers is subject to ageing effects. Over time, pump lasers may degrade, requiring replacement. Various techniques have been developed to monitor pump lasers, focusing on high pump power and injection current values [Rap23]. However, these methods have weaknesses, as they only detect degradations at high pump powers. Predictive maintenance (PdM) is an essential component in Industry 4.0, combining anomaly detection, prognosis, and diagnosis into one framework. Applying PdM to optical fiber amplifiers can enhance current monitoring and reduce network downtime risk. Ever higher data transmission rates are becoming necessary, particularly because of constant technological development. One approach is to widen the bandwidth, which entails

the use of multiband amplifiers. PdM for optical multiband amplifier is therefore of great importance as the number of amplifiers in the optical network increases and also the failure rate.

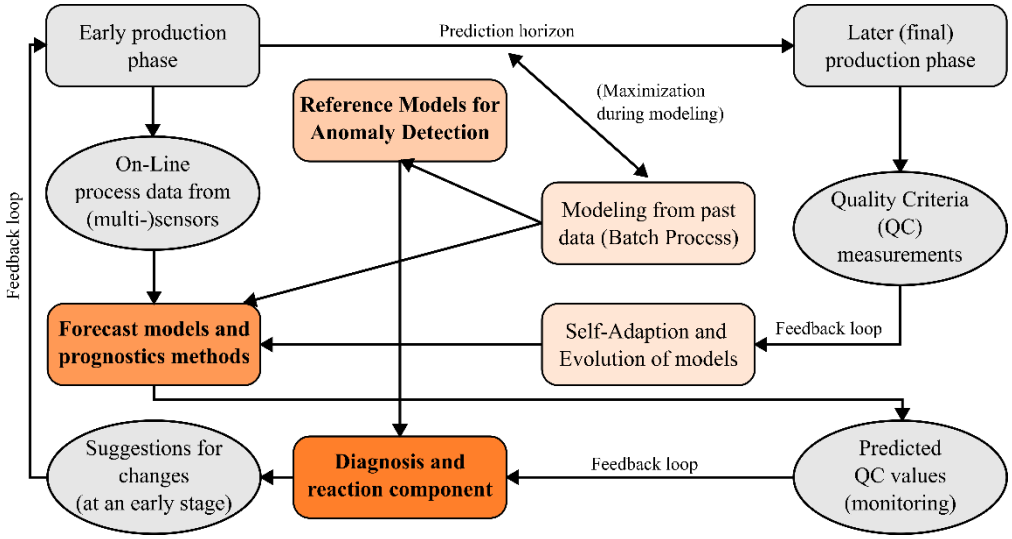

Figure 7.6-1: Generalized PdM framework [Lug19].

The PdM framework, proposed by [Lug19] and shown in Figure 7.6-1, consists of system models used for anomaly detection, prediction, forecasting, or diagnosis. These models describe system behavior under normal conditions and are adapted to the existing use case of multiband amplification. Advanced signal processing techniques are required to build robust models, which detect anomalous behavior and trigger prognosis and diagnosis components.

A PdM based prototype for improved supervision of optical fiber amplifiers has been developed, which can access high-quality historical data and monitor load and usage of components in combination with condition monitoring at the system level, and therefore enable (1) Anomaly Detection, (2) Prognosis and Forecasting and (3) Diagnosis and Fault Identification. This prototype accesses the system parameters of the multiband amplifier at defined inspection intervals and triggers the proposed PdM pipeline with subcomponents (1), (2) and (3).

7.6.2 Interfaces

S.No	Interface	Description
1	REST	This high level north-boud interface allows transport orchestrator to setup a service with specific requirementes in terms of vlan characterization, bandwidth assignment, time prioritization.
2	NETCONF PON	The prototype supports NETCONF to interact with OLT ports and control port activation/deactivation.
3	NETCONF SWITCH	The prototype supports NETCONF to interact with the spatial switch and control physical aggregation/disaggrgation of spatial lanes.

S.No	Interface	Description
1	T**elnet**	Telnet interface is used to acces the current state of the parameter of the amplifiers card

7.6.3 Status and Roadmap

S.No	Status and Roadmap	
1	Status	The current implementation of the PdM system uses the Telnet interface to access the system parameter of ADTRANs amplifier cards. All subcomponents of the PdM system are individual ML models. The current version of the PdM prototype was trained on C-Band EDFA data.
2	Roadmap	The current implementation of the interface of the PdM system will be adapted to a REST interface (Q2, 2025). The subcomponents of the PdM system will be merged into one large deep learning model, to minimize the model management efforts (Q3, 2025). The PdM prototype will be fine-tuned for the use on multiband amplifier (Q3, 2025).

7.6.4 Assessment

Investigations of the three subcomponents of the PdM system are presented below. (1) Anomaly detection uses a fuzzy clustering based method for identification of atypical behavior in time series of EDFA systems, combining fuzzy clustering procedures with entropy analysis (EA) and principal component analysis (PCA). EA is used for dynamic feature selection, reducing feature space and increasing computational performance. PCA extracts features from the raw feature space for generalization capability. Three different fuzzy clustering methods are evaluated in view of performance and generalization. The change detection framework (CDF) can detect changes in pump current time series at an early stage for arbitrary points of operation, compared to state-of-the-art predefined alarms in commercially used EDFAs. Experimental measurements of drifting pump currents show significant generalization under arbitrary operational conditions, detecting anomalies in time series with up to 4.9% drift from typical operating conditions. The algorithm can robustly detect anomalies in degenerative features and noisy data streams resembling normal operating conditions, as shown Figure 7.6-2[Sch24]. The CDF triggers the downstream models for (2) Prognosis and Forecasting and (3) Diagnosis and Fault identification.

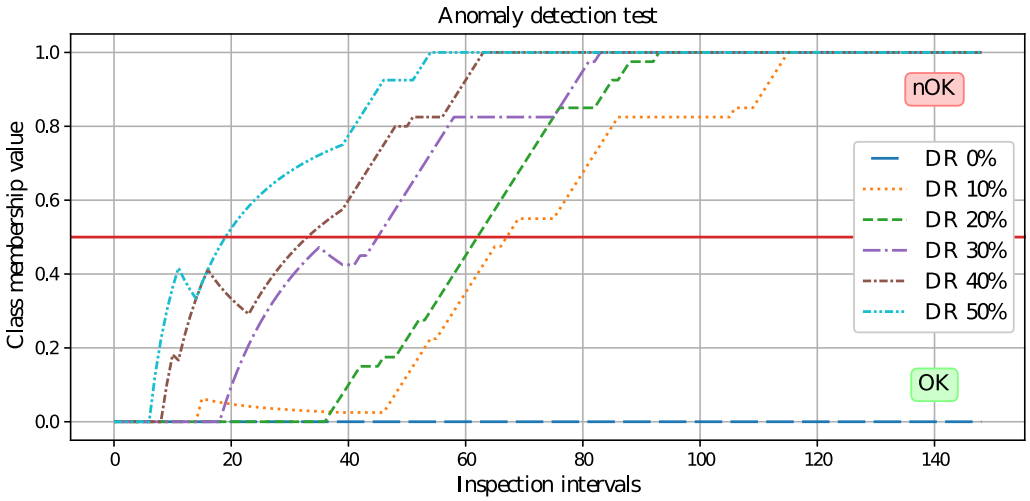

Figure 7.6-2: Anomaly identification test on different datastreams [Sch24].

(2) Remaining useful lifetime (RUL) prediction is an essential parameter in predictive maintenance techniques, ensuring reliability and safety. However, modern systems operate under complex conditions, making forecasting difficult. This PdM approach uses a novel RUL prediction method called sparse low-ranked self-attention transformer (SLAT) [Sch24b]. SLAT uses an encoder-decoder architecture, extracting features for sensors and time steps using a self-attention mechanism. The model reduces overfitting and increases generalization. Experimental application to optical fiber amplifiers shows that SLAT outperforms state-of-the-art methods. The run to failure (RTF) plot, shown in Figure 7.6-3, demonstrates the RUL prediction capability of SLAT for different failure types and degradation scenarios.

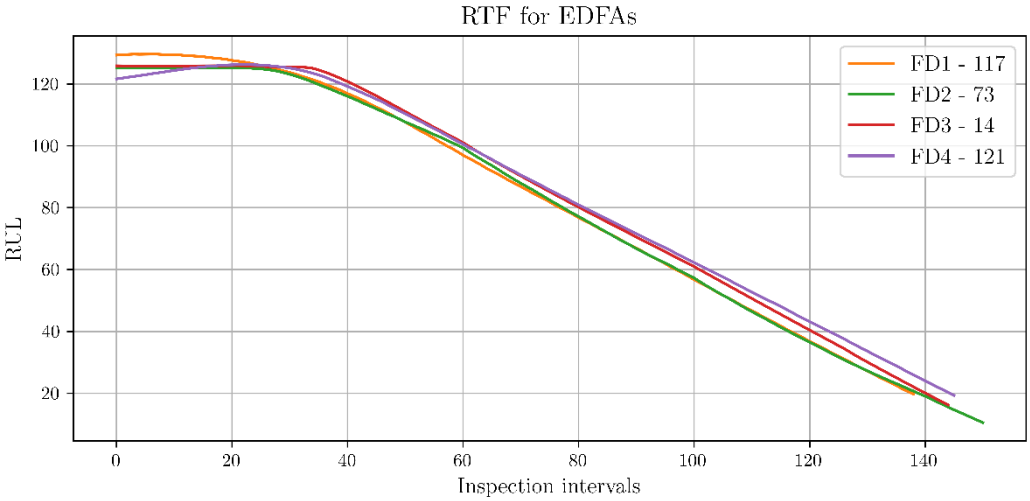

Figure 7.6-3: RTF for different faults and units of EDFAs [Sch24b].

The diagnosis component of the PdM prototype focuses on (3) identifying fault cases (FC) when system degradation has occurred, allowing for corrective measures to be initiated. Diagnosing FC is a classification task in the context of PdM, using system data at runtime. Data-driven models have evolved from statistical models to ML algorithms, with the most efficient using the

attention mechanism. Recent transformer-based models use convolutional layers for feature extraction, embedding with parallelization of three different-granulated feature maps. A novel transformer-based architecture, inverse triple-aspect self-attention transformer (ITST), is presented for diagnosing FC in optical fiber amplifiers [Sch24c]. ITST uses a triple aspect self-attention mechanism in three domains, extracting time, sensor, and frequency dependencies for improved generalization and performance. Figure 7.6-4 indicates, that ITST has a reliable classification capability for the FC with a worst misclassification rate of 15%, therefore the method is valid for diagnosing FC in complex systems like optical fiber amplifiers.

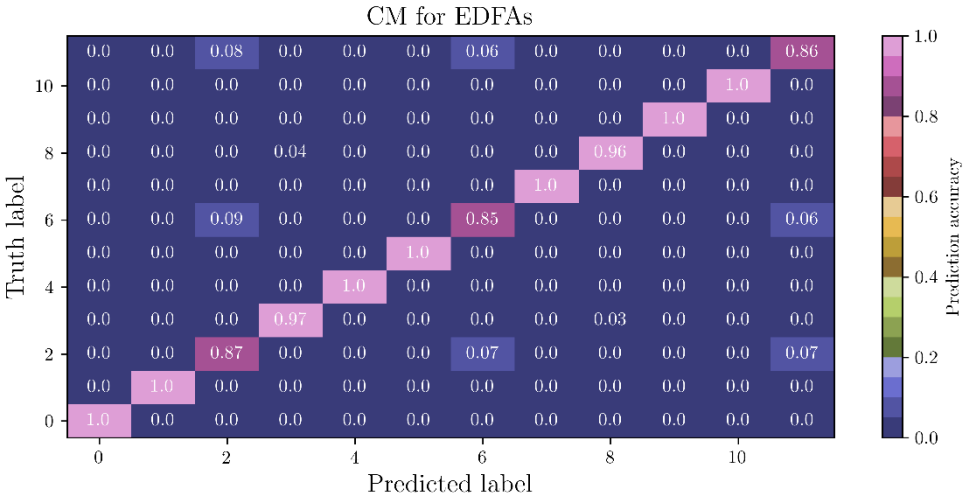

Figure 7.6-4: Confusion Matrix (CM) for FC in EDFAs [Sch24c].

This evaluation of the PdM prototype on the use case of an EDFA in the C-Band showed potential for early detection of degradation processes, prediction of RUL, and diagnosis of FC in optical fiber amplifiers, increasing the availability and reliability of optical communication networks. This work laid the foundations for the generation of a PdM for multiband amplifiers. Further investigations must be carried out with regard to adaptation of the deep learning models onto amplifier working in the MB and, if necessary, extension or fine-tuning of the individual models.

7.7 MONITORING SYSTEM AND TELEMETRY (C3.7)

7.7.1 Description

Fiber-optical networks are crucial for digital transformation, but guaranteeing their permanent availability requires continuous monitoring and fault localization [Eur23]. Most fibers are buried in the ground and susceptible to damage from human activities. Traffic interruptions are often caused by excavation and rodents [Fuj01]. Power levels monitored continuously for amplifier control can be used for detecting a faulty span, thus avoiding the installation of new hardware. The exact position of the cut within a span is determined using a mobile optical time domain reflectometer (OTDR) [Kum12]. This method saves equipment costs but delays restoration of data transmission. However, equipping networks with permanent OTDRs keeps repair time

small but is expensive. A fault localization technique that significantly reduces repair time at almost no additional equipment cost has been conceived and verified. Using the concept, the side of the fiber span closer to the cut is determined for reducing travel time and repair time.

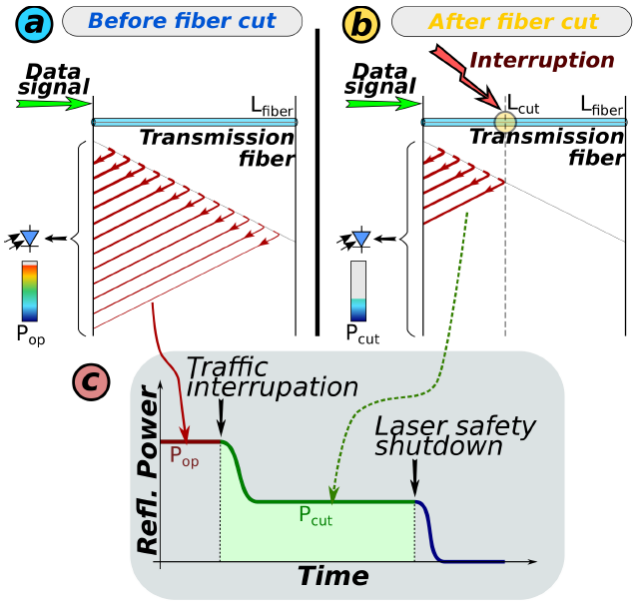

*Figure 7.7-1: Reflected power **a** without traffic interruption and **b** with traffic interruption. **c** Evolution of reflected power over time during a fiber break.*

The demonstrator set up in the laboratory uses data signals propagating in the fiber without requiring additional auxiliary lightwaves. Power components propagating back to the transmitter due to distributed reflections caused by Rayleigh backscattering are detected by a power monitor along the fiber axis. The total power measured at the fiber input represents the total power of all power components reflected back from different locations over the total length of the transmission fiber, as shown in Figure 7.7-1. When the fiber is cut, the measured power drops to a smaller level, and the position of the cut can be determined from the measured reflected power and the attenuation coefficient known from system installation.

The main goal of the invention is to provide an estimate of the location of a fiber cut at low cost. This becomes possible since the required hardware is present in almost all commercial amplifiers offering gain or output power control. In some cases, a small modification might be required, namely implementing the output monitoring capability by a 2x2-splitter in contrast to the frequently used 1x2-splitter. Since the conceived technique is to be implemented into an optical amplifier card and only requires a backward monitor comprising a splitter and a photodiode connected to a signal processing system, the demonstrator setup comprising only components required for verifying the technique is quite simple, as illustrated in Figure 7.7-2.

Dissemination Level	Public

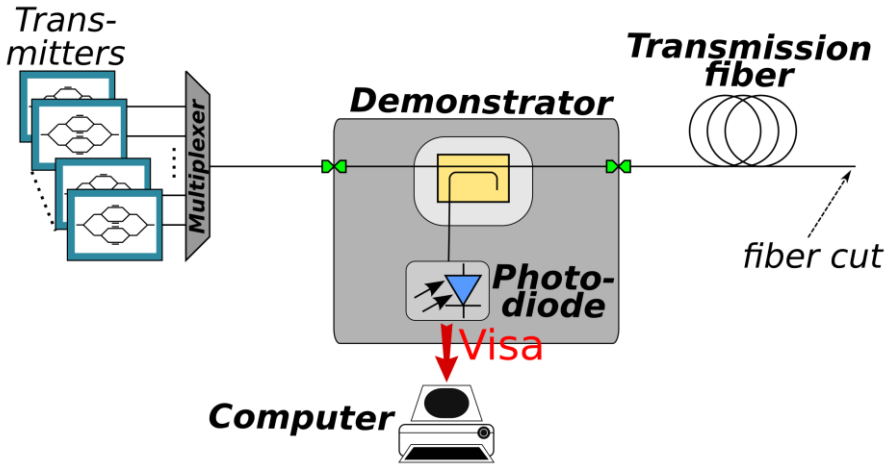

Figure 7.7-2: Demonstrator setup for demonstrating fault localization in fiber optical networks at low complexity by using optical components that are already implemented in most commercial amplifiers.

7.7.2 Interfaces

S.No	Interface	Description
1	VISA	The photodiode for power measurement is implemented in a measurement device, wheras this device is controlled remotely using a VISA interface.

7.7.3 Status and Roadmap

S.No	Status and Roadmap	
1	Status	The power that is reflected back to the fiber input is measured by an external photodiode. The measurement value from the photodiode is received using a VISA interface to the measurement device. A python script, which is manually triggered, calculated the approximated location of the fiber cut.
2	Roadmap	Provide a method to use node components to measure the reflected power at the fiber input (Q3, 2025). Implement a reading possibility to get the measurement value from the node component (Q3, 2025). Automate the triggering of the calculation script for fiber cut location approximation (Q3, 2025).

7.7.4 Assessment

The demonstrator has been verified by launching data signals into fibers of the same type but different lengths, with attenuation coefficients of 0.19 dB/km and 0.20 dB/km. The power

reflected back to the fiber input is measured and normalized to the power determined for the fiber with maximum length.

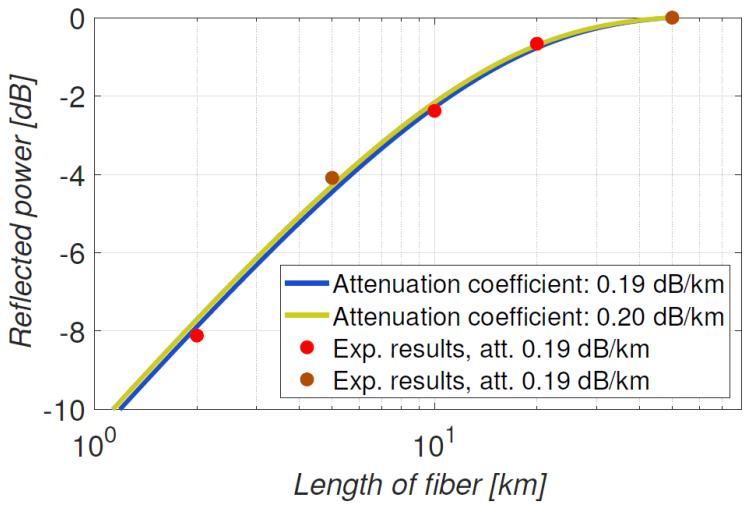

Figure 7.7-3: Experimental results showing reflected power versus fiber length.

The results in Figure 7.7-2 show an expected decrease in reflected power with decreasing fiber length. For an initial length of 60.9 km, the output of a photodetector monitoring power reflected back to the input of the fiber span is shown in Figure 7.7-3 versus time for a fiber cut. After the fiber cut, the length of the fiber segment connected to the transmit equipment is only 10.3 km, resulting in a power ratio of 61.6%.

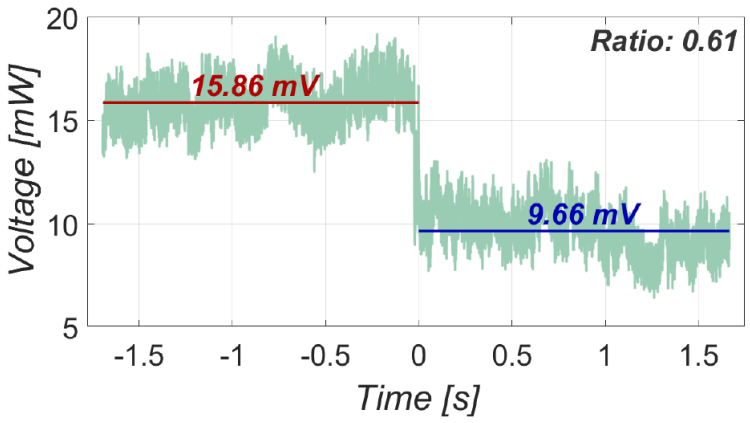

Figure 7.7-4: Output of the photodetector used for monitoring the reflected power with a power cut happening at zero on the time axis.

The demonstrator for fast fault localization in fiber optical networks is described, offering cost-effective and permanent monitoring, and ensuring high network availability by reducing repair time.

7.8 RESEARCH ACTIVITIES ON PLUGGABLE AMPLIFIERS (C3.8)

7.8.1 Description

EDFA is a low-cost amplifier used mainly for optical connections at fixed distance between datacenters. Its lack of variable gain makes it more suitable for applications with a fixed gain, where transmission conditions are established and predictable. Despite this limitation, the EDFA amplifier is advantageous in network access as it can be implemented to increase signal range without significant investment. With our architecture (Figure 7.8-1), we were able to establish an optical ring that comprises four nodes, using six channels via WDM. This ring allows the transmission of multiple signals through the same optical fiber, thus optimizing the use of existing infrastructure and increasing the overall capacity of the system.

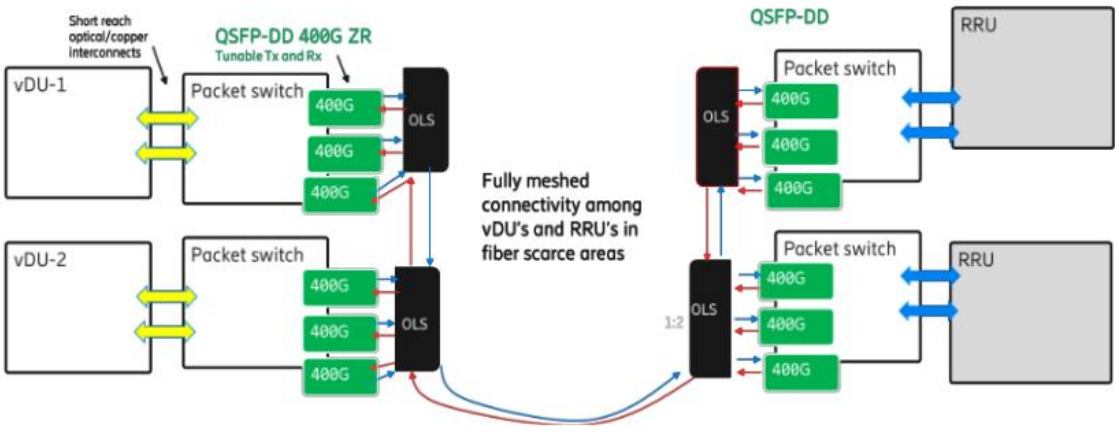

Figure 7.8-1: WDM horseshow mesh.

The network topology designed for the Fronthaul network segment presents a sophisticated infrastructure where vDUs and RRUs are seamlessly integrated with packet switches and OLS, utilizing 400G QSFP-DD transceivers to facilitate high-speed data transmission. The schematic diagram illustrates the network's core, where vDUs are connected to adjacent packet switches via short-reach optical or copper interconnects, signifying their proximity within the network. Each of these packet switches boasts 400G links to the OLS, which serves as the network's backbone, providing high-bandwidth data paths.

To optimize the network's performance in fiber-scarce regions, the OLS units are interconnected to create a fully meshed topology, extending over long distances as indicated by the 20-30km duplex fiber links that ensure bidirectional communication over a substantial reach. The network's periphery features RRUs connected to packet switches, which are in turn linked to the OLS, maintaining the consistency of the high-speed 400G connections throughout the network's architecture. These connections form a physical ring, as shown by the red and blue lines in the diagram, which also corresponds to a logical mesh network, offering redundancy and robustness for network reliability.

A key component of the network's design is the use of QSFP-DD 400G tunable transceivers, capable of adjusting both transmission and reception parameters for long-range, high-

throughput applications. This approach indicates a deliberate effort to ensure high bandwidth and adaptability for advanced telecommunications systems, such as those required by 5G networks. The entire network infrastructure is engineered for efficiency and scalability, particularly in environments with limited fiber resources, thereby maximizing network efficiency through a full mesh connectivity approach in sparsely populated areas.

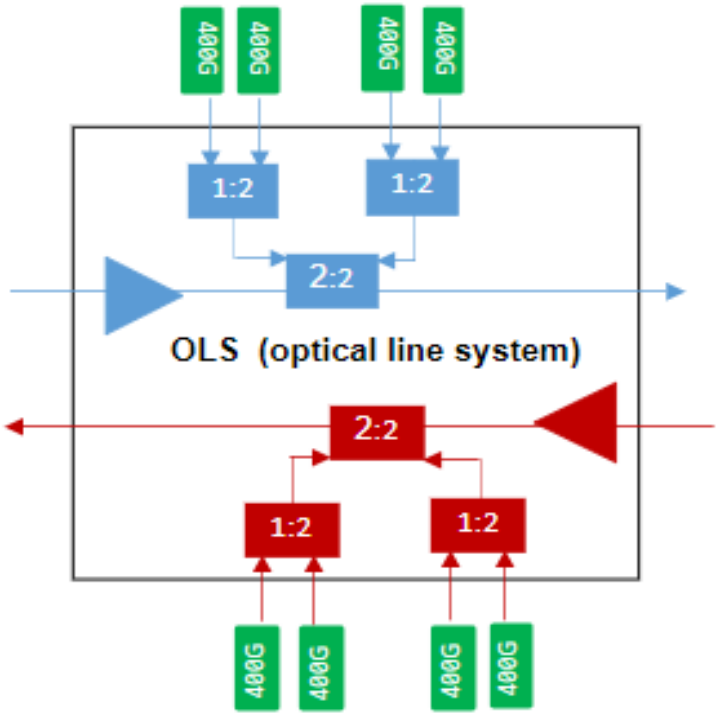

Figure 7.8-2: Filterless OADM node.

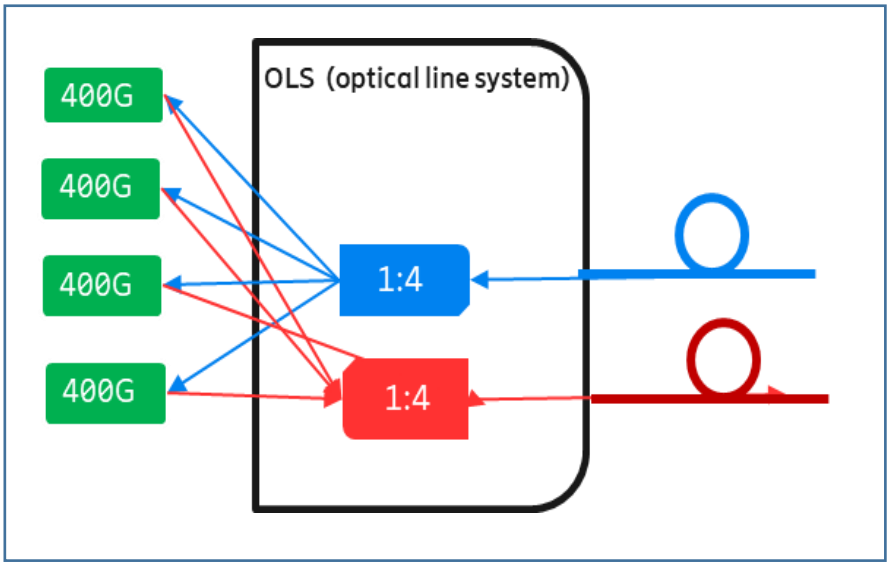

Figure 7.8-3: Filterless Terminal node.

The images depicted above (Figure 7.8-2 and Figure 7.8-3) are a zoomed-in view of an OLS, providing a detailed look at the internal configuration of the system, which includes splitters and couplers essential to support a ring topology. This close-up shows the strategic design choices made to facilitate efficient signal propagation through the network. The OLS depicted in the diagram is an integral part of the network infrastructure, with direct and non-selective splitting mechanisms indicating its reliance on simple but robust signal distribution methods. The presence of pluggable EDFAs within the system illustrates the inherent flexibility of the design, allowing for the dynamic addition or removal of channels as network demands evolve. Wavelength management is handled through precise tuning of the lasers within the 400G transceivers, ensuring the network can scale and adapt to a variety of requirements.

The system architecture, highlighted by “1:2” and “2:2” port configurations, emphasizes the system's capacity for high-speed data throughput, while interfaces labelled 400G highlight the high-capacity nature of the connections. The diagram effectively communicates the complex interaction of components within an advanced optical network, optimized not only for rapid data transfer but also to maintain signal strength and provide flexible wavelength allocation. Overall, the scheme captures the essence of a sophisticated optical network design that is both adaptable and scalable, capable of meeting the complex needs of modern high-speed data communication.

The comparative analysis table showcases the distinct capabilities of Dual and Single Amplifiers within a network system. Dual Amplifiers are designed to manage up to 8 channels, while Single Amplifiers can handle a significantly wider range, from 16 to 48 channels. Both types of amplifiers are equipped with features like AGC and APC, which provide the necessary adjustments for consistent performance, irrespective of the variations in input levels. A key differentiation is that Single Amplifiers have an added advantage of flatness control, ensuring uniform gain distribution across all channels, a feature not available in Dual Amplifiers. Furthermore, in terms of output power, Single Amplifiers have the flexibility to offer a slightly higher range, adjustable from 15 to 17 dBm, whereas Dual Amplifiers maintain a constant output of 15 dBm. This comparison clearly outlines the functional distinctions between the two amplifier types, highlighting that Single Amplifiers offer a higher degree of control and a broader operational range, making them suitable for more demanding applications that require fine-tuned signal management and greater flexibility.

Table 7.8-1: Comparison between Dual and Single Amplifier.

	Dual Amplifier	Single Amplifier
Channels	8	16-48
AGC	Yes	Yes
APC	Yes	Yes
Flatness Controll	No	Yes
Output Power	15 dBm	15-17 dBm

7.8.2 Assessment

EDFA amplifiers are fixed gain, while being cost-effective and easy to implement, they introduce constraints on network scalability. This is because the preset gain requires that the signals have

a well-defined input power to avoid over-amplifications or insufficient amplification. As a result, it is often necessary to adjust the length of the optical path-for example, by adding additional fiber cables to fit this fixed gain, a process that can increase the cost and complexity of the infrastructure. A significant improvement could come from the adoption of variable gain amplifiers. These devices allow for gain adaptability in response to dynamic changes in network conditions, such as changing the input power or adding new transmission channels. With the use of variable gain amplifiers, the network gains flexibility, as it is no longer necessary to adjust the length of the optical path for each specific signal. In addition, the use of a high-power transceiver that can operate at an output level of at least 0 dBm could help to increase the efficiency of the system. A high-power transmitter can compensate for line losses and interact more effectively with the amplifier.

However, the amplifiers used within the SEASON project offer gain variability but lack a flatness control system, this is essential to ensure a homogeneous amplification across all channels. Without this capability, some channels may be amplified more than others, leading to suboptimal signal balance and potentially transmission quality problems. To meet this challenge, it would be advisable to integrate a flatness control mechanism that automatically adjusts the gain for each channel, this ensures a consistent and reliable signal over the entire bandwidth.

In conclusion, optimizing EDFA amplifiers for greater scalability and operational flexibility requires a trade-off between cost, technological complexity, and performance benefits. The adoption of variable gain amplifiers, combined with high-power transmitters and a flatness control system, represents a promising path towards improving existing network infrastructure.

7.8.3 Interfaces

S.No	Interface	Description
1	Command line	The architecture of WDM horseshoes is developed in WP3. Is design the OLS (optical line system). The OLS features splitters, couplers, and pluggable EDFAs for efficient signal distribution, supporting a ring topology. It uses precise laser tuning in 400G transceivers for scalable and adaptable wavelength management

7.8.4 Status and Roadmap

S.No	Status and Roadmap	
1	Status	The Edgecore switch successfully supports P2P WDM transceiver using EDFA amplifier Optimizing EDFA amplifiers involves balancing cost, complexity, and performance. Variable gain amplifiers, high-power transmitters, and flatness control enhance scalability and flexibility in network infrastructure.
2	Roadmap	Identified an algorithm to appropriately adjust the amplifier gain in the ring without additional monitoring equipment.

7.9 RESEARCH ACTIVITIES ON SMARTNIC WITH COHERENT PLUGGABLE (C3.9)

7.9.1 Description

In the SEASON project, we propose the use of SmartNIC, also called Data Processing Unit (DPU), equipped with P2P and P2MP coherent transceivers as an innovative cost-effective *edge solution* providing converged packet, optical and computing resources in a single platform.

DPUs with coherent transceivers enable reduction of telecommunication equipment (e.g., aggregation routers / gateways) with benefits in terms of latency, power consumption and reduction of O/E/O conversions. Furthermore, they enable new and advanced optical and packet monitoring capabilities (as preliminarily investigated in D3.1 and D4.1 respectively).

A relevant use case of an edge node equipped with DPU encompassing coherent transceivers refers to the implementation of Distributed 5G Units (DU), as reported in Figure 7.9-1. On the left, we present the current scenario where the DU needs to be co-located with the RUs since the cell site is too far from the central office (e.g., rural areas, coverage of railways/highways). In this scenario, the cell site gateway manages only very few connections: the one from the central office to the server hosting the DU and the two/three connections towards the RUs. In SEASON, as shown in the figure on the right, we present the proposed scenario where the cell site GW is removed thanks to the use of network interface cards (NIC), equipped with P2MP coherent pluggable transceiver. The NIC is hosted in the server running the DU. Indeed, NICs/DPUs with up to four interfaces can be also exploited to directly reach the co-located RUs. This way, the Cell Site Gateway can be avoided, with significant benefits in terms of management and reliability, power consumption and latency (one less standalone element to power on, manage, monitor, and traverse). introduction of the DPU.

To support this innovative scenario, SEASON is proposing as innovative component a NIC/DPU supporting coherent pluggable modules.

Two main aspects need to be addressed.

The first aspect refers to the limited power provided to transceivers by current generation NICs/DPUs which does not allow to power on current generation of coherent pluggable transceivers. Such limitation requires a technological evolution which is beyond the project scope.

The second aspect, assuming the first one is successfully addressed, refers to the proper control of the transceiver. In SEASON this latter aspect is specifically addressed. A lightweight SDN Agent has been implemented to support the configuration of the optical transceiver equipped within the DPU, enabling the configuration of output power, frequency, and operational mode. Furthermore, in the case of P2MP transceivers, additional parameters need to be considered, such as specific hub-leaf configurations of the OpenXR module.

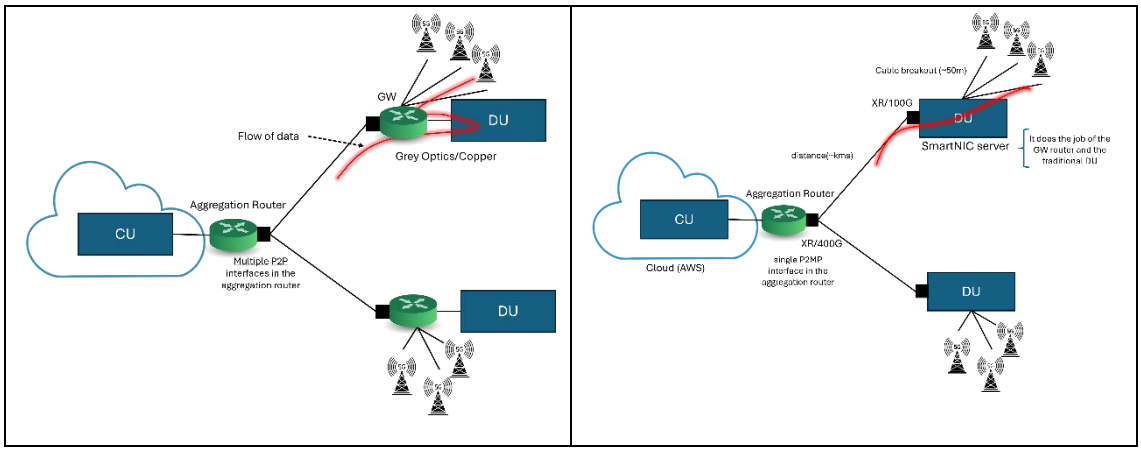

Figure 7.9-1: (left) state-of-the-art solution leveraging a standalone Cell Site Gateway router; (right) proposed approach within SEASON, eliminating – under specific conditions – the Cell Site GW.

7.9.2 Interfaces

S.No	Interface	Description
1	OpenConfig	A lightweight SDN Agent has been implemented in WP4 to support the configuration of the optical transceiver equipped within (*) the DPU. Specific parameters to be configured are the standard ones for a coherent P2P transceiver: output power, frequency, and operational mode. In the case of P2MP transceivers, additional parameters include specific hub-leaf configurations of the XR module.

(*) As of today, coherent transceivers cannot be directly inserted into DPUs due to electrical and heating constraints. For this reason, in SEASON, we insert them in packet-optical switches, but their control is performed as if they are plugged in the DPU, i.e., by software modules running within the DPU.

7.9.3 Status and Roadmap

S.No	Status and Roadmap	
1	Status	A server equipped with DPU is up and running, connected with an Edgecore switch hosting the coherent pluggable. The server also runs the Acceleran sw implementing DU functionalities The Edgecore switch successfully supports P2P transceiver, while the support of P2MP transvers by Infinera is in progress
2	Roadmap	Finalize the support of P2MP transceivers (by WP4). Expected by Q1 2025.

8 CONCLUSIONS

This deliverable reports on the activities of the WP3 during the second year of the SEASON project. The reference architecture, developed in WP2, has been taken as input in WP3. Key data plane solutions are presented to address the challenges posed by the growing demand to enable high-capacity, scalable, and energy-efficient optical networks. The main focus is on the design and implementation of multiband over spatial division multiplexing technologies to meet the stringent requirements of future data traffic and bandwidth demands. Project objectives and KPIs related to WP3 have been discussed, and their fulfilment status is also reported in this document.

Key advancements include the development of scalable optical network architectures that leverage MBoSDM to significantly increase network capacity while maintaining energy efficiency. By means of modeling and end-to-end transmission evaluation, SEASON has successfully explored solutions for MBoSDM and P2MP systems, optimizing network designs to reduce power consumption without compromising performance.

Innovative optical subsystems and devices have been prototyped and initially evaluated, including advanced transceivers, and switching solutions that supports MBoSDM operation. These technologies are crucial for enabling efficient, flexible, and high-capacity optical infrastructure, addressing different network segments.

The deliverable also reports considerable progress on the exploration of new network designs for front/mid-haul systems in the context of 5G and beyond, introducing solutions like spatial passive optical networks and optimized P2MP architectures. These developments will support the scalability and performance required to manage the increasing demands of next-generation mobile transport systems.

Additionally, the deliverable highlights advances in optical monitoring and power efficiency strategies, including the use of pluggable transceivers and advanced monitoring techniques. Finally, various data plane components developed within the SEASON project are detailed and initially assessed, including MBoSDM transceiver and node solutions, a predictive maintenance system for multiband amplifiers, monitoring systems, pluggable amplifiers and SmartNICs equipped with coherent pluggables

All these achievements are key steps towards fulfilling SEASON objectives, KPIs and goal, which aims to design and validate a transport network infrastructure able to support beyond 5G and new emerging services, relying on the joint usage of MBoSDM, spanning the access, aggregation, and metro/long-haul segments, supporting the requirements for x-haul, further integrating the packet/optical and computing layers, and targeting efficient networks in terms of capacity and energy efficiency.

This deliverable feeds WP4 and WP5, supporting the integration with the control plane for managing transceivers, nodes, and monitoring systems. It enables network flexibility, reconfiguration, and integration into the final demonstrations.

9 GLOSSARY

Acronym	Description
ADC	Analog-to-Digital Converter
ADSL	Asymmetric Digital Subscriber Line
AL	Ambitious Level
AR	Augmented Reality
ASE	Amplified Spontaneous Emission
ASIC	Application-Specific Integrated Circuit
AWG	Arrayed-Waveguide Grating
b2b	Back-to-Back
BNG	Broadband Network Gateway
BOL	Begin of Life
BVT	Bandwidth/bit rate Variable Transponder
CC-MCF	Coupled-Core Multi-Core Fiber
CD	Colorless Directionless
CDC	Colorless Directionless Contentionless
CDF	Change Detection Framework
CDN	Content Delivery Network
CM	Confusion Matrix
CO	Central Office
CSG	Cell Site Gateway
DAC	Digital-to-Analog Converter
DC	Data Center
DCM	Dispersion Compensation Modules
DD	Direct Detection
DPU	Data Processing Unit
DSB	Double Sideband
DSCM	Digital Supply Chain Management
DSP	Digital Signal Processor/Processing
DWDM	Dense Wavelength Division Multiplexing
E2E	End-to-End
EA	Entropy Analysis
ECL	External-Cavity Laser
EDFA	Erbium-Doped Fiber Amplifier
EON	Elastic Optical Networks
FC	Fault Case
FEC	Forward Error Correction
FIFO	First In First Out
FMF	Few-Mode Fiber
FOADM	Fixed Filter Optical Add-Drop Multiplexer
FTTH	Fiber-To-The-Home
FTTx	Fiber-To-The-x
GE	Gigabit Ethernet
GGN	Generalized Gaussian noise

GN	Gaussian Noise
GPON	Gigabyte Passive Optical Network
GPU	Graphics Processing Unit
GSNR	Generalized Signal-To-Noise Ratio
HLx	Hierarchical Level X
IM	Intensity Modulation
ISP	Internet Service Provider
ISRSGN	Inter-Channel Stimulated Raman Scattering
ITST	Inverse Triple-Aspect Self-Attention Transformer
KPI	Key Performance Indicator
MAN	Metropolitan Area Network
MB	Multiband
MBoSDM	Multiband over Space Division Multiplexing
MBT	Multiband Transmission
MC	Multi-Core
MCF	Multi-Core Fiber
MCS	MultiCast Switch
MDL	Mode-dependent loss
MIMO	Multi-input-multi-output
MMF	Multimode fiber
MPF	Mult-parallel fiber
MPLS	Multi-Protocol Label Switching
MW	Microwave
MZM	Mach-Zehnder Modulator
NIC	Network Interface Card
NLI	Nonlinear interference
NN	Neural Network
NOS	Network Operating System
O/E/O	Optical to Electrical to Optical
ODE	Ordinary differential equations
ODN	Optical Distribution Network
OFDM	Orthogonal Frequency Division Multiplexing
OLT	Optical Line Terminal
ONT	Optical Network Terminal
OPC	Optical Packet Core
O-RAN	Optical Radio Access Network
OSA	Optical Spectrum Analyzer
OSC	Optical Supervisory Channel
OSFP	Optical Small Factor Pluggable
OSNR	Optical Signal-to-Noise Ratio
OTDR	Optical Time Domain Refloctometer
OTN	Optical Transport Network
P2MP	Point-to-Multi-Point
P2P	Point-to-Point
PCA	Principal Component Analysis
PdM	Predictive Maintenance
PGW	Packet Data Network Gateway
PON	Passive Optical Network

QoT	Quality of Transmission
QSFP	Quad Small Factor Pluggable
RAN	Radio Access Network
RMA	Return Merchandize Authorization
ROADM	Reconfigurable Optical Add-Drop Multiplexer
RTF	Run-To-Failure
RUL	Remaining Useful Lifetime
S-BVT	Sliceable Bandwidth Variable Transceiver
SDM	Spatial division multiplexing
SE	Spectral Efficiency
SLAT	Sparse Low-Ranked Self-Attention Transformer
SMF	Single-Mode Fiber
SNR	Signal-To-Noise Ratio
SoA/SotA	State of the Art
S-OXC	Spatial Optical Cross Connect
SRS	Stimulated Raman Scattering
SSB	Single Sideband
SSMF	Standard Single Mode Fiber
TDFA	Thulium-Doped Fiber Amplifier
TF	Tunable Filter
TLS	Tunable Laser Source
UC-MCF	Uncoupled-Core Multi-Core Fiber
URLLC	Ultra-Reliable and Low-Latency Communications
VPN	Virtual Private Network
VR	Virtual Reality
WC-MCF	Weakly-Coupled Multi-Core Fiber
WDM	Wavelength Division Multiplexed
WSS	Wavelength Selective Switch
XGS-PON	10Gb Simmetric Passive Optical Network

10 REFERENCES

Fuj01	Alcoa Fujikura, “Alcoa Fujikura annual internet report (2001)”, 2001, Tokyo
Arp24	F. Arpanaei, J. M. Rivas-Moscoso, I. De Francesca, J. A. Hernandez, A. Sanchez-Macian, M. R. Zefreh, D. Larrabeiti, and J. P. Fernandez-Palacios, “Enabling seamless migration of optical metro-urban networks to the multi-band: unveiling a cutting-edge 6D planning tool for the 6G era,” Journal of Optical Communications and Networking, vol. 16, no. 4, pp. 463–480, 2024.
Arp24-2	F. Arpanaei, K. Ghodsifar, H. Beyranvand, J. A. Hernández, J. M. Rivas-Moscoso, C. Natalino, M. R. Zefreh, A. Napoli, J. P. Fernández-Palacios, and D. Larrabeiti, “Hyperaccelerated power optimization in multi-band elastic optical networks,” in 2024 Optical Fiber Communi- cations Conference and Exhibition (OFC), 2024, pp. 1–3.
Bar18	D. J. F. Barros and J. M. Kahn, “Comparison of Orthogonal Frequency-Division Multiplexing and On-Off Keying in Amplified Direct-Detection Single-Mode Fiber Systems,” Journal of Lightwave Technology, vol. 28, no. 12, pp. 1811–1820, 2010. 10.1109/jlt.2010.2048999.
Bha08	U. N. Bhat, “The general queue G/G/1 and approximations,” in An Introduction to Queueing Theory. Birkh¨auser, 2008, pp. 169–183.
Boi24	Fabien Boitier, Laia Nadal, F. Javier Vílchez, Petros Ramantanis, Josep M. Fàbrega, Alix May, Michela Svaluto Moreolo, Ramón Casellas, Patricia Layec, “Monitoring of Chromatic Dispersion in Multi-Domain Optical Transmission Systems”, submitted to ECOC 2024.
Bos19	G. Bosco, “Advanced modulation techniques for flexible optical transceivers: The rate/reach tradeoff,” Journal of Lightwave Technology, vol. 37, no. 1, pp. 36–49, 2019.
Cas23	C. Castro, A. Napoli, M. Porrega, et al., “Scalable filterless coherent point-to-multipoint metro network architecture”, Journal of Optical Communications and Networking, vol. 15, no. 5, pp. B53–B66, 2023.
Cas24	C. Castro, J. Sime, T. Eriksson, M. S. Erkilinç, M. Porrega, J. Pedro, Marco Quagliotti, E. Riccardi, C. Fludger, A. Napoli, “Power and Spectral Savings in Metro Aggregation Networks Exploiting Coherent Point-to-Multipoint Transceivers”, in European Conference on Optical Communications (ECOC) 2024.
Cas24-2	Piero Castoldi, Rana Abu Bakar, Andrea Sgambelluri, Juan Jose Vegas Olmos, Francesco Paolucci, and Filippo Cugini, “Programmable Packet-Optical Networks using Data Processing Units (DPUs) with Embedded GPU Monitoring devices”, OFC Conf. 2024.
Coh85	L. Cohen, “Comparison of Single-Mode Fiber Dispersion Measurement Techniques,” Journal of Lightwave Technology, vol. LT-3, no. 5, pp. 958–966, 1985. 10.1109/jlt.1985.1074327.
D1.1-13	FP7 IDEALIST Project Deliverable D1.1, “Elastic optical network architecture: Reference scenario, cost and planning,” [Online]. Available:.https://cordis.europa.eu/docs/projects/cnect/9/317999/080/deliverables/001-D11ElasticOpticalNetworkArchitecture.doc.
D2.1-24	“Definition of Use Cases, Requirements and Reference Network Architecture”, SEASON, V2.1, March 2024.
D2.2-25	“Techno-economic Analysis: First Results”, SEASON, January 2025.
D3.1-24	“End-to-end design of next generation smart optical networks”, SEASON, V2.0, June 2024.
Duh90	P. Duhamel, "Algorithms meeting the lower bounds on the multiplicative complexity of length-2/sup n/ DFTs and their connection with practical algorithms," in IEEE Transactions on Acoustics, Speech, and Signal Processing, vol. 38, no. 9, pp. 1504-1511, Sept. 1990, doi: 10.1109/29.60070.
Ess12	Essiambre, R.-J., Tkach, R.W., "Capacity Trends and Limits of Optical Communication Networks", Proceedings of the IEEE, Vol. 100, No. 5, 2012, pp. 1035-1055.
Eur23	European Commission, “Report on the state of the digital decade”, 2023.
Fer20	A. Ferrari, A. Napoli, J. K. Fischer, N. Costa, A. D’Amico, J. Pedro, W. Forysiak, E. Pincemin, A. Lord, A. Stavdas, J. P. F.-P. Gimenez, G. Roelkens, N. Calabretta, S. Abrate, B. Sommerkorn-Krombholz, and V. Curri, “Assessment on the achievable throughput of multi-band ITU-T G.652.d fiber transmission systems,” J. Light. Technol. 38, 4279–4291, 2020.

Ger22 O. Gerstel et al., “A control hierarchy for integrated packet-optical networks utilizing pluggable transceivers,” in OFC’22, 2022, pp. paper M4F–2.

Gio20 A. Giorgetti et al., “Control of open and disaggregated transport networks using the open network operating system (onos),” Journal of Optical Communications and Networking, vol. 12, no. 2, pp. A171–A181, 2020.

Gio23 A. Giorgetti, D. Scano, A. Sgambelluri, F. Paolucci, E. Riccardi, R. Morro, P. Castoldi, and F. Cugini, “Enabling hierarchical control of coherent pluggable transceivers in sonic packet–optical nodes,” Journal of Optical Communications and Networking, vol. 15, no. 3, pp. 163–173, 2023.

Gri10 S. Gringeri, B. Basch, V. Shukla, R. Egorov, and T. J. Xia, “Flexible architectures for optical transport nodes and networks,” IEEE Communications Magazine, vol. 48, no. 7, pp. 40–50, 2010.

Han24 S. J. Hand, D. F. Welch, V. Bhaskara, D. Naik, A. Wikman, M. Silvola, H. Su, T. Monteiro, F. Marques, P. Santos, N. Swenson, A. Napoli, D. Hillerkuss, and H. Bock, “A new operational paradigm for ipodwdm networks,” IEEE Access, vol. 12, pp. 56 050–56 061, 2024.

Her20 J. A. Hernandez, M. Quagliotti, E. Riccardi, V. Lopez, O. G. d. Dios, and R. Casellas, “A techno-economic study of optical network disaggregation employing open source software business models for metropolitan area networks,” IEEE Communications Magazine, vol. 58, no. 5, pp. 40–46, 2020.

IEEE17 IEEE Standards Association, “IEEE standard for ethernet amendment 10: Media access control parameters, physical layers, and management parameters for 200 Gb/s and 400 Gb/s operation”, 2017 [Online]. Available: https://standards.ieee.org/ieee/802.3bs/6748/.

IEEE22 IEEE P802.3df, “Adopted IEEE P802.3df timeline”, 2022 [Online]. Available: https://www.ieee802.org/3/df/projdoc/timeline 3df 221004.pdf.

IEEE23 IEEE P802.3dj, “Adopted IEEE P802.3dj timeline,”, 2023 [Online]. Available: https://www.ieee802.org/3/dj/projdoc/timeline 3dj 231128.pdf.

IEICE22 The Institute of Electronics, Information and Communication Engineers (Technical Committee on Photonic Network), “Japan photonic network model (JPNM)”, 2022 [Online]. Available: https://www.ieice.org/cs/pn/eng/jpnm en.html.

Inf22 Infinera, “XR Optics Solution Brief: Innovative Point-to-Multipoint Coherent that Slashes Aggregation Network TCO”, 2022 [online] available: https://www.infinera.com/wp-content/uploads/XR-Optics-SB-0217-RevF-0222.pdf.

Iso19 H. Isono, “Latest standardization status and its future directions for high speed optical transceivers,” in Metro and Data Center Optical Networks and Short-Reach Links II, (2019), p. 1094604.

Iwa12 Y. Iwai, H. Hasegawa, and K.-i. Sato, “Large-scale photonic node architecture that utilizes interconnected small scale optical cross-connect sub-systems,” in 2012 38th European Conference and Exhibition on Optical Communications, 2012, pp. 1–3.

Kaw20 H. Kawahara, M. Nakagawa, T. Seki, and T. Miyamura, “Experimental demonstration of wavelength-selective band/direction-switchable multi-band OXC using an inter-band all-optical wavelength converter,” in 2020 European Conference on Optical Communications (ECOC), 2020, pp. 1–4.

Kha24 L. Z. Khan, J. Pedro, N. Costa, A. Sgambelluri, A. Napoli and N. Sambo, "Model and data-centric machine learning algorithms to address data scarcity for failure identification," in Journal of Optical Communications and Networking, vol. 16, no. 3, pp. 369-381, March 2024, doi: 10.1364/JOCN.511863.

Kim20 G. Kim, L. Kull, D. Luu, M. Braendli, C. Menolfi, P.-A. Francese, H. Yueksel, C. Aprile, T. Morf, M. Kossel, A. Cevrero, I. Ozkaya, A. Burg, T. Toifl, and Y. Leblebici, “A 161-mw 56-gb/s adc-based discrete multitone wireline receiver data-path in 14-nm finfet,” IEEE J. Solid-State Circuits 55, 38–48 (2020).

Kin61] J. F. C. Kingman, “The single server queue in heavy traffic,” Mathematical Proceedings of the Cambridge Philosophical Society, vol. 57, no. 4, p. 902, October 1961.

Kum12	V. Kumar, D.Rajouria, “Fault detection technique by using OTDR: Limitations and drawbacks on practical approach of measurements“, in International Journal of Emerging Technology and Advanced Engineering, 2012, pp. 283-287.
Lug19	E. Lughofer, M. Sayed-Mouchweh, “Prologue: Predictive maintenance in dynamic systems”, in “Predictive Maintenance in Dynamic Systems”, Springer, 2019.
Moe16	D. A. Morero et al., "Design Tradeoffs and Challenges in Practical Coherent Optical Transceiver Implementations," in Journal of Lightwave Technology, vol. 34, no. 1, pp. 121-136, 1 Jan.1, 2016, doi: 10.1109/JLT.2015.2470114.
Mor23	R. Morro, E. Riccardi, D. Scano, A. Sgambelluri, P. Castoldi, F. Cugini, and A. Giorgetti, “First demonstration of mantra IPoWDM convergent SDN architecture using SONIC white box and 400ZR/ZR+ pluggables,” in 2023 International Conference on Optical Network Design and Modeling (ONDM), 2023, pp. 1–3.
Nad17	Laia Nadal, Michela Svaluto Moreolo, Josep M. FÃ brega, F. Javier Vilchez, ’Meeting the future metro network challenges and requirements by adopting programmable S-BVT with direct-detection and PDM functionality,’ Optical Fiber Technology, Volume 36, 2017, Pages 344-352, ISSN 1068-5200, https://doi.org/10.1016/j.yofte.2017.05.007.
Nad20	Nadal, L.; Moreolo, M.S.; Hernández, J.A.; Fabrega, J.M.; Casellas, R.; Muñoz, R.; Martínez, R. SDN-Enabled S-BVT for Disaggregated Networks: Design, Implementation and Cost Analysis. J. Light. Technol. 2020, 38, 3037–3043.
Nad22	L. Nadal et al, "SDN-enabled Multi-band S-BVT within Disaggregated Optical Networks," JLT.2022.
Nad23	Nadal, L.; Ali, M.; Vílchez, F.J.; Fàbrega, J.M.; Svaluto Moreolo, M. “The Multiband over Spatial Division Multiplexing Sliceable Transceiver for Future Optical Networks”, Future Internet, 15, 381, Dec. 2023.
Nad23-2	Nadal, Laia and Fàbrega, Josep M. and Vílchez, Francisco and Svaluto Moreolo, Michela, “Next-Generation Optical Transceiver and Switching Solutions Exploiting MB and SDM”, 13-15, 2023, 10.1109/IMOC57131.2023.10379777.
Nad24	Nadal, L., Martínez, R., Ali, M., Vílchez, F. J., Fàbrega, J. M., Svaluto Moreolo, M. and Casellas, R., “Advanced Optical Transceiver and Switching Solutions for Next-Generation Optical Networks”, accepted in JOCN, 16, 8, 2024.
Nad24-2	Nadal, L., Fàbrega, J. M., Ali, M., Vílchez, F. J. and Svaluto Moreolo, M., “Towards Extending Switching Capabilities in Future Optical Networks”, ICTON, Bari, July 2024.
Nal23	S. Nallaperuma, Z. Gan, J. Nevin, M. Shevchenko, and S. J. Savory, “Interpreting multi-objective reinforcement learning for routing and wavelength assignment in optical networks,” J. Opt. Commun. Netw. 15, 497–506 (2023).
Niw17	M. Niwa, Y. Mori, H. Hasegawa, and K.-i. Sato, “Tipping point for the future scalable OXC: what size MxM WSS is needed?” Journal of Optical Communications and Networking, vol. 9, no. 1, pp. A18–A25, 2017.
OIF23	https://www.oiforum.com/oifs-q3-technical-and-mae-committees-meeting-spurs-four-new-innovative-projects-link-training-for-224g-electrical-interfaces-1600zr-data-center-optical-network-coordination-energy-effi/, accessed on 12.3.24.
OpenConfig24	OpenConfig, “Openconfig web site. [online] available: http://www.openconfig.net/,” (2016-2024).
OpenROADM24	OpenROADM, “The open roadm multi-source agreement (MSA). (2024) [online] available: http://www.openroadm.org”.
OpenXR24	OpenXR Optics forum, “OpenXR Optics forum MSA”. (2024) [On-line]. Available:https://openxropticsforum.org/.
Ped15	J. Pedro and S. Pato, “On scaling transport networks for very high nodal degree ROADM nodes using state-of-the-art optical switch technology,” in 2015 17th International Conference on Transparent Optical Networks (ICTON), 2015, pp. 1–5.
Ped17	J. Pedro and S. Pato, “ROADM express layer design strategies for scalable and cost-effective multi-fibre DWDM networks,” in 2017 19th International Conference on Transparent Optical Networks (ICTON), 2017, pp. 1–7.

Ped20 J. Pedro, N. Costa, and S. Pato, “Optical transport network design beyond 100 GBaud [invited],” Journal of Optical Communications and Networking, vol. 12, no. 2, pp. A123–A134, 2020.

Rad24 M. Radovic, A. Sgambelluri, F. Cugini and N. Sambo, "Power-aware high-capacity elastic optical networks," in Journal of Optical Communications and Networking, vol. 16, no. 5, pp. B16-B25, May 2024, doi: 10.1364/JOCN.514067.

Rap03 L. Rapp, “Comparison of EDFA setups using either adaptive equalization filter or fixed gain-flattening filter with respect to noise figure”, Journal of Optical Communications, vol. 24, no. 5, pp. 185-188, 2003.

Rap21 L. Rapp, F. Azendorf, and W. Mönch, “Capturing Nonlinear Signal Distortions by the Spectral Correlation Method”., Optical Fiber Communication Conference, 2021.

Rap23 L. Rapp, “Method for Monitoring a Pump Laser of at Least One Optical Amplifier in an Optical Transmission Link in Operation”, United States of America Patentnr. US2023/0411924 A1, 2023.

Roo24 P. Roorda, B. Smith, P. Colbourne, S. McLaughlin, and M. Matthews, “Enabling technologies for scalable ROADMs,” in 2024 Optical Fiber Communications Conference and Exhibition (OFC), 2024, pp. 1–3.

Sah17 A. Sahara, H. Kawahara, S. Yamamoto, S. Kawai, M. Fukutoku, T. Mizuno, Y. Miyamoto, K. Suzuki, and K. Yamaguchi, “Proposal and experimental demonstration of SDM node enabling path assignment to arbitrary wavelengths, cores, and directions,” Opt. Express, vol. 25, no. 4, pp. 4061–4075, Feb 2017.

Sam24 N. Sambo, F. Cugini, P. Castoldi, “Toward high-capacity and energy-efficient optical networks”, ONDM 2024.

Sav08 S. J. Savory, “Digital filters for coherent optical receivers,” Optics express, vol. 16, no. 2, pp. 804–817, 2008.

Sch24 D. Schneider, L. Rapp, C. Ament, “ Anomaly detection in time series of EDFA pump currents to monitor degeneration processes using fuzzy clustering”, in IEEE International Conference on Machine Learning in Communications and Networking (ICMLCN), pp. 454-459, 2024, doi: 10.1109/ICMLCN59089.2024.10624870.

Sch24b D. Schneider, L. Rapp, “Sparse Low-Ranked Self-Attention Transformer for Remaining Useful Lifetime Prediction of Optical Fiber Amplifiers”, in IEEE Transaction on Machine Learning in Communications and Networking (TMLCN), submitted.

Sch24c D. Schneider, L. Rapp, C. Ament, “ Diagnosing Fault Cases in Optical Fiber Amplifiers using Inverse Triple Aspect Self-Attention Transformer“, in Optical Fiber Communication Conference (OFC), 2025, submitted.

Sen22 M. Sena et al., "DSP-Based Link Tomography for Amplifier Gain Estimation and Anomaly Detection in C+L-Band Systems," in Journal of Lightwave Technology, vol. 40, no. 11, pp. 3395-3405, 1 June1, 2022, doi: 10.1109/JLT.2022.3160101.

Sen22-2 M. Sena et al., "Advanced DSP-based Monitoring for Spatially resolved and Wavelength-dependent Amplifier Gain Estimation and Fault Location in C+L-band Systems," in Journal of Lightwave Technology, 2022, doi: 10.1109/JLT.2022.3208209.

Sev24 E. Seve, S. Bigo and P. Layec, “Identification of Optical Links with Heterogenous Fiber Types in a Production Network” in Optical Fiber Communications Conference (OFC), W3C.4, 2024.

Sga24 A. Sgambelluri, D. Scano, R. Morro, F. Cugini, J. Ortiz, J. M. Martinez, E. Riccardi, P. Castoldi, P. Pavon, and A. Giorgetti, “Failure recovery in the MANTRA architecture with an IPoWDM SONiC node and 400ZR/ZR+ pluggables,” J. Opt. Commun. Netw., vol. 16, no. 5, pp. B26–B34, May 2024.

Shi20 W. Shi, Y. Tian, and A. Gervais, “Scaling capacity of fiber-optic transmission systems via silicon photonics,” Nanophotonics, vol. 9, no. 16, pp. 4629–4663, 2020.

Sou22 A. Souza, N. Costa, J. Pedro, and J. Pires, “Benefits of counterpropagating Raman amplification for multiband optical networks,” J. Opt. Commun. Netw., vol. 14, no. 7, pp. 562–571, Jul 2022.

Sou24 A. Souza, N. Costa, J. Pedro, and J. Pires, “Comparative assessment of S+C+L-band and E+C+L-band systems with hybrid amplification,” in Optical Fiber Communication Conference (OFC) 2024. Optica Publishing Group, 2024.

Sou24-2 A. Souza, B. Correia, A. Napoli, V. Curri, N. Costa, J. Pedro, and J. Pires, “Cost analysis of ultrawideband transmission in optical networks,” Journal of Optical Communications and Networking, vol. 16, no. 2, pp. 81–93, 2024.

Sun20 H Sun. et al., ”800G DSP ASIC design using probabilistic shaping and digital sub-carrier multiplexing,” J. Lightwave Technol. 38, 4744-4756 (2020)

Tak11 K.Takenaga, Y.Arakawa, Y.Sasaki, S.Tanigawa, S.Matsuo, K.Saitoh, and M. Koshiba, “A large effective area multi-core fibre with an optimised cladding thickness,” in 2011 37th European Conference and Exhibition on Optical Communication, 2011, pp. 1–3.

Ter23 A. B. Terki, J. Pedro, A. Eira, A. Napoli, and N. Sambo, “Routing and spectrum assignment based on reinforcement learning in multi-band optical networks,” in PSC, (2023)

TIP22 TIP MANTRA Whitepaper, “Ipowdm convergent sdn architecture - motivation, technical definition and challenges, v1.0,” 2022.

Tre23 C. Tremblay, A. Mahmoudialami, P. Alain, N. Sigue, Y. Pei, D. Côté, D. Boertjes, D. Demeter, and C. Desrosiers, “Detection and root cause analysis of performance degradation in optical networks using machine learning,” in 2023 European Conference on Optical Communication (ECOC), (2023), pp. 1–4.

Vat20 B. Vatankhahghadim, N. Wary, and A. C. Carusone, “Discrete multitone signalling for wireline communication,” in 2020 IEEE International Symposium on Circuits and Systems (ISCAS), (2020), pp. 1–5.

Wel23 D. Welch, A. Napoli, J. Bäck, et al., “Digital subcarrier multiplexing: Enabling software-configurable optical networks”, Journal of Lightwave Technology, vol. 41, no. 4, pp. 1175–1191, 2023.

Ye14 F. Ye, J. Tu, K. Saitoh, and T. Morioka, “Simple analytical expression for crosstalk estimation in homogeneous trench-assisted multi-core fibers,” Opt. Express, vol. 22, no. 19, pp. 23007–23018, Sep 2014.

Zam24 T. Zami, N. Rossi and B. Lavigne, "Is unceasing increase of channel symbol rate the panacea for WDM transparent meshed networks?," 2024 Optical Fiber Communications Conference and Exhibition (OFC), San Diego, CA, USA, 2024, pp. 1-3.

Zef20 M. R. Zefreh and P. Poggiolini, “A real-time closed-form model for nonlinearity modeling in ultra-wide-band optical fiber links accounting for inter-channel stimulated Raman scattering and co-propagating Raman amplification,” 2020, arXiv:2006.03088,[eess.SP].